Volume 4 SEPTEMBER, 1933 Number 9

PHYSICS

A Journal of General and Applied Physics

Luminous Discharge Between Lecher Wires in a Partially Evacuated Tube*

W. D. HERSHBERGER, H. A. ZAHL AND M. J. E. GOLAY, *Signal Corps Laboratories, Fort Monmouth, New Jersey*

(Received May 5, 1933)

In experiments with a Gill-Morrell oscillator generating undamped waves less than a meter in length, a study was made of the potential difference between the Lecher wires coupled to the oscillator by enclosing these wires in an evacuated glass tube several wave-lengths long. The oscillator itself employed two type −52 tubes connected in push-pull and it set up radiofrequency currents of 2.5 amperes in the Lecher wires and potential differences in excess of several hundred volts between the wires at positions separated by half wave-length intervals. At these voltage loops for certain critical pressures, between the wires a discharge took place which was photographed as well as employed in a direct study of the standing waves in the wires. The gases used in the tube were air, helium, oxygen, mercury vapor and mixtures of these gases with air. The use of this tube made possible a visual study of the changes in potential distribution as various circuit adjustments were made. A series of double maxima was observed as the length of the line was changed by a half wave-length.

INTRODUCTION

IN an investigation of an ultra-high frequency oscillator generating undamped waves less than one meter in length, a pair of parallel conductors enclosed in a partially evacuated glass tube proved of some value. Experiments of this type were conducted in 1892 by Arons[1] who employed a Hertzian spark gap and oscillator to generate damped waves ranging from 1 to 2.5 meters in length. Thus, with considerable power at his disposal, he was able to study the standing waves set up on parallel wires enclosed in a vacuum by means of the discharges taking place between the wires at the voltage loops. More recently, Grimsehl[2] and Herold[3] used discharges in long tubes held adjacent to Seibt coils, which were tuned by their own distributed capacity, to show standing waves in the coils. However, these experimenters also used damped waves and employed comparatively long wave-lengths, as the use of a coil instead of parallel wires reduces the size of the apparatus to laboratory dimensions. The present experiments were conducted with undamped waves generated by a modified Barkhausen-Kurz oscillator and were possible only because considerable power was available. The usefulness of the method arises particularly in that it makes possible a visual study of the potential distribution in the entire tuning system as circuit adjustments are being made.

APPARATUS

The generator of undamped oscillations here employed has been described by Kozanowski[4] and uses two type-52 tubes connected in push-pull to produce oscillations of the Gill-Morrell variety. A diagram of the circuit and the enclosed Lecher wire system is shown in Fig. 1. Electrons leaving the filament of a tube are accelerated in the filament-grid space, since the grid is held at a potential 500 volts above that of the filament.

* Published with permission of the War Department.

[1] Arons, Ann. d. Physik **45**, 553 (1892).

[2] Grimsehl, Phys. Zeits. **8**, 484 (1907).

[3] Herold, Phys. Zeits. **33**, 418 (1932).

[4] Kozanowski, Proc. I. R. E. **20**, 957 (1932).

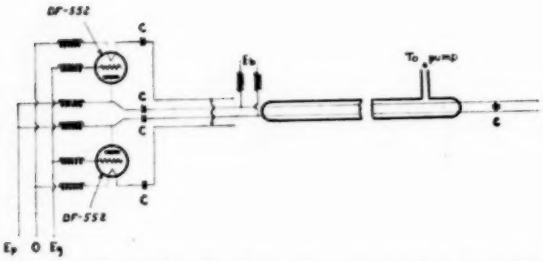

FIG. 1. Circuit for the short wave generator. Length of discharge tube = 180 cm; I.D. of discharge tube = 2 cm; separation of wires = 1.3 cm; diameter of wires = 0.005 in.; Eb = 0–400 volts; $Ep = -80$ volts; $Eg = +500$ volts; $C = 50 \mu\mu f$.

Those escaping capture by the grid are then retarded and finally the direction of travel is reversed in the grid-plate space, since the plate is held 80 volts negative with respect to the filament. Many of the accelerated electrons immediately lose their energy by striking the grid and are thus no longer available for the production of oscillations. The electrons avoiding the grid oscillate in the filament-plate space at a frequency partly determined by the flying time of the electrons and partly by the length of the transmission line coupled to the tubes, until they are finally picked up either by the grid or the plate. With this generator, currents of 2.5 amperes are set up in the line and the potential difference across it at current nodes exceeds several hundreds of volts as is shown by the setting up of an electrodeless discharge in a neon lamp held in the space between the wires. Several watts of radiofrequency power may be expended at any wave-length in the range 65 cm to 85 cm.

The evacuated glass tube is 180 cm long and has an inside diameter of 2.0 cm. The wires are of tungsten 0.005 inches in diameter and are spaced 1.3 cm apart. The characteristic impedance of the line is thus approximately 600 ohms. The line extends from the oscillator tubes through and beyond the glass tube, where a movable bridge is placed across it. In many cases a steady biasing potential difference of 400 volts or less is maintained between the wires to facilitate the discharge. Excitation from a Tesla coil was also found to be useful for this purpose.

RESULTS

The gases used are air, helium, oxygen, mercury vapor and mixtures of these gases with air. However, the most satisfactory discharges are obtained with air or with mercury vapor. When air is used the discharges of interest take place at pressures ranging from 0.5 mm to 0.1 mm of mercury. Fig. 2A shows a photograph of the discharge taking place in air at approximately 0.5 mm. The wire connected to the negative terminal of the biasing battery is encircled by a white sheath several times its own diameter, the sheath is surrounded by a dark space and finally a soft purple glow fills the entire tube. There is no variation in intensity in the glow surrounding the negative wire or in the purple glow along the length of the tube. On the other hand, the positive wire is surrounded by a steady and brilliant discharge, reddish-pink in color, which varies cyclically in size along the length of the wire, attaining maxima at the voltage loops and disappearing at the voltage nodes. As the pressure is decreased the uniform glow throughout the tube gradually dies out, leaving a pink discharge about the positive wire, in-

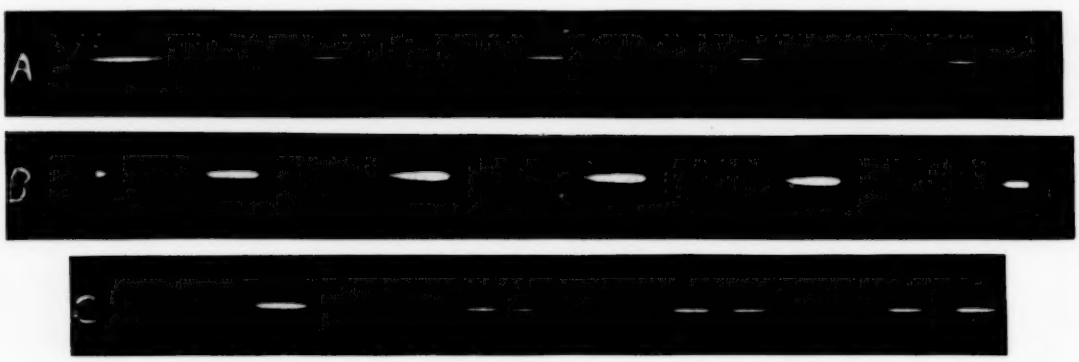

FIG. 2. Photographs of the discharge.

creasing in brilliancy and becoming intermittent in character, rapidly playing back and forth from one loop to another. Fig. 2B shows a photograph of this type of discharge. A further decrease in pressure to 0.1 mm or less is attended by the complete disappearance of the uniform glow while the pink discharge is further enhanced and its intermittent character becomes more marked. Finally, at lower pressures no discharge is obtained. However, the exact pressure at which the various types of discharge take place depends somewhat on the magnitude of the biasing voltage as well as on the amplitude of oscillation. When mercury vapor is used the color of the discharge is blue and the loading effect of the discharge on the line is marked. There is first a brilliant arc-like discharge which loads the line to the extent that oscillations almost die out, thus extinguishing the discharge; then oscillations are resumed at their former amplitude and the cycle is repeated.

The discharge tube was found to be particularly useful in a study of the potential distribution in the transmission line as a whole, as its length was varied a full half wave-length. One particular set of observations was begun when the maxima were sharply defined and uniformly spaced as in Fig. 2B. As the bridge was moved towards the oscillation generator, each maximum advanced toward the driving end with the intervals between them continuing of equal but diminished length, indicating that because of the reaction of the line on the source a slightly higher frequency was being generated. As the bridge was moved still nearer the source, relatively feeble "satellite" discharges appeared which were uniformly spaced but with the intervals separating them longer than those between the main discharges. These "satellite" peaks increased in brilliance and the intensity of the original peaks decreased as the motion of the bridge toward the source continued until the two sets were of equal intensity and, finally, the original peaks died out, with the "satellites" taking their positions but with the entire line a half wave-length shorter than at the beginning of the experiment. Fig. 2C shows the discharge when the "satellites" and main peaks were nearly equal in intensity. This type of discharge is made up of two series of overlapping and uniformly spaced peaks with each series characterized by the common length of the interval between members in it. If the transmission line is made longer, the series with the greater spacing disappears and if the line is made shorter, the other set disappears.

The theory advanced by Tonks,[5] Roder[6] or Hikosaburo[7] to explain double-hump resonance in lines driven at a fixed frequency does not account for the two series of maxima since in the present case the line partly determines frequency. While no attempt is being made at this time to present a complete picture of the actual mechanism of the oscillations giving rise to two sets of voltage loops, the following description of such a mechanism is suggested by the experiments. When the bridge terminating the transmission line is so situated as to place the tubes at a voltage loop of the line, at a frequency determined by the tubes, the reaction of the line on the tubes is a minimum and, obviously, tube voltage and maximum line voltage are equal. However, by moving the bridge, say towards the tubes, the line voltage may be made to exceed the tube voltage and the reaction of the line on the tubes begins to make itself felt. Presently such a position is found, for which the voltage in the line attains a maximum value. Finally, by further shifting in the position of the bridge, the tubes are geometrically situated at a voltage node but the reaction of line on tubes becomes a maximum and tends to modify frequency. The frequency may be either increased slightly or decreased slightly so that for a certain range of bridge positions the tube places itself on either side of the voltage node to feed the line. Both modes of oscillation are unstable and the two modes succeed each other with such rapidity that the discharge tube is continually lighted and thus the two series of maxima are observed.

[5] Tonks, Physics **2**, 1 (1932).
[6] Roder, Proc. I. R. E. **21**, 290 (1933).
[7] Hikosaburo, Proc. I. R. E. **21**, 303 (1933).

Fluctuation Noise Due to Collision Ionization in Electronic Amplifier Tubes

STUART BALLANTINE, *Boonton Research Corporation*

(Received May 24, 1933)

Ions formed by collision in electronic amplifier tubes move toward the cathode and control-grid and produce momentary increases in the space-charge limited current (current pulses). These current pulses are random in time and produce fluctuation noise analogous to the shot-effect. An approximate theory is presented, applicable to cathodes of large diameter (*ca.* 0.1 cm). Both the noise and the increase in the average value of the electron current due to the presence of ionization are calculated in terms of the "size of the elementary event" or the integral of the current pulse. It is not feasible to calculate the latter directly but it may be evaluated indirectly by measurements of the increase of average current. The noise calculated from the values so obtained and from the ionization probability data of Smith, Bleakney and Tate is in close agreement with that observed experimentally. The production of noise in tubes with oxide cathodes containing mercury vapor, argon and the gases naturally evolved from the electrodes and tube walls is investigated experimentally as affected by pressure and electron current density. In the case of a tetrode containing mercury vapor or evolved gases the variation with pressure is linear up to 10^{-3} mm; in the case of argon the noise varies as the 1.1 power of the pressure. In the mercury vapor tetrode a variation as the 3/2 power of the plate current was found, as compared to a 5/3 law, expected theoretically. These measurements were made at 620 kilocycles. The noise per frequency interval was measured as a function of frequency over the range 500–1500 k.c. At pressures of the order of 10^{-4} mm in mercury vapor a decrease at the higher frequencies was observed; with argon the noise was uniform. With mercury vapor at higher pressures (*ca.* 4×10^{-3}) the noise spectrum became peaked, the frequencies of the peaks depending upon the electron current flowing (electrode potentials). The hypothesis that these peaks are due to oscillations of positive ions in the potential trough surrounding the cathode is in accord with the principal experimental facts. With further increase in pressure continuous oscillations are produced, sustained apparently by a regenerative action of the space charge upon the oscillating ions. The frequencies of these oscillations are affected only by the electrode potentials and not at all by the external electrical circuit.

SINCE Schottky in 1918 predicted, on theoretical grounds, the existence of two important fluctuation effects in vacuum tube amplifiers (shot and thermal effects), occasioned by the finite size of the electrical carriers, a number of experimental investigations of the several sources of noise in such tubes have been undertaken. Of these phenomena the simplest and most recondite from a theoretical and experimental viewpoint is the pure *shot-effect* successfully studied by Hull and Williams. In amplifier tubes as employed technologically, the noise production is complicated by a number of so-called "abnormal" effects. The present paper is devoted to one of these effects—the rôle played by gas ionization. That noise is produced by ionization in electron tubes has been known since the invention of the audion itself but no systematic investigation seems to have been reported. The present investigation is restricted to the noise produced in the plate circuit, particularly at radiofrequencies (500–1500 kilocycles).

1. Experimental Technique

It will be convenient to represent the noise generated in the tube by an equivalent temperature-saturated current I_s which, flowing in the tube between plate and cathode, would generate the same amount of noise by pure shot-effect. We shall, therefore, speak of a certain number of milliamperes of noise. This method of representing the noise lends itself to a very simple experimental arrangement as shown in Fig. 1.

In shunt to the plate circuit of the tube under investigation is connected a diode, carrying a temperature-saturated electronic current whose value is adjusted by varying the filament temperature. The conductance of this diode is usually negligible in comparison with the circuit admittances over the range of current employed. This can ordinarily be assured by adjustment of the coupling transformer conductance. The noise produced by this current is due (within one or two percent) to pure shot-effect. Since the frequency is high (10^5-10^6 cycles/sec.) the noise

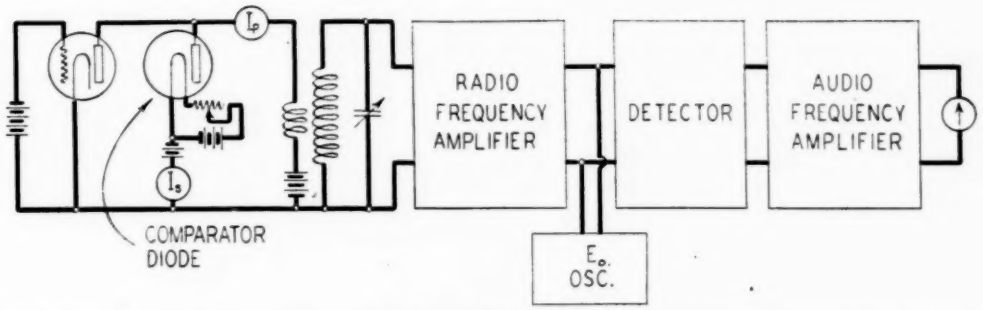

FIG. 1. Arrangement for measurement of noise per frequency interval in terms of temperature-saturated current producing a pure shot-effect.

due to the Johnson-Schottky flicker effect is negligible.

An additional radiofrequency voltage E_0 of the same frequency f_0 as that of the portion of the noise spectrum under investigation is impressed upon the detector. The high frequency noise components beat with this voltage in the square-law detector and are transformed into low frequency components which are amplified and measured by means of a thermocouple milliammeter. If the amplitude of E_0 is large compared with those of the noise components the effects due to beating in the detector between the noise components themselves are negligible. The deflection of the square-law output meter is then proportional to the noise energy. The theory of the transmission of elementary noise pulses through a system of this type has been given in previous papers.[1]

The procedure in making a measurement of noise is as follows: The tube being studied is operated with its input (control-grid) terminals shorted and the amplifier gain adjusted to give a certain deflection of the output meter (due to noise). The current through the comparator diode is then increased from zero until this deflection is exactly doubled. This value of diode current then represents the noise.

In special circumstances, such as in measurements of tetrodes, when the conductance of the tube can be made negligible in comparison with that of the transformer, a simplified procedure may be employed as follows: With the main tube cold the diode current is set at some convenient value, say 1 m.a. and the amplifier gain adjusted for a reading of 1 m.a. on the output meter. The diode current is then reduced to zero and the readings with the main tube operating are then directly in noise current. Any variation in amplifier gain may be compensated by frequent re-setting by means of the diode comparison current.

There will generally be a residual noise reading due to noise generated behind the tube (e.g., thermal noise in the secondary of the transformer). Since the noise deflections are additive the residual noise may be taken care of by a mechanical displacement of the zero of the output meter or by subtraction. In general, it is convenient to reduce the transformer conductance (by reducing the primary turns) until this residual deflection becomes excessive.

The amplitude of carrier voltage E_0 and the operating voltages of the detector are chosen to secure square-law operation to comply with the theory. Upon plotting noise output against the square of the carrier, the carrier amplitude may be selected to be well within the linear range of this curve.

This technique avoids the calibration of the amplifier for gain and selectivity which is necessary in the precise procedure of Hull and Williams.[2] The accuracy is adequate for most purposes. The extra voltage E_0 applied to the detector also increases the sensitivity so that fewer stages of amplification are required with a corresponding gain in experimental convenience.

2. EXPERIMENTAL TUBES

Experimental studies of this type of noise have been carried out by using the four-electrode tube

[1] Stuart Ballantine, J. Frank. Inst. **206**, 159 (1928); Proc. Inst. Radio Engs. **18**, 1377 (1930).

[2] A. W. Hull and N. H. Williams, Phys. Rev. **25**, 154 (1925).

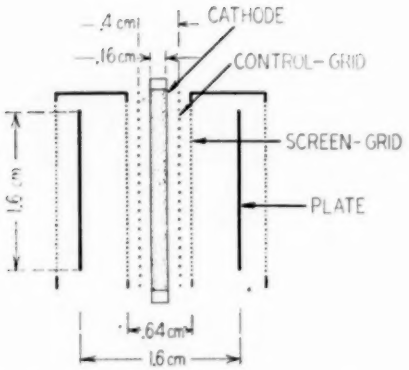

FIG. 2. Section through electrode structure of experimental screen-grid tetrode.

shown in Fig. 2. Mercury vapor was employed from the outset on account of its ionizability, large mass and relatively small effect upon the thermal electron emission from the filament. The tube was prepared in the usual way and thoroughly baked and degassed. Mercury was distilled into the bulb, which was then sealed off. While the mercury was kept condensed in the upper part of the bulb by immersion of this part in CO_2 slush, a magnesium "getter" was flashed and the oxide cathode activated and aged. No residual gases could be detected by the Buckley ionization gauge connection with the tube walls at -78°C. In the experimental work, the mercury vapor pressure was adjusted by varying the temperature of the glass wall of the tube by means of an alcohol bath. The bulb temperature was measured by two copper-constantan couples attached to the wall of the tube. These were calibrated against a pentane thermometer.

In view of the difference in temperature between the wall of the tube and the space in which ionization takes place, a correction for thermal effusion seems necessary. Let T_w represent the temperature of the walls, T that of the electrodes, p_w and p the corresponding pressures. Then:

$$p = p_w(T/T_w)^{\frac{1}{2}}. \tag{1}$$

At low pressures the number of ions formed is proportional to the density, that is to:

$$p/T = p_w/(TT_w)^{\frac{1}{2}}. \tag{2}$$

In view of the small size of the cathode and uncertainty as to the accommodation coefficient between it and mercury ions, T was taken as the temperature of the plate electrode. This was determined by measurements with a tube of identical construction containing a copper-constantan couple welded to the plate. The temperature of the plate was found to vary by an entirely negligible amount over the range of temperatures of the tube wall and to be equal to 152°C. The values employed for the saturated mercury vapor pressure as a function of the bulb temperature were those given in the *International Critical Tables*.[3]

Experiments have also been carried out with argon and with the gases naturally evolved from the glass walls and metal parts in vacuum tubes of this kind. The dimensions of the tubes used in these cases were identical with those of the tube (Fig. 2) containing mercury vapor.

It may be of interest to preface an account of the experimental results with an examination of the theoretical expectations, worked up necessarily in the simplest possible way.

3. Production of Noise by Ions

Owing to their large mass, the motions of ions are comparatively slow; they therefore exert a large effect upon the space-charge-limited electron current. When an ion appears in the space between the electrodes, the average electron current increases and undergoes a variation with time which depends upon the subsequent motion and life of the ion. The resulting change of electron current may be regarded as the "elementary event" in the production of this kind of noise. If the precise form of the current pulse as a function of time were known, an analysis would yield its frequency distribution and enable us to compute the noise so produced. Unfortunately, the effects are so complicated that there is little hope of performing this microscopic calculation. A rough qualitative examination of the possibilities is, however, not without interest.

The principal sources of ions in normal amplifier tubes are: (1) ionization by collision, (2) thermionic emission from the cathode, (3) ionization at the cathode surface of atoms of gas or vapor present in the tube. We shall be concerned here mainly with those of class (1). Ions may be formed when the molecules of the residual gas

[3] Int. Crit. Tab. 3, 206.

collide with electrons having energies (by virtue of their velocities in the electric field) in excess of the ionization or critical potentials of the molecule. Equilibrium is maintained by the disappearance of the ions by (*a*) recombination, (*b*) diffusion from the ends of the electrode structure or through mesh electrodes with subsequent neutralization at the tube walls, (*c*) discharge at the cathode and control-grid electrode.

(*a*) The exact part played by recombination is difficult to estimate because of the scarcity of reliable data.[4] In view, however, of the rather high velocities of the electrons and ions under the action of the electric field it seems safe to assume that the effect of recombination at low pressures is small in comparison with the normal rate of discharge at electrodes and other surfaces.

(*b*) Ions escape by diffusion from the ends of the electrode structure. In the range of pressures in which we are interested the mean-free-path is large compared with physical dimensions so that we may expect the coefficient of diffusion to be constant. A constant fraction of ions will therefore escape which is independent of the pressure.

(*c*) The ions, as soon as they are formed, are urged toward the grid or cathode by the electric field. At low pressures, in tubes having cathodes of relatively large dimensions, a considerable fraction of them move directly toward the cathode and strike it at the first passage, since the radial velocities acquired under the action of the field are very much larger than the tangential component of velocity due to thermal agitation. The average velocity of a singly-charged ion due to thermal agitation may be expressed in equivalent volts as follows:

$$v = 3kT/2\epsilon = 1.3\times 10^{-4}T \text{ volt}, \qquad (3)$$

where T is the temperature in absolute degrees. For most of the parent atoms $T = 300°$, approximately, so that the average velocity of the ion is that which would correspond to motion through a potential difference of 0.04 volt. Whether an ion misses the cathode at the first passage or not depends largely on the cathode diameter. In a diode with a cathode of radius r_1 an electron starting from a point distant r from the cathode, where the potential is V_r will miss the cathode if the component of velocity transverse to the field exceeds[5]

$$v_0(\text{volts}) > (r/r_1)^2 V_r. \qquad (4)$$

In a typical case of a 6 mil filament ($r_1 = 0.003''$) let $r = 0.15''$; $V = 100$ volts; $v_0 = 0.04$ volt at $T = 20°\text{C}$; about 1/12th of the ions would miss the cathode at the first passage. However, for a large cathode ($r_1 = 0.03''$) of the equipotential indirectly heated type as employed in commercial tubes, only ions having initial velocities in excess of 4 volts would miss. In this case a considerable fraction of the ions would flow directly to the cathode in spite of the lower potential of the control grid. Also, because of the small diameter of wire usually employed for the control grid, many of the ions miss it at the first passage and so perform several passages around the wires before finally discharging at cathode or grid. Kingdon found that in such cases the life of the ion was apparently determined by its kinetic-theory life but it varied as $1/p^{\frac{1}{2}}$ (p = pressure) instead of $1/p$, principally because of diffusion from the ends of the structure.[6] The probability of an ion formed by a *one-stage* collision between electrons and molecules becoming trapped in the potential minimum surrounding the cathode is assumed to be negligible.

4. Approximate Theory for Tubes having Cathodes of Large Diameter

As an approximation, let us neglect the irregularities in the interelectrode potential distribution produced by the control-grid. Let the electrode potentials be E_d(screen-grid) = 70 volts, E_p (plate) = 180 volts. The potential distribution between cathode and screen-grid under space-charge conditions may be calculated by the method of Langmuir and Blodgett[7] and is shown in Fig. 3 (dotted curve). The potential between screen-grid and plate may be approximated by correcting the normal logarithmic distribution for space-charge. It will be noticed that, at the electrode voltages selected, the potential distri-

[4] I. Langmuir and K. T. Compton, Rev. Mod. Phys. **2**, 197 (1930); I. Langmuir, Phys. Rev. **31**, 403 (1928).

[5] A. W. Hull, Phys. Rev. **18**, 31 (1921).

[6] K. H. Kingdon, Phys. Rev. **21**, 412 (1923).

[7] I. Langmuir and K. B. Blodgett, Phys. Rev. **24**, 49 (1924).

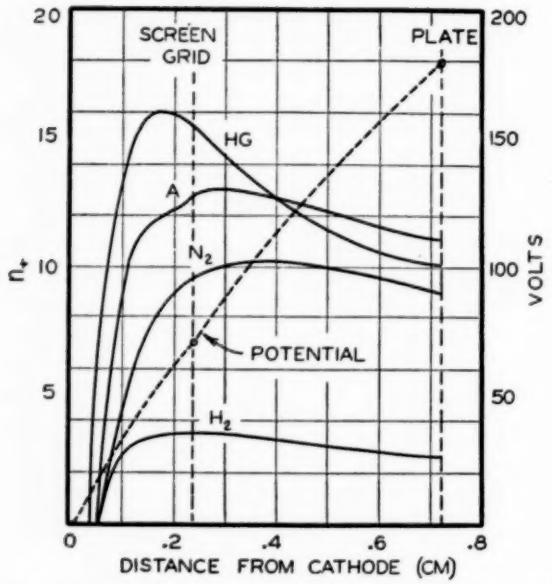

FIG. 3. Dotted curve, approximate potential distribution in tetrode (Fig. 2), screen-grid voltage = 70, plate voltage = 180; solid curves, distribution of ionization for several gases computed from data of Smith, Bleakney and Tate.

bution is very nearly linear, as in the case of plane electrodes.

The ionization probabilities in several gases at fixed pressures have been determined experimentally by Smith,[8] Bleakney[9] and Tate.[10] The *efficiency of ionization*, $P(V)$, as defined by Smith, represents the number of positive ions formed by one electron having a velocity of v volts in a 1 cm path length at 1 mm pressure and temperature of 0°C. The number of ions formed per second in a volume element of length dl in the direction of the electron current will be therefore:

$$dn = I_e P(v) p\ 273\ dl/\epsilon T \qquad (5)$$

where I_e represents the electron current entering the element, ϵ the elementary charge, p the pressure (mm of mercury) and T the absolute temperature.

From these experimental data for $P(v)$ for several gases and the calculated potential distribution (Fig. 3) the number of ions formed per second in an annular element of volume $dv = 2\pi r dr$ may be estimated and is also shown in Fig. 3. It is assumed that the current is uniform across the tube; as a matter of fact the current in the space between cathode and screen-grid plate is usually greater than that between screen-grid and plate by the amount of the screen-grid current and in later calculations it will be necessary to allow for this.

The probabilities for mercury vapor have been reduced 25 percent below the published values.[11]

Most of the ions in a tube of the dimensions shown in Fig. 2 discharge at the cathode. The proportion reaching the grid may be estimated from measurements of the grid current at known pressures and calculation from the data of Fig. 3. At $p = 10^{-4}$ mm, $I_p = 4.6$ m.a., $I_2 = 2.05$ m.a., the observed grid current I_g in the tube (Fig. 2) connected as a tetrode was 7×10^{-7} amp. The ratio of the number of positive ions striking the grid to the total number formed is approximately

$$n_g/n = (I_g/I_e p) \int_0^R P(v) dr. \qquad (6)$$

Allowing for the current of 6.65 m.a. in the space between cathode and screen-grid and 4.6 m.a. between screen-grid and plate, it is found by calculation that only 8 percent of the ions reach the control-grid. Those that do not strike the cathode, but strike the control-grid at the first passage, have a small effect upon the noise. The remainder, circling more than once, seems so small as to be negligible. Presumably, then, 90 percent of the ions flow to the cathode and we may, therefore, with small error consider only the effects of these in the production of noise.

In moving to the cathode (or grid) each ion produces an increase in the average electron current or *current pulse*, whose instantaneous value depends upon the position of the ion at that instant. If the pulses due to individual ions are independent events their effects are additive statistically. Denote the increase of electron current due to a single ion by $i(t)$. The microscopic calculation of the relation between $i(t)$ and the position of the ion under space-charge conditions is difficult, especially in the cylindrical case. The case of plane electrodes is somewhat more recondite.

[8] P. T. Smith, Phys. Rev. **36**, 1293 (1930); **37**, 808 (1931).

[9] Walker Bleakney, Phys. Rev. **35**, 139 (1930); **36**, 1303 (1930).

[10] J. T. Tate and P. T. Smith, Phys. Rev. **39**, 270 (1932).

[11] See H. D. Smyth, Rev. Mod. Phys. **3**, 362 (1931).

Emersleben[12] has calculated the relation between the position of a point charge between plane electrodes and the charge induced on one electrode. In accordance with the Langmuir-Van der Bijl theorem, assume that the electron current is in equilibrium when the total charge induced at the cathode (or virtual cathode) by the electronic space-charge, anode and ion charges is zero. Let the charge induced upon the cathode by the ion be $\sigma(x, d, t)$ then:

$$i' = I_e + i = k[V_p/4\pi d + \sigma(x, d)]^{\frac{1}{2}}, \qquad (7)$$

where x is the distance of the ion from the cathode and d the distance between cathode and anode.

Near the cathode the surface density σ increases as $1/x^2$ at a point directly opposite the ion. The current cannot approach infinity because of temperature saturation. At other points the current remains finite or is limited by saturation. On account of the high values which σ can assume, our assumption of statistical superposition may fail on account of the 3/2 power law when the ion gets near the cathode.

The probable shape of the current pulse in the cylindrical case (mercury vapor), based upon an examination of the plane case, is represented in Fig. 4. The ions may be divided into classes depending upon the annular element in which they are formed. The current pulses for three classes are shown in Fig. 4, corresponding to ions formed at distances 0.1 cm, 0.2 cm, and 0.32 cm from the cathode. The pulses for other kinds of ions may be obtained by dividing the abscissae by the square root of the ratio of the molecular weight of Hg and the other ion.

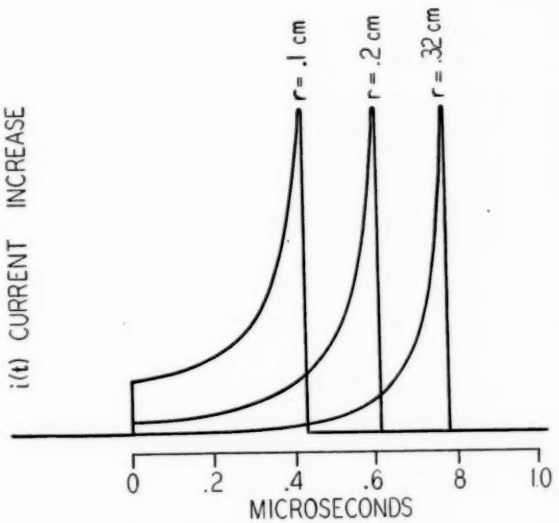

FIG. 4. General forms of current pulses (increase in average electron current) due to ions of mercury vapor formed at various distances from cathode.

[12] O. Emersleben, Ann. d. Physik **82**, 713 (1927).

If the form of the $i(t)$ pulse is known the *noise function* $nI^2(f)$ may be calculated by a method previously described.[1] The noise per frequency interval is:

$$nI^2(f) = n\left\{\left[\int_{-\infty}^{\infty} i(t)\cos 2\pi ft \cdot dt\right]^2 + \left[\int_{-\infty}^{\infty} i(t)\sin 2\pi ft \cdot dt\right]^2\right\}, \qquad (8)$$

where n is the number of pulses of a given class per second. The total noise is otbained by adding up the noise produced by various classes of ions, assuming complete microscopic independence.

At frequencies low compared with the reciprocal of the time of transit of the ion, the noise approaches the value:

$$nI^2(0) = n\left[\int_{-\infty}^{\infty} i(t)\cdot dt\right]^2, \qquad (9)$$

which shall be designated as the *low frequency noise.*

Let x represent the distance between the ion and cathode and r the distance between cathode and the point where the ion is formed. Since the field in the experimental case under consideration is approximately linear the motion of the electron is of a simple type and

$$x = r - \epsilon E t^2/m, \qquad (10)$$

where ϵ is the ionic charge, E the electric force (V/d) and m the mass. Hence

$$t = [2m(r-x)/\epsilon E]^{\frac{1}{2}}. \qquad (11)$$

The total low frequency noise is

$$nI^2(0) = \int_0^R n(r)\left[\int_0^r i(t)dt\right]^2 dr. \qquad (12)$$

Denote the relation between the increment of electron current and the position of the ion by $f(x)$. By means of (11), change the variable of

integration in (12) from dt to dx; then:

$$nI^2(0)=\frac{m}{2\epsilon E}\int_0^R n(r)\left[\int_0^r \frac{f(x)dx}{(r-x)^{\frac{1}{2}}}\right]^2 dr. \quad (13)$$

If the effect of the ion is confined to small x, then the chief contribution to the integral will be obtained while $(r-x)^{\frac{1}{2}}$ is constant so that:

$$nI^2(0)=\frac{m}{2\epsilon E}\left[\int_0^r f(x)dx\right]^2\int_0^R \frac{n(r)dr}{r}. \quad (14)$$

Let i' represent the total electron current as given by an expression of the type of (7)

$$i'=I_e+i=k[V_p/4\pi d+\sigma(x)]^n; \quad (15)$$

then

$$i=f(x)=(\partial i'/\partial\sigma)\sigma(x)=nk^{1/n}I^{(n-1)/n}\sigma(x). \quad (16)$$

Substituting this into (14) and making use of (5)

$$nI^2(0)=\frac{273}{T}\frac{pmI^{(3n-2)/n}J^2}{2E\epsilon^2}\int_0^R \frac{P(v)dr}{r} \quad (17)$$

where

$$J=nk^{1/n}\int_0^r \sigma(x)dx.$$

The noise may be expressed in terms of an equivalent shot-noise current I_s by means of the relation

$$I_s=nI^2(0)/\epsilon.$$

If the conduction follows the 3/2 power law $(n=3/2)$

$$I_s=\frac{273}{T}\frac{pmI^{5/3}J^2}{2\epsilon^3E}\int_0^R \frac{P(v)dr}{r}. \quad (18)$$

The average electron current will be increased by an amount ΔI_e by ionization. According to the above theory,

$$\Delta I_e=\int_0^R n(r)\int_0^r \frac{f(x)}{(r-x)^{\frac{1}{2}}}dx\,dr$$

$$=\frac{273pI_e^{4/3}J}{T}\left(\frac{m}{2\epsilon^3E}\right)^{\frac{1}{2}}\int_0^R \frac{p(v)}{r^{\frac{1}{2}}}dr, \quad (19)$$

assuming uniform current distribution along the cathode and the 3/2 power law. There is, therefore, no simple relation between ΔI_e and the low frequency noise; nevertheless (19) is of interest in that it enables us to estimate J from measurements of ΔI_e. If J is calculated from (19) and substituted in (17) we obtain:

$$I_s=TS_2(\Delta I_e)^2/273pI_eS_1^2, \quad (20)$$

where

$$S_1=\int_0^R P(v)dr/r^{\frac{1}{2}},$$

$$S_2=\int_0^R P(v)dr/r.$$

Here I_s represents the low frequency noise in terms of shot-current.

5. Experimental Results

The results of an experimental test of the relation (18) between noise and plate current are shown in Fig. 5. The ordinates represent the noise measured at the pressures recorded minus the basic noise due to other causes, as measured with the tube immersed in CO_2 slush ($p=10^{-8}$ mm). The noise is expressed in equivalent shot-current. The plate and screen voltages were 180 and 72, respectively, and the plate current was varied by varying the control-grid voltage. Measurements at 1400 k.c. gave lines of the same shape as those shown (620 k.c.). The slope of the

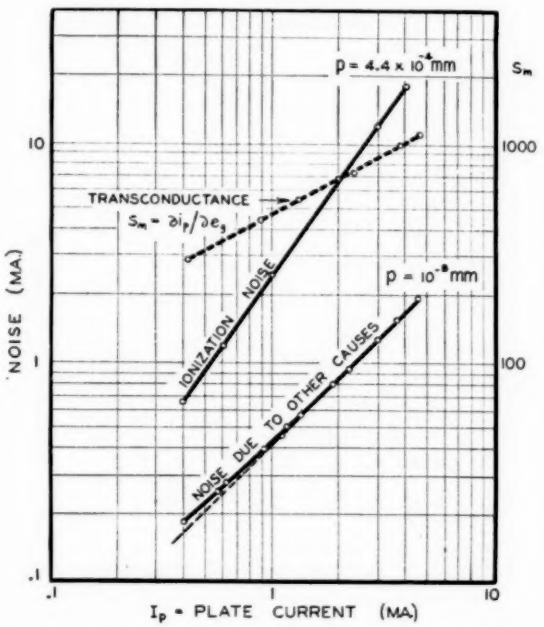

Fig. 5. Noise as a function of plate current, constant pressure; tetrode; mercury vapor.

curve of ionization noise is unaffected by pressure and corresponds to variation as the 3/2 power of plate current I_p. This is somewhat less than that predicted by (18), *viz.* 5/3 (1.66). The variation of the noise due to other causes (shot-effect, secondary emission, etc.) with plate current, in the absence of ionization, is shown by the curve for $p = 10^{-8}$ mm. The relation is, in this case, more nearly linear.

A factor which expresses the performance of a vacuum tube as regards freedom from noise when used as an amplifier is the noise-signal ratio as referred to the input or control-grid terminals. This is I_s/s_m^2, where I_s represents the noise as expressed in equivalent shot-current and s_m is the transconductance $\partial i_p/\partial e_g$. The transconductance of this tube was measured against plate current at $p = 2.64 \times 10^{-4}$ mm (Fig. 5), the plate current as before being controlled by varying the grid bias. It was found that $s_m \sim i_p^{0.54}$ so that the noise factor I_s/s_m^2 decreases as the grid is made more negative. Low electron currents are therefore conducive to quiet operation when appreciable ionization is present.

According to Eq. (16) the noise should be proportional to the molecular concentration (i.e., to p/T). The temperature T in the inter-electrode space is but little affected by the variation of the temperature of the walls of the tube, so that the noise should be proportional to the true pressure in the inter-electrode space. The results of an experiment to test this relation, by using the mercury vapor tetrode, are shown in Fig. 6. The cathode was at its normal operating temperature. The plate voltage was 180 and three combinations of screen and control-grid voltages were used, as marked on the curves. The ordinates represent values of the noise observed (in m.a.) minus the basic noise due to other causes, the basic noise being obtained by measurement with the tube immersed in CO_2 slush. The noise was corrected for the rise in i_p at higher pressures, due to ionization, by means of the $i_p^{\frac{1}{2}}$ law. The measurements were made at a frequency of 620 kilocycles. Corrections of the pressures were made for thermal effusion so that the abscissae in Fig. 6 represent the true pressures in the inter-electrode space.

Thus the expected linear relation between ionization noise and pressure is observed experimentally in the case of mercury vapor up to *ca.* 10^{-3} mm.

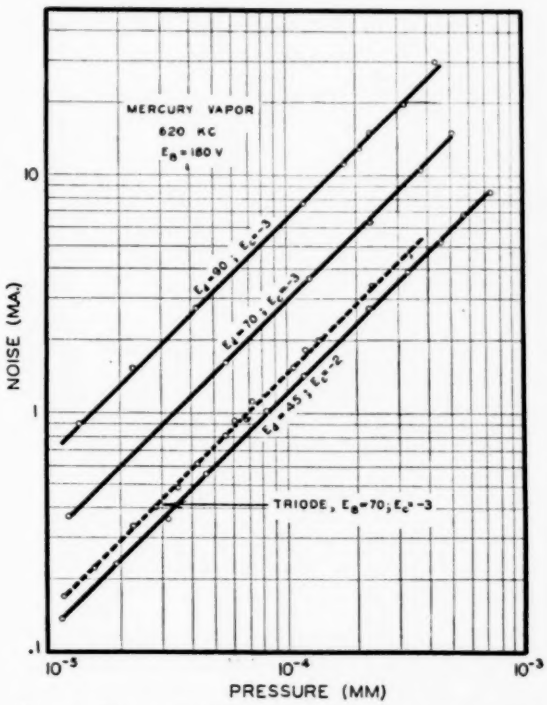

FIG. 6. Noise as a function of pressure, mercury vapor; tetrode connection; plate voltage = 180; dotted curve, triode connection, plate voltage = 70; grid voltage = −3.

Since the noise has been found to vary as $I_p^{\frac{1}{2}}$, the values of noise current divided by $I_p^{\frac{1}{2}}$ have been plotted in Fig. 7. This brings out the fact, of some technological interest, that variations of screen and bias voltages over a wide range have but little effect on the noise aside from their effect upon the plate current.

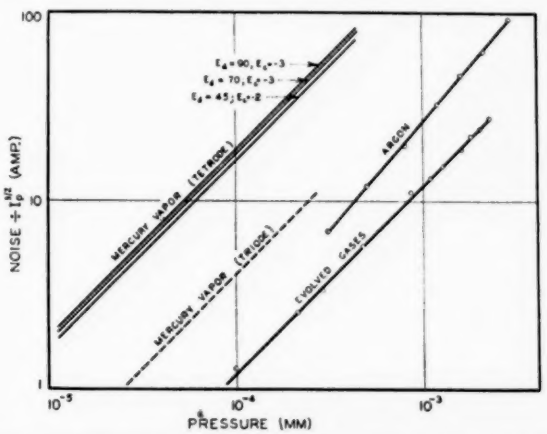

FIG. 7. Summary of results for several gases, tetrode; dotted curve, triode, mercury vapor.

The ionization noise in a tube of similar dimensions containing argon is shown also in Fig. 7. The gas was taken directly from a commercial cylinder (Matheson Company) and dried, but no attempt was made to purify it. In this case, which is typical of several runs, the relation between noise and pressure is not strictly linear over the range employed. Measurements at lower pressures than those shown were not considered reliable because other gases evolved from the system at such a rate as to contaminate the argon during the time required for measurement. The control-grid current varied more nearly linearly with pressure and the noise, as measured against grid current with variable pressure, varied as $i_g^{1.2}$. This test was made in order to check the possibility of errors in the McLeod gauge. No further investigation of the apparent nonlinearity in the case of argon was made.

The ionization noise due to the residual gases likely to be present in vacuum tubes as commercially manufactured is of some technological interest. The results of an experiment on this point are shown also in Fig. 7. A tetrode of the dimensions shown in Fig. 2 was constructed, thoroughly exhausted, baked, degassed and the cathode activated and aged. The pump was then cut off and a series of measurements were made as the pressure increased by the slow evolution of gas from the metal parts and walls of the tube. The pressures were measured by means of a McLeod gauge and corrected for thermal effusion. The partial pressures of condensible gases, if present, were not, therefore, indicated. Fig. 7 represents the results of an average of several runs, all of which gave a linear relation between noise and pressure.

The positive-ion currents to the control-grid were also measured during this experiment and are shown in Fig. 8. These data may be useful to those working with tubes of this type in estimating the pressures in gassy tubes from measurements of grid current. Measurements of the control-grid current in the cases of mercury vapor and argon are also shown in this figure.

According to Eq. (16) the relative noise production in various gases depends upon the quantity:

$$M\int_a^R P(v)dr/r, \qquad (21)$$

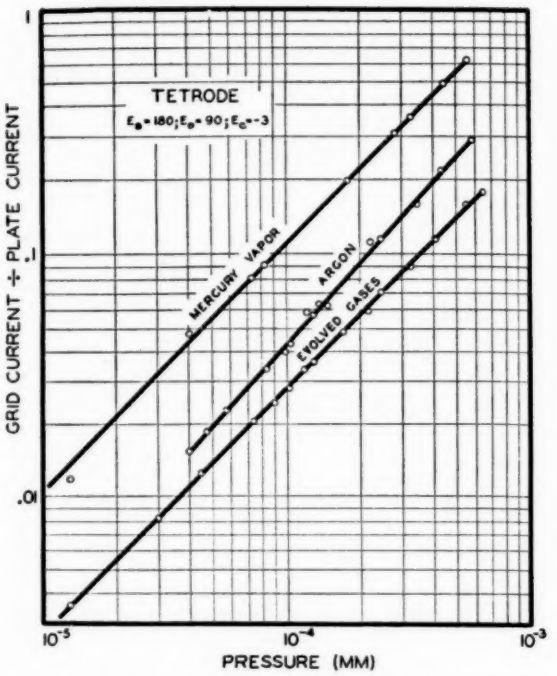

FIG. 8. Relation between pressure and grid current in tetrode (Fig. 2) for several gases; grid current in microamperes, plate current in milliamperes.

where M is the molecular weight and the other symbols have their previously assigned meanings. For the experimental tetrode, with Smith's ionization data for Hg and A, those of Tate and Smith for CO ,O_2 and those of Hogness and Lunn for N_2, the calculated relative amounts of noise to be expected with these gases is as shown in Table I.

TABLE I.

Gas	Noise
Mercury vapor	1.00
Argon	0.12
Oxygen	.08
Carbon monoxide	.075
Nitrogen	.07

A comparison with the experimental values can be made in the case of argon and Hg vapor. Over the range of pressures in which the observations overlap the ratio between the A noise and the Hg noise varies from 0.12 to 0.14 (see Fig. 7) as compared with the calculated value 0.12. For the gases evolved from the tube parts the experimental ratio is about 0.07. This is of the order of the calculated values for N_2, O_2 and CO.

The possibility of checking this theory of noise production by means of measurements of the average increase in electron current, I_e, has been referred to above. The size of the elementary event, J, can be calculated from values of ΔI_e by means of Eq. (19). The noise, expressed in shot-current, is then given by (20) in terms of ΔI_e. For this purpose measurements of ΔI_e were made during the measurements of the noise in the mercury vapor tetrode, with $E_p=180$, $E_d=70$ volts. The integrals S_1 and S_2 were computed for the distribution of ionization shown in Fig. 3. The current to the screen grid was 1.36 m.a. and to the plate 2.81 m.a. The total current between cathode and screen-grid (4.17 m.a.) was therefore 48 percent greater than that between screen-grid and plate so that the values of n in the region between cathode and screen-grid must be increased by this amount over those shown in Fig. 3. In accordance with previous calculations we may allow 10 percent off for ions which do not reach the cathode but which discharge at the control grid. In addition, a reduction in the number of ions in the region between plate and screen-grid will be caused by ions discharging at the screen-grid. This is estimated at 25 percent from the cross-sectional area of the screen grid conductors. The number of multiply-charged ions is small and relatively ineffective, so they may be ignored. Under these conditions the quantities S_1 and S_2, by numerical integration, have the following values:

$$S_1=15.7, \qquad S_2=37.9.$$

Values of noise (in I_s, m.a.) calculated from (20) and observed are given in Table II.

TABLE II. Comparison of observed values of low frequency noise (expressed in equivalent shot-current) and values calculated from increment of plate current, ΔI_p. Mercury vapor tetrode. $E_p=180$ v, $E_d=70$ v, 620 kc, $T=425°$K.

p	I_p	ΔI_p	*Noise* (m.a.)		Calc.
mm	m.a.	m.a.	Calc.	Obs.	Obs.
7.06×10^{-5}	2.85	0.044	2.08	2.2	0.95
10.7	2.88	.067	3.15	3.31	0.95
20.4	2.94	.130	6.08	6.00	1.01
25.9	3.00	.170	8.02	8.1	0.99
38.4	3.06	.250	11.30	12.4	0.91
47.4	3.11	.305	13.7	15.5	0.89

The calculated values are somewhat low but the agreement is excellent and perhaps partly accidental in view of uncertainties as to the true molecular concentration in the inter-electrode spaces and the approximate nature of the theoretical considerations involved. Besides confirming the other points of the theory this agreement may be regarded as substantiating our fundamental assumption that the chief effects of the ions upon the electronic current is confined to the immediate neighborhood of the cathode.

Measurements of ionization noise with the mercury vapor tetrode used as a triode (3-element tube) by connecting plate and screen-grid together are shown in Figs. 6 and 7 (dotted curves). In this case the ions formed in the space between plate and screen-grid are not acted upon by an electric force and reach the cathode only after diffusion through the screen-grid. Calculations of the noise from measured values of I_e gave values 10 percent high, which again is in sufficiently good agreement. The discrepancy, moreover, is in the proper direction to be accounted for by diffusion.

6. Frequency Distribution

The distribution of noise energy per frequency interval, as a function of frequency for the approximate current pulses shown in Fig. 4, can be calculated by means of Eq. (8). The dotted curve in Fig. 9 represents the case of mercury vapor and is chiefly characterized by a gradual decrease in the noise above 10^6 cycles. For other gases the

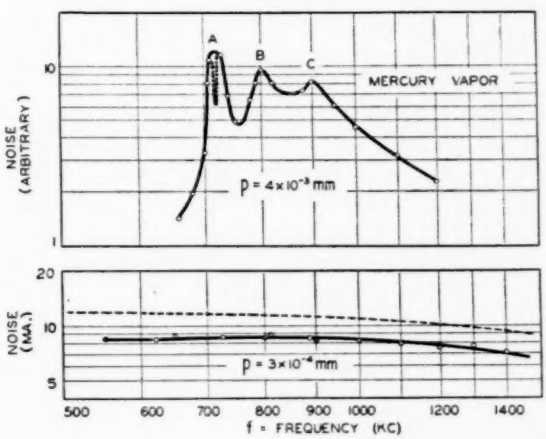

FIG. 9. Lower curve, distribution of noise energy as a function of frequency, medium pressures, tetrode, mercury vapor; upper curve, peaked spectrum obtained at higher pressures, mercury vapor, triode.

curves would be of the same form but displaced along the frequency axis according to the ratio, M_{hg}/M, of the mass of the mercury ion to that of the ion of the gas in question. Thus, for argon, the same decrease in the noise per frequency interval which is obtained in mercury vapor at 10^6 cycles would be obtained at 2.25×10^6 cycles. This is in accordance with the experimental facts. Over the frequency range investigated, 300–1500 kc, the frequency distribution in the case of argon was substantially uniform ($p=10^{-4}$ mm).

The measured frequency distribution with mercury vapor at low pressure ($p=3\times10^{-4}$ mm) is shown by the heavy curve in Fig. 9. This curve is of the same general shape as that expected theoretically (dotted). The decrease in noise with increasing frequency would seem to make possible the employment at very high radiofrequencies (*ca.* 100,000 kc) of tubes containing quantities of gas which would totally unfit them for service at the more usual frequencies.

The results at higher pressures in mercury vapor were rather unexpected. When pressures of the order of 4×10^{-3} mm are reached the spectrum becomes peaked and the noise varies considerably over the region investigated (600–1500 kc). The frequencies of these peaks depend upon the current flowing, electrode voltages, pressure, etc. and not at all upon the constants of the external circuits. These phenomena are of a critical nature and develop rapidly over a small range in pressure, the peaks increasing in amplitude until a pressure is reached at which self-sustained continuous oscillations are obtained.

On account of the sensitivity of the phenomena to pressure, difficulty was experienced in keeping the pressure sufficiently constant over the period required for accurate measurements over the frequency range. A rough survey of the noise spectrum at a pressure of about 4×10^{-3} mm is shown in the upper curve of Fig. 9. In this figure no correction has been made for the variation of amplifier sensitivity with frequency.

In general, more than one peak was present, the number increasing with the electron current. The frequencies of the peaks in the case of a triode connection of the tube are shown in Fig. 10 as a function of the electron current. The screen-grid and plate were connected together and held at 70 volts potential while the electron current

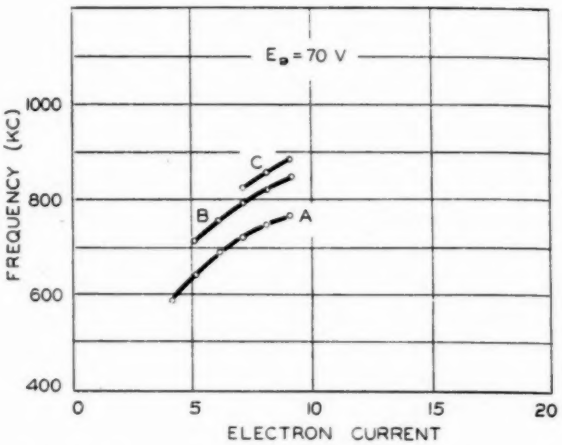

FIG. 10. Relation between frequencies of noise peaks and electron current from cathode, mercury vapor, triode, plate voltage = 70.

was varied by means of the control-grid voltage. The strongest peak was that marked *A*, of lowest frequency. This is accompanied by a peak of double frequency (not shown), which is evidently its second harmonic. Peak *A* got stronger as the current increased. Above 5 m.a. it could be resolved into a double peak whose components were separated about 0.7 percent in frequency. The energy distribution in the double peak is shown in Fig. 11.

In the case of the triode connection, the frequencies of the peaks increased with increase in electron current and plate voltage and decreased with increase in cathode temperature. The mag-

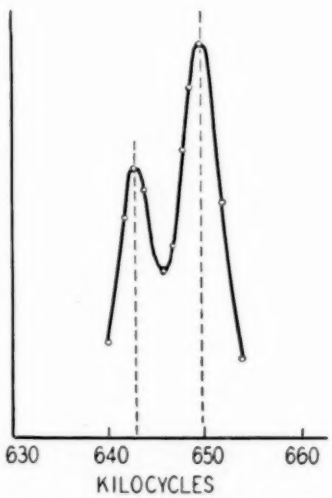

FIG. 11. Structure of double peak *A*.

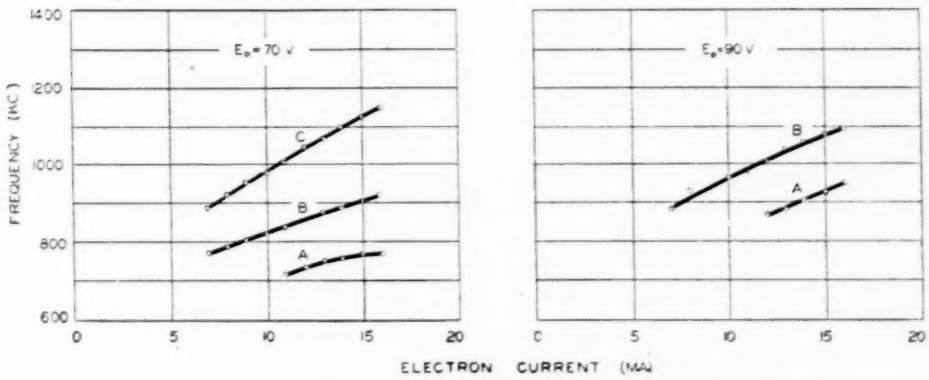

FIG. 12. Frequency of noise peaks as function of electron current from cathode, mercury vapor, tetrode; plate voltage = 180.

nitude of the peaks increased with pressure and decreased with increasing plate voltage.

The peak frequencies with the tube connected as a tetrode are shown in Fig. 12 for two screen-grid voltages, 70 and 90. In this case the frequencies vary in the same manner with the variables listed, as in the case of the triode, except that the frequency decreases slightly with increase in plate-voltage.

Tonks and Langmuir have reported[13] the observation in a mercury vapor discharge of noise peaks in this frequency range and also continuous oscillations at 1380 kc. Their discharge was of the plasma type and the phenomena were ascribed to plasma positive ion oscillations. While there is a certain descriptive resemblance between these observations and those reported here, true plasma discharge conditions did not exist in the present experiments, so that another explanation must be sought.

The appearance of these critical frequencies at the higher pressures may be due to oscillations of positive ions. Several modes of ionic oscillation are possible: (1) In the potential trough surrounding the control-grid wires; (2) in the potential trough surrounding the cathode; (3) paths encircling the cathode.

Paths of type (3) observed by Kingdon[14] in the case of filamentary cathodes of small diameter, are not probable in view of the large size of the cathode employed here.

Oscillations around the grid wires (diameter = 0.012" cm) are probable but in this part of the tube the ions may be expected to have a relatively small effect upon the electron current. Moreover, calculations of the critical frequencies to be expected in this type of oscillation, employing potential distribution data obtained from probe measurements on a three-dimensional model, yield frequencies considerably higher than the range of the present measurements. These considerations, together with the previous calculation that only about 10 percent of the ions would be expected to participate in such oscillations, seem to discourage this explanation.

The most promising explanation appears to reside in the possibility of the temporary imprisonment of positive ions in the potential trough surrounding the cathode. Oscillations of this type have been observed by Charleton and Kingdon in the case of caesium ions formed by contact ionization at a hot cathode surface. Evidence of ionic imprisonment, but without oscillation, has also been obtained by Donal[15] in studies of the effect of atoms of tungstous and tungstic oxide upon fluctuation noise.

The success of this explanation depends upon finding a satisfactory source of ions in the trough which, in order to conform to the experimental absence of peaks at low pressures, must increase with pressure at a rate greater than the first power. Only those ions are trapped which enter the trough ($V = 0$) with zero radial velocity. This virtually requires that the ions be formed in the

[13] Lewi Tonks and Irving Langmuir, Phys. Rev. **33**, 195 (1929).

[14] K. H. Kingdon, Phys. Rev. **33**, 1011 (1929).

[15] J. S. Donal, Phys. Rev. **36**, 1172 (1930).

trough. The number of ions formed from unexcited atoms in the trough by simple electron impact is negligible since the number of electrons of Maxwellian emission velocities in excess of the ultimate ionizing voltage is of the order of 10^{-40}. There are, however, a number of possible cumulative ionization processes yielding ionic densities which vary as a higher order of pressure than the first. Of such processes involving excited atoms, those involving metastable states appear most probable on account of the known longevity of this state. Ionizing encounters between metastable atoms and neutral atoms, metastable atoms or positive ions are possible. Unfortunately, experimental data concerning these processes is so meager as to preclude an accurate quantitative assessment of their probabilities. In all cases the ionization would vary as p^2 or a higher power of p and in the last two cases, as the square of the electron current. Measurements by Messenger[16] indicate that metastable atoms of Hg increase with voltage in approximately the same way as do the positive ions.

The formation of ions at the cathode surface also offers interesting possibilities. While it is true that such a process will yield an ionic density varying only as the first power of pressure, yet a higher order increase in this effect may be accounted for by regeneration. As a matter of fact the ultimate appearance of self-sustained oscillations at sufficiently high pressures favors a regenerative explanation. If enough positives are trapped, the electric field is affected by their motion, they are urged into step and the random vibration gives way to a synchronized motion capable of sustaining itself.

Attempts to calculate the natural frequencies of oscillation of ions in the potential trough by the method employed by Kingdon and Charleton give values which are too high. This method rests upon Langmuir's calculations of the potential distribution for purely electronic conduction with Maxwellian emission velocities. In the present case, at the pressures involved, the density of positive space charge due to the ionization is significant in comparison with the electronic space charge and affects the shape of the potential trough. The difficult mathematical problem presented is fundamental for the theory of gas discharges and has not yet been elucidated. In a general way it can be shown, by means of approximations, that for a given depth of the trough (i.e., for a given electron current density) the total trough width is increased by the presence of the positive ionic charge. The frequencies will therefore be lower than those which would be found for trapped ions at lower pressures. This is in accordance with the experimental facts. The broadening of the trough will obviously increase with increased ionization.

No satisfactory explanation has been found for the multiplicity of peaks. It was at first thought that the peaks having frequencies higher than the mercury vapor peak A might be due to the presence of lighter ions. In particular, ions of barium, barium oxide, strontium and strontium oxide may be present due to evaporation and sputtering from the cathode. The characteristic frequencies of Ba and BaO are in the ratios of 1.22 and 1.16 to that of mercury vapor. The ratio of B peaks to the A peaks in Fig. 12 is 1.16; in Fig. 10; $B/A = 1.1$ and $C/A = 1.16$. The expected ratios do not always appear consistently. In the tetrode at 45 volts screen-grid voltage and high current densities, as many as seven peaks have been observed.

The doubling of the peak of lowest frequency may be due to the isotopic character of mercury. According to Aston[17] the known isotopes of mercury in the order of abundance are of atomic weights: 202, 200, 199, 198, 201, 204. Of these 202 and 200 are outstanding. If the peaks are due to these two isotopes, their frequencies should differ by about $\frac{1}{2}$ percent. The average separation observed experimentally is about 0.7 percent. The higher frequency component is observed to be invariably of greater strength than that of lower frequency, which is rather singular in view of the reported greater abundance of the 202 isotope.

[16] H. A. Messenger, Phys. Rev. **28**, 962 (1926).

[17] F. W. Aston, Phil. Mag. **49**, 1199 (1925); Nature **116**, 208 (1925).

The Interpretation of the Resistivity Prospecting Method for Horizontal Structures

L. B. SLICHTER, *Massachusetts Institute of Technology*

(Received May 29, 1933)

The direct problem of deducing from electrical potentials observed at the surface of a horizontally uniform earth the unknown variation of the conductivity with depth reduces to a boundary value problem of unusual type. Its solution for the isotropic case is developed in Part I, following. In Part II the more usual inverse problem is solved for some special classes of conductivity functions and graphical examples are given as an aid in guiding the interpretation work. In Part III, the anisotropic case is discussed.

PART I. AN UNUSUAL BOUNDARY VALUE PROBLEM AND ITS SOLUTION—ISOTROPIC CASE[1]

1.0. Statement of the problem

In almost all the problems of potential theory, the physical constants of material which enter are considered to be known functions of position; the solution of the problem is the potential function which satisfies the partial differential equation involved and the prescribed boundary conditions. The present problem is unusual in that the function to be solved is the one which expresses the unknown variation of the constant of material with position, whereas the potential function itself is considered to be known on the boundary. The problem is one which arises in the investigation of shallow geological structures by the resistivity method, as well as in the study of the electrical resistivity of the earth's crust at great depths.[2] The question of the proper interpretation of the field data obtained in this process has long been a fundamental theoretical difficulty. A common application of the resistivity method, which is the particular subject of this paper, may be described as follows. A small electrode is supposed to supply direct current to the earth at its surface.[3] The ground is assumed to be a horizontally uniform, infinite, half-space. Thus the conductivity will depend on the depth alone; electrical anisotropy, if present, is also restricted to vary only with depth and in any horizontal plane the conductivity is supposed to be independent of direction. Under these restrictions, symmetry will exist about a vertical axis through the electrode. Thus the assumptions, besides being useful analytically, will be capable of easy experimental test. The electrical potentials resulting at the surface are observable and are assumed to be known within a large area centering about the electrode. From these potentials we desire to deduce the unknown value of the conductivity as a function of the depth. This problem, in the form stated above in which it really arises, appears to have received little or no attention in the literature. Instead, the simpler *inverse* problem is studied,[4] that is to say, the unknown conductivity function is assumed to be known and the problem is then solved for the potential field at the surface. These potentials are compared with the observed values and unless the original choice of the conductivity function was felicitous, the assumption is revised until a satisfactory fit is obtained. The inter-

[1] The writer takes pleasure in acknowledging his indebtedness to Professor R. E. Langer, of the University of Wisconsin, who kindly investigated the unusual boundary value problem proposed in § 1.3 of this section and who furnished the solution there outlined. His complete mathematical discussion of this problem is to appear in the Bulletin of the American Mathematical Society.

[2] C. M. Schlumberger, *Electrical Studies of the Earth's Crust at Great Depth*, Trans. A. I. M. E. "Geophysical Prospecting" (1932).

[3] For simplicity, the second electrode is considered to be removed at an effectively infinite distance. But regardless of its position, its effect may be at once included after solving the single electrode problem, because of the restriction as to horizontal uniformity.

[4] For a thorough treatment of the potential problem for a layered earth, with references to the chief theoretical papers on the subject, see Morris Muskat, Physics **4**, 129 (1933).

pretation process is thus one of cut and try. Furthermore, the postulated structures have been quite restricted in geological type, consisting of a number of discrete layers, usually not more than three, each of uniform conductivity. By varying the thickness and conductivities assigned to the layers, it is usually possible to fit tolerably well the observed potential distribution and the structure so obtained is used as an approximation to the reality. It is, perhaps, surprising that this rather crude process of interpretation has met with as much practical success as has been the case.

In Part I of the present paper the direct problem is solved for the unknown conductivity function. In Part II, some illustrative results and graphical examples are computed for special classes of conductivity functions. In Part III, the anisotropic case is considered.

1.1. Solution of the general problem

The condition of zero divergence for the current, in the case of an anisotropic conductivity, is

$$\text{div}\,(i\sigma_x\partial\varphi/\partial x+j\sigma_y\partial\varphi/\partial y+k\sigma_z\partial\varphi/\partial z)=0,$$

where the coordinate axes are oriented in the directions of the principal conductivities, σ_x, σ_y, σ_z; and φ is the electrical potential. If $\sigma_x=\sigma_y$ and the conductivities depend only on z then

$$\sigma_x\nabla^2\varphi+(\sigma_z-\sigma_x)\frac{\partial^2\varphi}{\partial z^2}+\frac{\partial\sigma_z}{\partial z}\frac{\partial\varphi}{\partial z}=0 \qquad (1.1)$$

or, in cylindrical coordinates ρ, z with origin at the electrode,

$$\sigma_\rho\left(\frac{\partial^2\varphi}{\sigma\rho^2}+\frac{1}{\rho}\frac{\partial\varphi}{\partial\rho}\right)+\sigma_z\frac{\partial^2\varphi}{\partial z^2}+\frac{\partial\sigma_z}{\partial z}\frac{\partial\varphi}{\partial z}=0, \quad (1.2)$$

where σ_ρ has been written for σ_x. This equation is separable and yields, if $\varphi(\rho, z)=R(\rho)Z(z)$, a Bessels' equation:

$$d^2R/d\rho^2+(1/\rho)(dR/d\rho)+\lambda^2R=0 \qquad (1.3)$$

in R; and in Z, the Sturmian equation:

$$(d/dz)(\sigma_z dZ/dz)=\lambda^2\sigma_\rho Z$$

or

$$\frac{d^2Z}{dz^2}+\frac{\sigma_z'}{\sigma_z}\frac{dZ}{dz}-\lambda^2\frac{\sigma_\rho}{\sigma_z}Z=0. \qquad (1.4)$$

Here λ is a parameter independent of ρ or z.

The boundary conditions to be satisfied by φ are the following: (1) φ is everywhere finite and vanishes at infinity; (2) $d\varphi/dz=0$ at the surface $z=0$, except at the electrode. At the surface of the electrode, assumed for convenience to be a small disk of radius a, we shall require the current distribution to be the same as for a disk at constant potential supplying current to a uniform half space. This is equivalent to the assumption that the change in conductivity is small in a distance comparable to the diameter of the disk.

Since the potential remains finite at $\rho=0$, the appropriate solving function for Eq. (1.3) is $J_0(\lambda\rho)$. Since σ_z is always positive, the solutions of Eq. (1.4) will be non-oscillatory; one of the solutions vanishes at infinity, whereas the other becomes infinite. Let the solution which vanishes at infinity be denoted by $Z_1(z, \lambda)$, the other by $Z_2(z, \lambda)$.

Then the required solution for the potential which satisfies the prescribed boundary conditions may be written in the form:

$$\varphi(\rho, z)=\frac{-C}{2\pi\sigma_z(0)}\int_0^\infty\frac{\sin\lambda a}{\lambda a}J_0(\lambda\rho)\frac{\lambda Z_1(z,\lambda)}{\dot{Z}_1(0,\lambda)}d\lambda. \quad (1.5)$$

Here C is the total current, and $\dot{Z}_1(z, \lambda)$ denotes the derivative of Z_1 with respect to z. If in Eq. (1.4) σ_z' is zero and $\sigma_\rho=\sigma_z$ it is easily verified that Eq. (1.5) reduces to Weber's[5] well-known solution for the corresponding problem of a *uniform*, isotropic half-space.

1.2. The relation between the surface potentials and the function $k(\lambda)$

At the surface, if $A\equiv C/2\pi\sigma_z(0)$ the potential[6] is:

$$\varphi(\rho, 0)=A\int_0^\infty\frac{\sin\lambda a}{\lambda a}J_0(\lambda\rho)\left\{-\lambda\frac{Z_1(0,\lambda)}{\dot{Z}_1(0,\lambda)}\right\}d\lambda. \qquad (1.6)$$

[5] H. Weber, Crelle **75**, 75 (1872).

[6] It is shown by Langer that when $\sigma(z)$ is bounded from zero, $\sigma(z)\geqq c>0$, then $-\lambda Z(0,\lambda)/\dot{Z}(0,\lambda)\equiv k(\lambda)$ is bounded. It follows that the integral in Eq. (1.6) is convergent and the formula valid.

It will appear shortly that the function, $-\lambda Z_1(0, \lambda)/\dot{Z}_1(0, \lambda)$, which appears in this integral, has especial significance in the theory of the interpretation of the present problem and it will therefore be designated by $k(\lambda)$, and referred to as the "kernel." Eq. (1.6) may be solved for $k(\lambda)$ by the use of Hankel's Fourier-Bessel inversion formula

$$F(\mu) = \int_0^\infty J_0(\mu\rho)\rho d\rho \int_0^\infty F(\lambda) J_0(\lambda\rho)\lambda d\lambda.$$

This formula is valid[7] when (a) $\int_0^\infty F(\lambda)\lambda^{\frac{1}{2}} d\lambda$ exists and is absolutely convergent. If

$$F(\lambda) \equiv A \frac{\sin \lambda a}{\lambda a} \frac{k(\lambda)}{\lambda}$$

the condition (a) is satisfied and the inversion formula yields

$$A \frac{\sin \lambda a}{\lambda a} \frac{k(\lambda)}{\lambda} = \int_0^\infty \varphi(\rho, 0) J_0(\lambda\rho)\rho d\rho. \tag{1.7}$$

Experimentally, knowledge of $\varphi(\rho, 0)$ is restricted to some finite interval $(0, l)$. Hence the actual data will define a function $k(\lambda, l)$ through the formula

$$A \frac{\sin \lambda a}{\lambda a} \frac{k(\lambda, l)}{\lambda} = \int_0^l \varphi(\rho, 0) J_0(\lambda\rho)\rho d\rho. \tag{1.7a}$$

When $\lambda > 0$, the integral on the right possesses a limit as l becomes infinite whenever φ behaves as ρ^{-n}, where $\frac{1}{2} < n < 2$.[8] In the physical problem under consideration φ will certainly satisfy[9] this restriction, so that the convergence of the integral in (1.7a) and (1.7) is assured. The derivative $dk(\lambda, l)/dl$, is proportional to $J_0(\lambda l)\varphi(l, 0)l$; since $\varphi(l, 0)$ is of order l^{-1}, $k(\lambda, l)$ will become independent of l when λl is large. Hence the function $k(\lambda, l)$ approaches the kernel $k(\lambda)$ when λl is large. (The degree of accuracy of the approximation here involved is fortunately readily estimated in the mechanical method[10] here used for evaluating integrals of this type. The integral curves are drawn mechanically and their asymptotic behavior clearly exhibited.)

Thus the experimental data furnish knowledge of the function $k(\lambda)$ as the limit approached by $k(\lambda, l)$ for large λl. This is *all* the information that the surface potentials are capable of yielding, as is clear from the fact that Eqs. (1.6) and (1.7) are precisely equivalent. It may therefore be concluded that the observational data restrict the unknown conductivity function only by the condition that it be consistent with the known function $k(\lambda, l)$ and the differential Eq. (1.4).

1.3. Determination of $\sigma(z)$ from the function $k(\lambda)$ (isotropic case)

The key problem of solving the differential Eq. (1.4) when $\sigma(z)$ is unknown, and when the boundary condition, $k(\lambda) = -\lambda Z_1(0, \lambda)/\dot{Z}(0, \lambda)$, is given, has recently been accomplished by Langer.[11] His neat method for the determination of $\sigma(z)$ is briefly as follows: If the substitution $Z_1(z, \lambda)/\dot{Z}_1(z, \lambda) = -v_1(z, \lambda)$ is introduced into Eq. (1.4) this equation may be written:

---

[7] G. N. Watson, *Theory of Bessel's Functions*, paragraph 14.4, Cambridge Press (1922).

[8] See Gray, Mathews, McRoberts, *Treatise on Bessel Functions*, p. 65 (1931).

[9] Ultimately φ may be assumed to vanish as ρ^{-1} without appreciable influence upon the practical interpretation problem. This problem obviously involves a limitation on the depth to which the conductivity function may be explored, a limit set by the fact that experimental knowledge of the surface potentials is restricted to some *finite* interval. At depths of an order of magnitude greater than the limit to which the interpretations apply, a constant conductivity, σ_2, may be postulated without effect on the interpretable problem. In this case the surface potentials will ultimately vanish as $(c/2\pi\sigma_2)\rho^{-1}$.

[10] V. Bush, J. Frank. Inst. **212**, 447 (1931).

[11] R. E. Langer, to appear in the Bulletin of the American Mathematical Society.

$$\sigma'/\sigma = \frac{\dot{v}_1(z,\lambda)+1}{v_1(z,\lambda)} - \lambda^2 v_1(z,\lambda). \tag{1.8}$$

For large values of λ, the solutions of Eq. (1.4) approach $\sigma^{-\frac{1}{2}}(z)e^{\mp\lambda z}$, therefore $v_1(z,\lambda)$ approaches $1/\lambda$ as λ becomes infinite. Therefore $v_1(z,\lambda)$ may be expanded in the form:

$$v_1(z,\lambda) = \frac{1}{\lambda}\left(1+\frac{\alpha_1(z)}{\lambda}+\frac{\alpha_2(z)}{\lambda^2}+\cdots\right), \tag{1.9}$$

where $\alpha_i(z)$ are unknown functions of z. For large λ, the known function, $k(\lambda)=\lambda v(0,\lambda)$, therefore has the expansion

$$k(\lambda) = 1+a_1/\lambda+a_2/\lambda^2+\cdots, \tag{1.10}$$

where

$$\alpha_i(z)\to a_i \quad \text{as} \quad z\to 0. \tag{1.11}$$

When λ is sufficiently large, the series (1.9) is absolutely convergent. Its substitution in (1.8) yields the rearranged series

$$\sigma'/\sigma = -2\alpha_1(z)+\frac{\alpha_1'+\alpha_1^2-2\alpha_2}{\lambda}-\frac{\alpha_1^3-2\alpha_1\alpha_2+2\alpha_3+\alpha_1\alpha_1'-\alpha_2'}{\lambda^2}+\cdots, \tag{1.12}$$

but this function is necessarily independent of λ, so that all the terms in the expansion must vanish except the first, $\alpha_1(z)$. Hence it follows that:

$$\begin{aligned}
\alpha_1'(z) &= -\alpha_1^2(z)+2\alpha_2(z),\\
\alpha_1''(z)/2! &= \alpha_1^3(z)-2\alpha_1(z)\alpha_2(z)+2\alpha_3(z),\\
\alpha_1'''(z)/3! &= \tfrac{1}{3}(8\alpha_1^2\alpha_2-3\alpha_1^4-4\alpha_1\alpha_3-2\alpha_2^2+4\alpha_4),\\
&\cdots\cdots\cdots\cdots\cdots\cdots
\end{aligned} \tag{1.13}$$

By Eqs. (1.10) and (1.11) these are all known at $z=0$; they are the coefficients in the Taylor's series for $\alpha_1(z)$. It therefore follows from Eq. (1.12) that the desired solution for the conductivity is

$$\sigma(z) = \sigma_0 \exp\left[-2\int_0^z \alpha_1(z)dz\right]. \tag{1.14}$$

This formula, then, is the unique solution for the isotropic conductivity function. It is concluded that *knowledge of the surface potentials alone suffices to determine uniquely the variation of the conductivity with depth.*

Part II. Some Special Solutions Useful in Guiding the Interpretations, with Graphical Examples

It was seen in Part I that a unique solution exists for the interpretation problem and a method of determining the conductivity function as an infinite power series in z was outlined. However, for some types of functions, $k(\lambda)$, it may be inconvenient to evaluate enough coefficients in the expansion of $\sigma(z)$ for its satisfactory representation. It will sometimes be more expedient to identify directly the given function $k(\lambda)$ with known type forms for $\sigma(z)$. When the fit, however obtained, is within the experimental error in the determination of $k(\lambda)$, the interpretation problem may, of course, be considered satisfactorily solved. The present section is devoted to a somewhat detailed examination of special cases of the "inverse" problem, for the purpose of exhibiting a variety of functions $\sigma(z)$ and their associated kernels $k(\lambda)$ which may be of value in guiding the practical interpretation work.

2.1. Solutions involving the Bessel functions $K_\nu(\lambda z)$

If Eq. (1.4) is written in the normal form by the substitution $z=\sigma^{-\frac{1}{2}}(z)u(z)$, then $u(\lambda z)$ satisfies

$$u_{zz}(\lambda z)-(1+(2\dot{p}+p^2)/4\lambda^2)u(\lambda z)=0, \quad (2.1)$$

where $p\equiv\sigma'(z)/\sigma(z)$. The corresponding transformation of the Bessel's equation for $I_\nu(x)$, yields, if $I_\nu(x)=x^{-\frac{1}{2}}U(\lambda x)$, the similar equation in U

$$U_{xx}(x)-(1+(4\nu^2-1)/4x^2)\,U(x)=0.$$

Hence, provided

$$2\dot{p}+p^2=(4\nu^2-1)/z^2, \quad (2.2)$$

the solutions of Eq. (1.4) are

$$Z(z,\lambda)=\sigma^{-\frac{1}{2}}(z)(\lambda z)^{\frac{1}{2}}I_{\pm\nu}(\lambda z).$$

The particular solution in interest which vanishes at infinity may be written, if $K_\nu(x)$ has its usual meaning,[12]

$$Z_1(z,\lambda)=\sigma^{-\frac{1}{2}}(z)(\lambda z)^{\frac{1}{2}}K_\nu(\lambda z). \quad (2.3)$$

After introducing the substitution $p(z)\equiv q(z)/z$, Eq. (2.2) yields for p,

$$p=1/z+\frac{2\nu}{z}\left(\frac{Az^{2\nu}-1}{Az^{2\nu}+1}\right),$$

where A is an arbitrary constant. Hence, upon integrating, the conductivity σ is found to be

$$\sigma=Bz^{1-2\nu}(1+Az^{2\nu})^2, \quad (2.4)$$

where B is necessarily positive. The factor B may be disregarded, however, since the conductivity enters only as the ratio σ'/σ.

2.2. Character of the above family of conductivity functions

If, in Eq. (2.4), a linear change in the z scale is introduced by the substitution

$$\xi\equiv|A^{1/2\nu}|z, \qquad A\neq 0,$$

it appears that the conductivity function is essentially symmetrical in ν

$$\sigma=\xi(\xi^{-\nu}\pm\xi^{\nu})^2 \quad \begin{matrix}+\text{for } A>0\\ -\text{for } A<0.\end{matrix} \quad (2.4a)$$

Clearly σ is either infinite or zero at the origin (unless $\nu=\frac{1}{2}$) but such values will be avoided by introducing the translation $z=z+c$. If c is negative, an infinity or zero in the conductivity will then occur at depth $z=|c|$ and it will be necessary to introduce appropriate boundary conditions at this depth in forming the solution. To avoid this necessity, therefore, only positive values of c will be contemplated at present, to insure a positive argument for σ.

Unless $A=0$, $\sigma(z)$ is infinite at the origin when $|\nu|>\frac{1}{2}$ and zero for $|\nu|<\frac{1}{2}$; at infinity it is infinite for all ν; $\sigma(z)$ possesses at most a single extremum, which occurs at

$$Z=(A(2\nu+1)/(2\nu-1))^{-1/2\nu}.$$

When A is *positive*, it is a minimum or maximum according as $|\nu|\gtrless\frac{1}{2}$, but the maximum for $|\nu|<\frac{1}{2}$ is barred by the restriction that z be positive real. For $|\nu|\leq\frac{1}{2}$ and A positive, the conductivity increases steadily for all positive z. If A is *negative*, $\sigma(z)$ also approaches infinity or zero at the origin, according as $|\nu|$ is greater or less than $\frac{1}{2}$. In the former case, $\sigma(z)$ decreases steadily to zero at $z=|A|^{-1/2\nu}$, in the latter it attains a maximum at

$$z=(|A|(1+2\nu)/(1-2\nu))^{-1/2\nu}$$

before decreasing (as before) to zero at $z=|A|^{-1/2\nu}$. In either case, however, the additional boundary condition involved in the vanishing of the conductivity must be taken into account in the solution. This necessity will be avoided for the present by restricting A to be *positive* or zero.

When $\nu=0$, the conductivity function is linear and, as will appear, the kernel has the simple form $K_0(\lambda c)/K_1(\lambda c)$.

Kernels associated with the above conductivity functions. Substitution of Eq. (2.4) in Eq. (2.3) yields

$$Z_1(z,\lambda)=f(\lambda)\,\frac{[\lambda(z+c)]^\nu K_\nu[\lambda(z+c)]}{A(z+c)^{2\nu}+1}.$$

Whence it results that

$$1/k_\nu(\lambda)=\frac{K_{\nu-1}(\lambda c)}{K^\nu(\lambda c)}+\frac{2\nu}{\lambda c}f(\nu,A,c), \quad (2.5)$$

where the function $f(\nu,A,c)\equiv Ac^{2\nu}/(1+Ac^{2\nu})$. Under the restrictions introduced above that A

[12] G. N. Watson's definitions of Bessel's functions are adopted throughout this paper, see reference 7.

and c be positive, the factor f will have a value between zero and unity.

The kernels will, of course, exhibit a symmetry in ν corresponding to that noted for the conductivity functions. Thus, if the scale factor represented by $|A_\nu^{1/2\nu}|$ is unchanged when $-\nu$ replaces ν (i.e., if $A_\nu A_{-\nu}=1$), then $k_{-\nu}=k_\nu$. This may easily be confirmed from Eq. (2.5) on noting that

$$K_{\nu+1}(\lambda c)-K_{\nu-1}(\lambda c)=(2\nu/\lambda c)K_\nu(\lambda c).$$

When A is zero, the relation between $k(\lambda)$ and $\sigma(z)$ exhibits a rather surprising feature. For if we consider the reciprocal conductivity function $\sigma_2=(z+c)^{1-2\nu_2}$, where $1-2\nu_2=-(1-2\nu_1)$ the corresponding kernel $k_2(\lambda)$ is, (since $K_{-\nu}(\lambda)=K_\nu(\lambda)$)

$$k_2(\lambda)=\frac{K_{\nu_2-1}(\lambda c)}{K_{\nu_2}(\lambda c)}=\frac{K_{\nu_1}(\lambda c)}{K_{\nu_1-1}(\lambda c)}=\frac{1}{k_1(\lambda)}. \quad (2.6)$$

That is, when the conductivity functions are *any power functions*, reciprocal *conductivity functions* correspond, respectively, to *reciprocal kernels*.[13] Because of this simple relation, the case $A=0$ may also be considered adequately covered by consideration of positive ν only.

If ν is half an odd small integer, $\nu=(2n+1)/2$, the series for $K_\nu(\lambda)$ contains only a few terms; thus when $\sigma(z+c)$ has the form

$$\sigma(\xi)=\xi[\xi^{-(2n+1)/2}+\xi^{(2n+1)/2}]^2$$

especially simple expressions for $k(\lambda)$ result.

TABLE I. *The conductivity functions,* $\sigma_\nu(\xi)=\xi(\xi^{-\nu}+\xi^{\nu})^2$.

ξ	$\sigma_{1/2}(\xi)=(1+\xi)^2$	ξ	$\sigma_{3/2}(\xi)$	ξ	$\sigma_{5/2}(\xi)$
0	1.0	0	∞	0	∞
0.01	1.02	0.0465	464	0.0631	63,100
.03	1.06	.1	100	.1	10,000
.05	1.10	.2	25.37	.2	625
.075	1.15	.3	11.32	.3	123.5
.10	1.21	.4	7.06	.4	39.8
.2	1.44	.5	5.00	.5	16.95
.3	1.69	.641	3.86	—	—
.5	2.25	.75	3.595	.75	4.83
.75	3.06	.86	3.62	—	—
1.0	4.00	1.0	4.00	1.0	4.0
1.5	6.25	1.5	8.48	1.5	14.50
2.0	9.00	2.0	20.25	2.0	68.00
3.0	16.00	3.0	87.2	2.377	185.40
5.0	36.00	4.0	264.2	3.0	734.00
7.5	72.25	4.32	359	4.0	4,100.00

Computed examples.[14] In the accompanying Table I, the conductivity function, Eq. (2.4*a*), is tabulated for $\nu=1/2$, $3/2$, and $5/2$; in Table II the corresponding kernels (see Eq. 2.5) are tabulated as functions of λc, for five values of the factor $f(\nu, A, c)$, in its possible range, $0\leq f\leq 1.0$. Graphical representation of Table I is shown in Fig. 1 and of Table II in Figs. 2, 3 and 4. In the case of the linear conductivity function, the parameter c may, with convenience, be suppressed by adopting as the unit of length the distance in which unit change in the conductivity occurs. For such a convention, c is necessarily unity.

TABLE II. *The kernels* $k_\nu(\lambda)$.

λc	$k_{1/2}(\lambda)$ $f=0$	$f=1/100$	$f=1/10$	$f=\frac{1}{2}$	$f=1.0$	$k_{3/2}(\lambda)$ $f=0$	$f=1/100$	$f=1/10$	$f=\frac{1}{2}$	$f=1.0$	$k_{5/2}(\lambda)$ $f=0$	$f=1/100$	$f=1/10$	$f=\frac{1}{2}$	$f=1.0$
0	1	0	0	0	0	∞	0	0	0	0	∞	0	0	0	0
0.2	1	0.953	0.667	0.286	0.167	6.03	3.17	0.638	0.13	0.066	15.0	3.16	0.390	0.079	0.0339
.5	1	.98	.834	.50	.333	3.0	2.545	1.072	.30	.159	6.34	3.88	.865	.194	.0985
1	1	.99	.909	.667	.50	2.0	1.886	1.25	.50	.286	3.5	2.98	1.272	.359	.189
2	1	.995	.953	.80	.667	1.5	1.466	1.225	.706	.462	2.165	2.05	1.405	.584	.338
3	1		.968	.857	.75										
5	1		.980	.910	.834	1.2	1.19	1.12	.882	.700	1.433	1.412	1.253	.835	.589
10	1	1.00	.990	.952	.909	1.1	1.096	1.065	.954	.828	1.21	1.202	1.140	.935	.754
15	1	1.00		.968	.938										
20	1	1.00	.996	.976	.953	1.05	1.05	1.035	.974	.908	1.1	1.096	1.050	.966	.862

[13] It has been noted by R. E. Langer that this reciprocal relation is perfectly general. Thus, if $\sigma_2(z)\sigma_1(z)=1$, then $\sigma_2'/\sigma_2=-\sigma_1'/\sigma_1$. We now write: $\dot{U}+(\sigma_2'/\sigma_2)\dot{U}-\lambda^2U=0$ and $\dot{Z}+(\sigma_1'/\sigma_1)\dot{Z}-\lambda^2Z=0$. Multiply the first by $\dot{Z}$, the second by $\dot{U}$, add and integrate from 0 to ∞. Then,

$$\dot{U}\dot{Z}|_0^\infty=\lambda^2UZ|_0^\infty.$$

Both sides are zero at ∞, whence $\dot{U}(0)/\lambda U(0)=\lambda Z(0)/\dot{Z}(0)$, i.e., $1/k_2=k_1$.

[14] The writer is much indebted to Dr. Charles Müson Gewertz for his assistance in the computing of these examples.

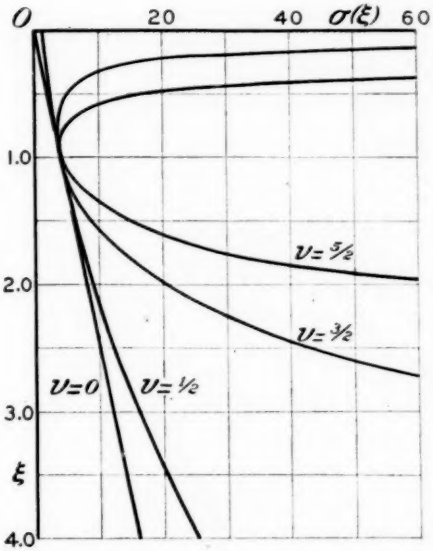

FIG. 1. The conductivity functions $\sigma_\nu(\xi)=\xi(\xi^{-\nu}+\xi^{\nu})^2$ for $\nu=0,\ 1/2,\ 3/2,\ 5/2$.

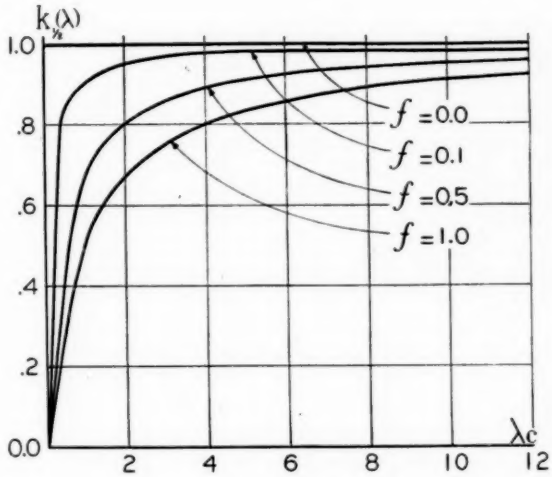

FIG. 2. The kernel, $k_{1/2}(\lambda)$.

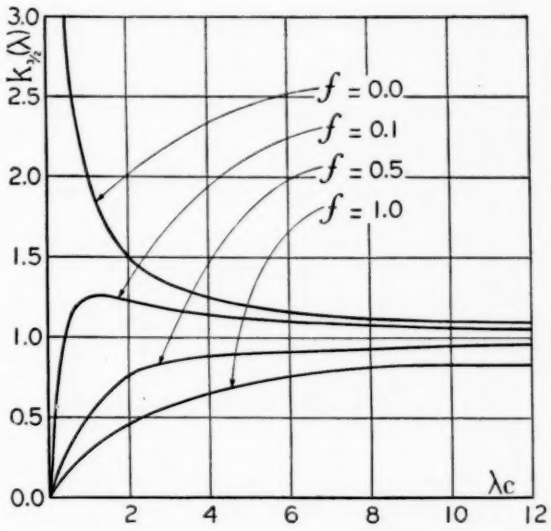

FIG. 3. The kernel, $k_{3/2}(\lambda)$.

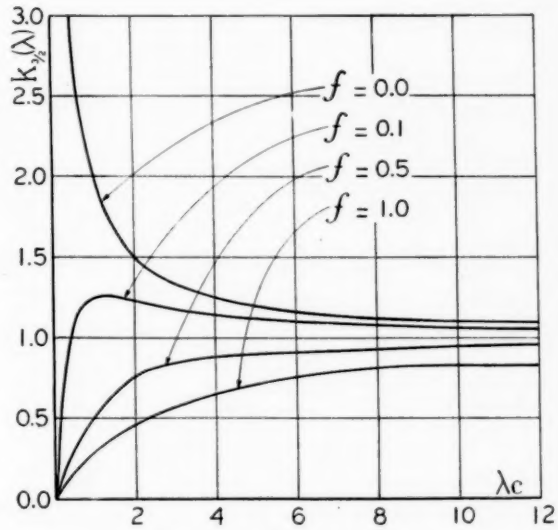

FIG. 4. The kernel, $k_{5/2}(\lambda)$.

2.3. Exponential conductivity functions

When the conductivity function is exponential, $\sigma=\sigma_0 e^{2bz}$, the differential equation (1.4) has constant coefficients; and its solutions are

$$z_1=\exp\{-bz[1+(1+(\lambda/b)^2)^{\frac{1}{2}}]\},$$

$$z_2=\exp\{-bz[1-(1+(\lambda/b)^2)^{\frac{1}{2}}]\}.$$

In this case, then,

$$k(\lambda)=\frac{+\lambda/b}{1+[1+(\lambda/b)^2]^{\frac{1}{2}}}. \qquad (2.7)$$

As b becomes small, the solution approaches that for a half space of constant conductivity and $R(\lambda)$ approaches unity for all λ. The factor, b, however, is conveniently suppressed by a suitable choice of the unit of length; i.e., if the unit of length is defined as the distance in which the conductivity changes by a factor e, the factor b is

unity. In Table III the functions $\sigma(z)$ and $k(\lambda)$ are tabulated and in Fig. 5 $\sigma(z)$ and $k(\lambda)$ are plotted against their arguments, when b is unity.[15]

2.4. Hyperbolic conductivity functions

If the conductivity function is one of the following hyperbolic types

$$\text{(a)}\ \sigma = A\sinh^2\omega(z+c), \qquad \text{or} \qquad \text{(b)}\ \sigma = A\cosh^2\omega(z+c)$$

the solutions of Eq. (1.4) are, respectively,

$$\text{(a)}\ Z = e^{\mp(\lambda^2+\omega^2)^{\frac{1}{2}}z}/[\sinh\omega(z+c)] \qquad \text{or} \qquad \text{(b)}\ Z = e^{\mp(\lambda^2+\omega^2)^{\frac{1}{2}}z}/[\cosh\omega(z+c)],$$

corresponding to which we have

$$\text{(a)}\ k(\lambda) = \lambda c/\{[(\lambda c)^2+(\omega c)^2]^{\frac{1}{2}}+\omega c\coth\omega c\}, \qquad \text{(b)}\ k(\lambda) = \lambda c/\{[(\lambda c)^2+(\omega c)^2]^{\frac{1}{2}}+\omega c\tanh\omega c\}. \quad (2.8)$$

TABLE III. *The conductivity function e^{2z} and its kernel.*

z	$\sigma(z)=e^{2z}$	λ	$k(\lambda)$
0	1.0	0	0
0.1	1.2214	0.1	0.0499
.2	1.4918	.2	.0990
.3	1.8221	.3	.1467
.5	2.7183	.5	.2362
.75	4.4817	1.0	.4145
1.0	7.3891	2.0	.6181
1.5	20.086	5.0	.8207
2.0	54.598	10.0	.9060
3.0	403.0	20.0	.9520
5.0	22,026	50.0	.9800

TABLE IV. *The conductivity functions $\sinh^2\omega z$ and $\cosh^2\omega z$.*

ωz	$\sinh^2\omega z$	$\cosh^2\omega z$
0	0	1.0
0.2	0.0405	1.040
0.5	0.2715	1.27
1.0	1.382	2.382
1.5	4.525	5.53
2.0	13.15	14.13
2.5	36.6	37.6
3.0	100.2	101.2
3.5	273.0	274.6

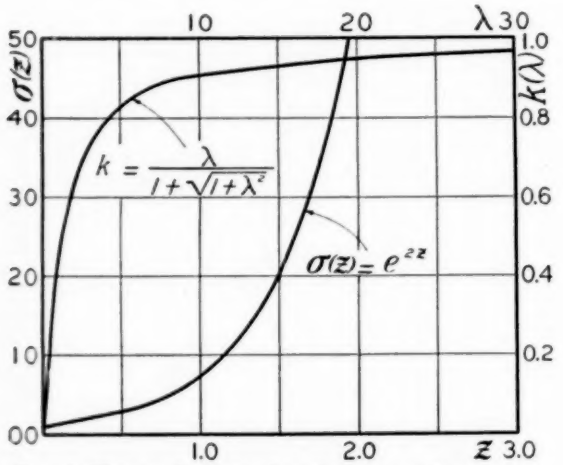

FIG. 5. The conductivity function, e^{2z}, and its kernel.

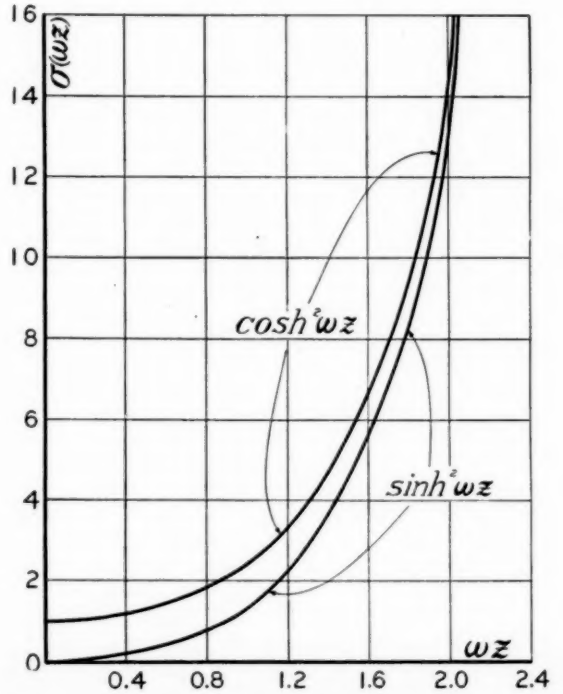

FIG. 6. The conductivity functions $\cosh^2\omega z$ and $\sinh^2\omega z$.

[15] The case for negative b, when the integral in Eq. (1.4) is divergent, has been treated in detail by S. Stefanesco in Volume II of his *Études Théoriques sur la Prospection du Sous-Sol* (Institutul Geologic al României. Vol. XIV, Fasciola II, 1932, Bucuresti). This work has just come to the author's attention. It seems to be little known in this country and well deserves to be called to the notice of those interested in the theoretical aspects of electrical prospecting.

TABLE V. *The kernels* k_1, *and* k_2 *corresponding to* $\sigma = \sinh^2 \omega(z+c)$ *and* $\sigma = \cosh^2 \omega(z+c)$ *for several values of* ωc.

λc	$\omega c = 0$	$\omega c = 0.2$	$\omega c = 1$	$\omega c = 3$	$\omega c = 6$
			$k_1(\lambda)$		
0	0	0	0	0	0
0.2	0	0.154	0.0859	0.0332	0.01667
0.5	0	.322	.2058	.0827	.0417
1	0	.492	.367	.162	.0828
2	0	.662	.564	.302	.1623
5	0	.832	.78	.565	.362
10	0	.908	.88	.743	.566
20	0	.952	.938	.862	.745
			$k_2(\lambda)$		
0	1	0	0	0	0
0.2	1	0.622	0.112	0.0345	0.016675
0.5	1	.867	.266	.0831	.0417
1	1	.945	.46	.1628	.0828
2	1	.977	.668	.3035	.1622
5	1	.922	.854	.568	.362
10	1	.997	.925	.746	.5665
20	1	.999	.963	.862	.744

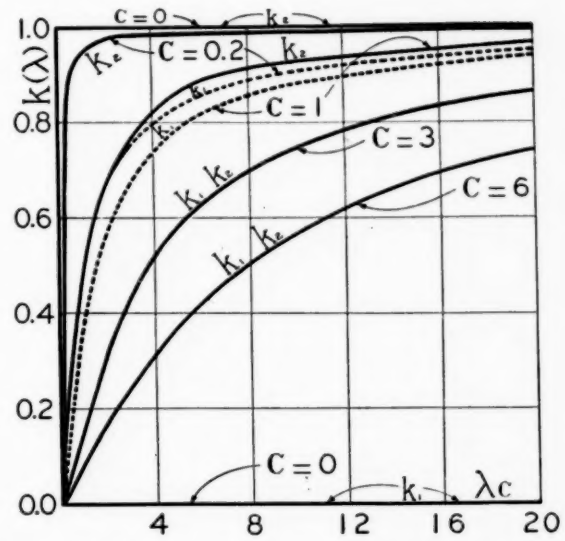

FIG. 7. The kernels, k_1 and k_2, corresponding respectively to $\sigma = \cosh^2 \omega z$ and $\sigma = \sinh^2 \omega z$.

The basic forms of these conductivity functions,

$$\sigma = \sinh^2 z; \qquad \sigma = \cosh^2 z$$

are plotted in Fig. 6, as functions of ωz; and in Fig. 7 the corresponding kernels $k(\lambda)$ are plotted against λc for several different values of the parameter ωc. The data for these curves appear in Tables IV and V, respectively.

2.5. Composite conductivity functions

If, at certain levels, the analytic form of the conductivity function changes, or if the conductivity becomes zero or infinite, the problem will involve two or more regions, in each of which the solution for the potential will be of individual type. These solutions are such as insure the continuity of the normal component of the current and the continuity of the potential function at all interfaces; thus, at the ith boundary, $z = h_i$,

$$\sigma_i(\partial\varphi_i/\partial z) = \sigma_{i+1}(\partial\varphi_{i+1}/\partial z); \qquad \varphi_i = \varphi_{i+1}. \tag{2.9}$$

Since these equalities are satisfied for all ρ, they lead directly to the following equations between the two distinct solutions, Z_1 and Z_2, of Eq. (1.4),

$$\sigma_i[A_i\dot{Z}_{1,i}(h_i, \lambda) + B_i\dot{Z}_{2,i}(h_i, \lambda)] = \sigma_{i+1}[A_{i+1}\dot{Z}_{1,i+1}(h_i, \lambda) + B_{i+1}\dot{Z}_{2,i+1}(h_i, \lambda)],$$

$$A_iZ_{1,i} + B_iZ_{2,i} = A_{i+1}Z_{1,i+1} + B_{i+1}Z_{2,i+1}. \tag{2.10}$$

In the region below the lowest, or nth boundary, the function $B_{n+1}(\lambda)$ is necessarily zero, since φ_{n+1} vanishes at infinity. In the upper layer, $0 \leq z \leq h_1$, the condition at the free surface imposes the additional relation

$$A_1(\lambda)\dot{Z}_{11}(0, \lambda) + B_1(\lambda)\dot{Z}_{21}(0, \lambda) = -\lambda. \tag{2.11}$$

A region involving n boundaries at depth, furnishes then, a system of $2n+1$ equations of the following type for determining the $2n+1$ functions $A_1(\lambda)\cdots A_n(\lambda)$, $A_{n+1}(\lambda)$, $B_1(\lambda)\cdots B_n(\lambda)$

$$\begin{aligned}
&\dot{x}_1(0)A_1 + \dot{y}_1(0)B_1 && = -\lambda,\\
&x_1(h_1)A_1 + y_1(h_1)B_1 - x_2(h_1)A_2 - y_2(h_1)B_2 && = 0,\\
&\dot{x}_1(h_1)A_1 + \dot{y}_1(h_1)B_1 - r_1\dot{x}_2(h_1)A_2 - r_1\dot{y}_2(h_1)B_2 && = 0,\\
&x_2(h_2)A_2 + y_2(h_2)B_2 - x_3(h_2)A_3 - y_3(h_2)B_3 && = 0,\\
&\dot{x}_2(h_2)A_2 + \dot{y}_2(h_2)B_2 - r_2\dot{x}_3A_3 - r_2\dot{y}_3B_3 && = 0,\\
&\quad\cdots\cdots\cdots

The cases (a'') and (b), like the one mentioned in footnote (15), yield a logarithmic potential for large ρ and a divergent integral in Eq. (1.6).

(c) If the boundary is one between two linearly varying regions, continuous at $z=h$, the expression for $k(\lambda)$ is the unwieldy one

$$\bar{k}(\lambda)=\frac{K_0(b_0)[I_1(b_1)K_0(b_2)+I_0(b_1)K_1(b_2)]+I_0(b_0)[K_0(b_2)K_1(b_1)-K_0(b_1)K_1(b_2)]}{K_1(b_0)[I_1(b_1)K_0(b_2)+I_0(b_1)K_1(b_2)]-I_1(b_0)[K_0(b_2)K_1(b_1)-K_0(b_1)K_1(b_2)]},$$

where $\sigma=\alpha_1(z+c_1)$ for $0<z<h$, $\sigma=\alpha_2(z+c_2)$ for $z>h$; and $b_0\equiv\lambda c_1$, $b_1\equiv\lambda(h+c_1)$, $b_2\equiv\lambda(h+c_2)$.

The slopes of the conductivity functions, α_i, do not appear explicitly in any of the above expressions. They are, however, implied in the constants c_1 and $h+c_2$, through the relations of the type $\sigma_0=\alpha_1 c_1$; $\alpha_1(h+c_1)=\alpha_2(h+c_2)$, etc.

(d) *Trigonometric conductivity function.* The functions of type, (a) $\sigma(z)=A\cos^2\omega(z+c)$ or (b) $\sigma(z)=A\sin^2\omega(z+c)$ should perhaps receive brief mention because of the possibility of representing by them (as well as by the functions of paragraph (2.1)) conductivities containing a maximum or minimum. The solutions of the differential Eq. (1.4) for these cases are:

$$\text{(a)}\quad Z(z,\lambda)=Ae^{\mp(\lambda^2-\omega^2)^{\frac{1}{2}}z}/\cos\omega(z+c),$$

$$\text{(b)}\quad Z(z,\lambda)=Ae^{\mp(\lambda^2-\omega^2)^{\frac{1}{2}}z}/\sin\omega(z+c).$$

Since the conductivity eventually decreases to zero, an additional boundary condition must be introduced either at this depth or at a lesser one. The form of $\bar{k}(\lambda)$ will, of course, depend upon the nature of the conductivity function below the boundary, but in any case, the formulae for $\bar{k}(\lambda)$ will be very unwieldy. They may be readily computed if desired by use of the general formulae (2.13) and (2.14).

2.6. Sequence of homogeneous layers

The case in which the medium is representable by a sequence of uniform layers is of interest because this is the simplest of the multiple boundary problems and because certain classes of conductivity functions are most readily approximated by the assumption of discontinuities of the step type. As has been said, the problem of one, two, and three layers superimposed on a uniform infinite half space was solved in convenient form by Stefanesco and Schlumberger[16] who also indicated the nature of the solution for the general case of n layers. The determinants of order $2n$ which occur in this solution may be simplified by a minor modification of Stefanesco's procedure, so that their evaluation in the general case is much facilitated.

In the case of a sequence of uniform layers, the functions x_i and y_i in Eq. (2.12) will all be of type $e^{\mp\lambda z}$. Thus $y_i=1/x_i$, $\dot{x}_i=-\lambda x_i$, $\dot{y}_i=\lambda/x_i$. If we denote $e^{-\lambda h_i}$ by x_i and substitute these values in Eq. (2.12), the result is

$$\begin{aligned}
A_1-\quad B_1 &= 1,\\
x_1A_1+(1/x_1)B_1-\ x_1A_2-(1/x_1)B_2 &= 0,\\
-x_1A_1+(1/x_1)B_1+r_1x_1A_2-(r_1/x_1)B_2 &= 0,\\
x_2A_2+\cdots &= 0,\\
-\ x_2A_2+\cdots &= 0,\\
\cdots\cdots\cdots\cdots &\\
x_nA_n+(1/x_n)B_n-\ x_nA_{n+1} &= 0,\\
-x_nA_n+(1/x_n)B_n+r_nx_nA_{n+1} &= 0.
\end{aligned}\qquad (2.15)$$

[16] S. Stefanesco and C. M. Schlumberger, J. d. Phys. et le Rad. **1**, 132 (1930).

If, in the determinant of this system, the $2d$ row is added to the third, the fourth to the fifth, etc., and the notations $a_i \equiv 1+r_i$; $b_i \equiv 1-r_i$ are introduced, the following expression for B_1 is obtained

$$B_1(\lambda) = \frac{\begin{vmatrix} -x_1 & -x_1 & -1/x_1 & 0 & \cdots & & & & & \\ 0 & -x_1b_1 & -a_1/x_1 & 0 & \cdots & & & & & \\ 0 & x_2 & 1/x_2 & -x_2 & -1/x_2 & 0 & \cdots & & & \\ 0 & 0 & 2/x_2 & -x_2b_2 & -a_2/x_2 & 0 & \cdots & & & \\ 0 & 0 & 0 & x_3 & \cdots & & & & & \\ \cdots & \cdots & \cdots & \cdots & \cdots & \cdots & \cdots & \cdots & \cdots & \cdots \\ & & & & & & & x_n & 1/x_n & -x_n \\ & & & & & & & 0 & 2/x_n & -b_nx_n \end{vmatrix}}{\Delta}$$

Here $\Delta \equiv D-N$, where N is the determinant in the numerator, and D is like N except its first column reads $1/x_1, 2/x_1, 0, \cdots$ instead of $-x_1, 0, 0, \cdots$. In the determinant N it is to be noted that the subminors of type

$$\begin{vmatrix} 1/x_i - 1/x_i \\ 2/x_i - a_i/x_i \end{vmatrix} \quad \text{and} \quad \begin{vmatrix} 1/x_i - x_i \\ 2/x_i - x_ib_i \end{vmatrix}$$

reduce respectively to the simple terms b_i/x_i^2 and a_i, on account of the relation $a_i+b_i=2$. Upon utilizing this relation, the determinant N may be conveniently expanded directly, beginning at the lower right corner. It will be noted in carrying out this evaluation that the sign of each term is positive. For example, if $n=5$ (ordinarily designated as the "six" layer case) the result of the expansion may be expressed by the following scheme:

$$N_5 = 1 \begin{cases} b_5\xi_5 \begin{cases} b_3/\xi_4 \begin{cases} b_3\xi_3 \begin{cases} b_2/\xi_2 \times b_1\xi_1 \\ a_2 \times a_1 \end{cases} \\ a_3 \begin{cases} b_2\xi_2 \times a_1 \\ a_2 \times b_1\xi_1 \end{cases} \end{cases} \\ a_4 \begin{cases} b_3/\xi_3 \begin{cases} b_2\xi_2 \times a_1 \\ a_2 \times b_1\xi_1 \end{cases} \\ a_3 \begin{cases} b_2/\xi_2 \times b_1\xi_1 \\ a_2 \times a_1 \end{cases} \end{cases} \end{cases} \\ a_5 \begin{cases} b_4\xi_4 \begin{cases} b_3/\xi_3 \begin{cases} b_2\xi_2 \times a_1 \\ a_2 \times b_1\xi_1 \end{cases} \\ a_3 \begin{cases} b_2/\xi_2 \times b_1\xi_1 \\ a_2 \times a_1 \end{cases} \end{cases} \\ a_4 \begin{cases} b_3\xi_3 \begin{cases} b_2/\xi_2 \times b_1\xi_1 \\ a_2 \times a_1 \end{cases} \\ a_3 \begin{cases} b_2\xi_2 \times a_1 \\ a_2 \times b_1\xi_1 \end{cases} \end{cases} \end{cases} \end{cases} \tag{2.16}$$

Here the notation $\xi_i \equiv x_i^2$ has been introduced. In this schematic representation, all possible 16 products indicated by the brackets are to be formed and the terms added with the positive sign. If the abbreviations $k_i \equiv b_i/a_i = (\sigma_i - \sigma_{i+1})/(\sigma_i + \sigma_{i+1})$ are introduced, it is seen that:

$$\frac{N_5}{a_1a_2a_3a_4a_5} = \sum_{i=1}^{5} \xi_i k_i + (\xi_1\xi_3\xi_5/\xi_2\xi_4)k_1k_2k_3k_4k_5 + k_5k_1\xi_5\xi_1(k_2/\xi_2 + k_3/\xi_3 + k_4/\xi_4) + k_5k_2\xi_5\xi_2(k_3/\xi_3 + k_4/\xi_4)$$
$$+ k_5k_4k_3\xi_5\xi_3/\xi_4 + k_4k_1\xi_4\xi_1(k_2/\xi_2 + k_3/\xi_3) + k_4k_3k_2\xi_4\xi_2/\xi_3 + k_3k_2k_1\xi_3\xi_1/\xi_2.$$

The schematic representation of D_5 is the same, except that the factors $b_1\xi_1$ and a_1, in the extreme right-hand column of Eq. (2.16) are to be replaced respectively by a_1, and b_1/ξ_1; so that, finally

$$D_5/a_1a_2a_3a_4a_5 = 1 + k_5\xi_5\sum_{i=1}^{4} k_i/\xi_i + k_4\xi_4\sum_{i=1}^{3} k_i/\xi_i + k_3\xi_3\sum_{i=1}^{2} k_i/\xi_i + k_2\xi_2k_1/\xi_1 + k_5k_4k_3k_2\xi_5\xi_3/\xi_4\xi_2$$
$$+ k_5k_4k_3k_1\xi_5\xi_3/\xi_4\xi_1 + k_5k_4k_2k_1(\xi_5/\xi_4)(\xi_2/\xi_1) + k_5k_3k_2k_1(\xi_5/k_3)(\xi_2/\xi_1) + k_4k_3k_2k_1\xi_4\xi_2/\xi_3\xi_1.$$

The number of terms in N_i and D_i *doubles* for each additional layer present; and from the recurrence rules evident from inspection of the schematic representation, Eq. (2.16), it will be clear how this scheme may be extended to provide for the evaluation of the determinants for N and for D of any order. But obviously, the arithmetic quickly becomes too cumbersome for computational purposes; the above sixteen term determinants occurring in the six layer case should be convincing on this point. The corresponding eight and four term expressions occurring in the five and four layer cases are more tractable, especially if simplification is introduced by postulating equal layer thicknesses. The five and four layer formulae are easily obtained from the six layer formula above by setting $k_5 = 0$ and $k_4 = 0$, successively.

It is seen from Eqs. (2.14) and (2.12) that whenever the uppermost layer is uniform, the kernel is simply

$$\bar{k}(\lambda) = A_1(\lambda) + B_1(\lambda) = 1 + 2B_1(\lambda).$$

Hence the function $2B_1(\lambda)$ determines the net perturbing effect of the underlying horizons upon the surface potentials, i.e.,

$$\varphi(\rho, 0) = (C/2\pi\sigma_0)\left(1/\rho + \int_0^\infty (\sin \lambda a/\lambda a) J_0(\lambda\rho) 2B_1(\lambda) d\lambda\right).$$

2.7. A comparison involving the surface potentials, kernels and conductivity functions

The comparisons in the preceding examples were drawn between conductivity functions and their corresponding kernels. The kernel, it will be recalled, and the observed surface potentials are essentially equivalent functions; either may be derived from the other by a quadrature. Thus the foregoing comparisons also involve indirectly the conductivity and the observed potentials. However, since these potentials are the primary experimental data of the problem, it is desirable to illustrate directly the effect of small changes in conductivity function upon the observed surface potentials. The conductivity functions chosen for the purpose are those shown in Fig. 8*b* and numbered I to III. These functions are similar in general type, but differ in detailed form. The first one increases linearly, with unit slope, from an initial value of 0.6 at the surface; II is like I except it remains constant after attaining the value 3.0, at depth 2.4; III is a step function zigzagging across the other two; its value is as follows:—for $0 < z < 1.0$, $\sigma_3(z) = 1.0$; when $1.0 < z < 2.0$, $\sigma_3(z) = 2.0$; and when $z > 2.0$, $\sigma_3(z) = 4.0$.

TABLE VI. *Kernels for the three conductivity functions in Fig. 9.*

λ	$1/\lambda$	$k_1(\lambda)$	λ	$1/\lambda$	$k_2(\lambda)$	λ	$1/\lambda$	$k_3(\lambda)$
0	∞	0	0	∞	0.200	0	∞	0.250
0.033	30	0.0806	0.033	30	.246	0.05	20	.314
.066	15	.134	.066	15	.285	.1	10	.374
.100	10	.177	.100	10	.318	.15	6.66	.431
.166	6	.246	.166	6	.374	.2	5	.484
.333	3	.367	.233	4.29	.420	.3	3.33	.579
.500	2	.449	.333	3.0	.476	.4	2.5	.657
.833	1.2	.558	.500	2.0	.546	.6	1.66	.776
1.666	0.6	.700	.833	1.2	.634	.8	1.25	.853
2.50	.4	.771	1.333	0.75	.722	1.2	0.833	.937
3.33	.3	.814	2.000	.5	.785	1.6	.625	.972
4.16	.24	.844	2.666	.375	.821	2.4	.417	.995
5.00	.2	.865	3.330	.3	.851	3.2	.312	.999
8.33	.12	.912	4.166	.24	.875			
16.66	.06	.953	5.000	.2	.892			
25.00	.04	.969						
33.33	.03	.976						
50.00	.02	.984						
83.33	.012	.990						

The formulae for the kernels in these cases are, respectively

$$k_1(\lambda)=\frac{K_0(0.6\lambda)}{K_1(0.6\lambda)}$$

$$k_2(\lambda)=\frac{K_0(0.6\lambda)\{I_1(3\lambda)+I_0(3\lambda)\}+I_0(0.6\lambda)\{K_1(3\lambda)-K_0(3\lambda)\}}{K_1(0.6\lambda)\{I_1(3\lambda)+I_0(3\lambda)\}-I_1(0.6\lambda)\{K_1(3\lambda)-K_0(3\lambda)\}}$$

$$k_3(\lambda)=\frac{3-e^{-2\lambda}(2/3+e^{-2\lambda})}{3+e^{2\lambda}(4/3+e^{-2\lambda})}.$$

These three kernels are tabulated in Table VI, and plotted in Fig. 9. The surface potentials resulting from the three conductivity functions were computed[17] by the use of formula (1.6). The ratios, φ_i/φ_0, of these potentials to the normal potentials which would have resulted had the conductivity remained constant at its surface value, are plotted in solid line in Fig. 8*a* against the radial distance from the electrode.

TABLE VII. *The ratio, ϕ_i/ϕ_0, of the surface potentials, for the three conductivity functions of Fig. 9.*

ρ	φ_1/φ_0	ρ	φ_2/φ_0	ρ	φ_3/φ_0
0	1.0	0	1.0	0	1.0
0.0666	0.842			1/9	0.957
.20	.687			1/3	.877
.40	.557			2/3	.767
.60	.47	1.0	0.471	1.0	.664
1.20	.34	2.0	.350	2.	.45
1.8	.242	3.0	.306	3.	.36
3.6	.138	6.0	.243	6.	.270
5.4	.090	9.0	.220	9.	.258

[17] The integrals were evaluated mechanically with the Bush integraph (see reference 10).

The graphical comparisons in Figs. 8 and 9 illustrate a typical feature of the mutual interdependence of the three types of functions $\sigma(z)$, $k(\lambda)$, and $\varphi(\rho)$. This dependence may be exhibited more directly if the potential ratios are compared with the function $k(1/\lambda)$, instead of $k(\lambda)$. In this case *both* types of functions are accurately known for *small* values of the agument, whereas they become less satisfactorily established as the argument becomes large. The dotted curves in Fig. 8*a* represent the three functions $k_i(1/\lambda)$, plotted against $1/\lambda$ as abscissa. For large values of $1/\lambda$ these curves approach asymptotically the respective curves for φ_i/φ_0. The asymptotic values are, respectively, the three ratios $\sigma_1(0)/\sigma_1(\infty)=0$, $\sigma_2(0)/\sigma_2(\infty)=0.2$ and $\sigma_3(0)/\sigma_3(\infty)=0.25$. At the origin, the functions have the common value unity and for intermediate values their similarities reflect the similarities existing between their respective conductivity functions $\sigma_1(z)$, $\sigma_2(z)$ and $\sigma_3(z)$. Comparison of the curves in Figs. 8 and 9 affords an indication of the "sensitivity" (or lack of it) of the functions

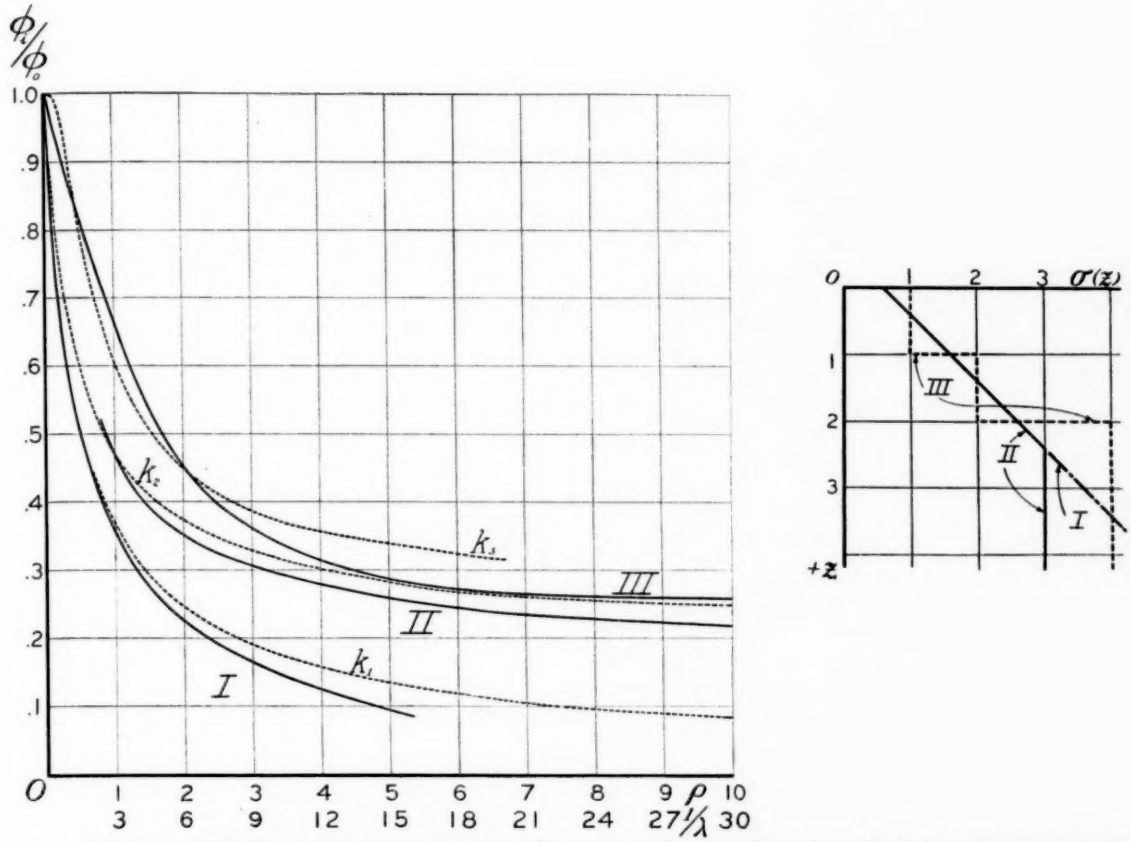

FIG. 8, *a* and *b*. Comparison between the surface potentials, kernels, and conductivities for some similar conductivity functions. φ_i/φ_0 is represented by the solid line; k_i is represented by the broken line.

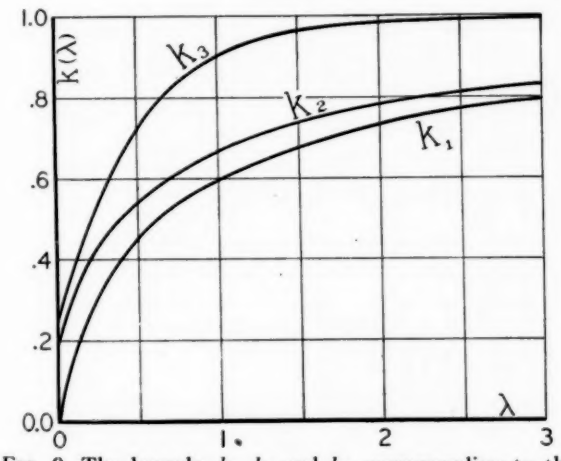

FIG. 9. The kernels, k_1, k_2 and k_3, corresponding to the three conductivity functions in Fig. 8.

$k(\lambda)$, and $\varphi(\rho)$ to moderately small changes in the form of the conductivity function.

PART III. THE ANISOTROPIC CASE

The anisotropic (but horizontally isotropic) problem differs from the isotropic case only in occurrence of the function $q^2(z) \equiv \sigma_\rho/\sigma_z$ which multiplies λ^2 in Eq. (1.4).[18] A solution for this case may readily be obtained by the same methods used in Part I, but it is perhaps simpler to reduce the anisotropic problem to an equivalent isotropic one. This is always easily done, as follows. If a new independent variable, $w(z)$, is introduced, the quantities $Z(z, \lambda)$, $\sigma(z)$ and $q(z)$ may be denoted, as functions of w, by $W(w, \lambda)$, $s(w)$, and $r(w)$, respectively. Then Eq. (1.4) may be written:

$$\frac{d^2W}{dw^2} + \left[\frac{\ddot{w}}{\dot{w}^2} + \frac{ds/dw}{s}\right]\frac{dW}{dw} - \lambda^2\frac{r^2(w)}{\dot{w}^2}W = 0. \quad (3.1)$$

[18] A discussion, with examples, of the conditions under which the potentials in a current flow problem remain invariant at homologous points under transformation of the space metric and of the conductivity tensor is given by R. Maillet and H. G. Doll, Gerlands Beitr. z. Geoph. Ergänzungs Hefte für Angewandte Geoph. 3, 109–124 (1932). Their general results include most of those deduced, by other methods, in this section.

$$\text{If} \qquad \left.\begin{aligned} w &= \int_0^z q(z)dz, \text{ so that} \\ dw/dz &= q(z) = r(w) \end{aligned}\right\} \tag{3.2}$$

then Eq. (3.1) is obviously that for an isotropic space ρ, w in which the conductivity, $u(w)$, satisfies

$$\frac{du/dw}{u} = \frac{\dot{w}}{\dot{w}^2} + \frac{ds/dw}{s} = \frac{dr/dw}{r} + \frac{ds/dw}{s}. \tag{3.3}$$

Integration yields the following expression for the equivalent isotropic conductivity,

$$u(w) = Ar(w)s(w) = Aq(z)\sigma_z(z). \tag{3.4}$$

The constant A is to be so chosen as to preserve the equivalence of the anisotropic and isotropic cases, insofar as the observable potentials are concerned. From Eq. (1.5) it is evident that such equivalence implies the relation

$$\frac{1}{u(0)} \frac{W_1(w, \lambda)}{(d/dw)W(w, \lambda)|_{w=0}} = \frac{1}{\sigma_z(0)} \frac{Z_1(z, \lambda)}{[dZ(z, \lambda)/dz]|_{z=0}}.$$

Since

$$Z_1(z, \lambda) = W(w, \lambda) \quad \text{and} \quad \frac{dW(0, \lambda)}{dw} \cdot q(0) = \frac{dZ(0, \lambda)}{dz}$$

the above relation is satisfied if $u(0) = \sigma(0)q(0)$. This fixes the constant in Eq. (3.4) as unity. Hence if $u(w) = \sigma_z(z)q(z)$, and $w = \int_0^z q(z)dz$, the potentials in the isotropic space will be identical with those at homologous points in the anisotropic one. In general, the function $q^2(z)$ is unknown, so that the occurrence of anisotropy renders the interpretation problem non-unique. However, in an actual geological application, geological arguments may sometimes be effective in restricting the range of pertinent interpretations. In all cases, the equivalent conductivity $u(w)$ which is deduced by assuming isotropy, *is the geometric mean* of the two component conductivities σ_ρ and σ_z. The form of the conductivity function $u(w)$ may often be correlated with the existence of known geological horizons —some of these will be known *a priori* to be essentially isotropic and to others an approximate value for q^2 may be assigned. This value will usually be a small number, greater than unity because of a well-known characteristic of horizontal rock structures. Usually q^2 will be less than 10 and only in exceptional cases, such as in a graphitic slate, will it attain a large value. Since it enters only as the square root, moderate errors in its estimation will not prove serious.

When the electrical anisotropy of the rocks which may occur in the given problem can be expressed as a function of their conductivity, then the anisotropic problem becomes completely determinate. This is clear from the following. If $q(z) = f(\sigma_z)$ where $f(\sigma_z)$ is a known function of σ_z, then Eq. (3.4) supplies knowledge of σ_z as a function of the variable u and therefore, since $u(w)$ is known, as a function of w also. Thus one may write $q(z) = F(w)$, where $F(w)$ is known. If this value is introduced into Eq. (3.2), this equation becomes

$$dw/F(w) = dz, \tag{3.5}$$

which is the formula which supplies the desired connection between corresponding values of the variables w and z. Hence, the additional relationship $q(z) = f(\sigma_z)$ furnishes the solution for the anisotropic problem, $\sigma_z(z)$ and z, in terms of the corresponding known quantities $u(w)$ and w for the isotropic space.

Since $q(z)$ always exceeds unity in a geological problem of the type being discussed, it is to be noted that the effect of anisotropy is always to *reduce* the depth to be associated with a given conductivity on the isotropic depth-conductivity curve to a value less than that indicated in the equivalent isotropic problem.

The writer desires to acknowledge the helpful suggestions and interest of Professor R. E. Langer who kindly criticized this paper in manuscript.

An Extension of a Maxwell Mutual-Inductance Formula to Apply to Thick Solenoids

H. B. DWIGHT AND S. H. CHEN, *Massachusetts Institute of Technology*

(Received April 13, 1933)

The formula for the mutual inductance of two concentric solenoids which is used probably more than any other is the one originally given by Maxwell. Since the solenoids were taken to have negligible thickness in the above formula and since the effect of the thickness is often appreciable in practical cases, additional terms to give the effect of the thickness have been calculated and are presented in this article.

AS given by Maxwell,[1] the formula included terms as far as the one in a^4/A^4 of Eq. (4) of this paper. The term in a^6/A^6 was added by E. B. Rosa and L. Cohen.[2] The formula was further extended to include the term in a^{14}/A^{14} by E. B. Rosa and F. W. Grover.[3]

The effect of the thickness of two coaxial solenoids on their mutual inductance may be found in accordance with the general method described by Maxwell.[4]

The mutual inductance of two coils may be described as being proportional to the voltage at the terminals of one coil when unit alternating current flows in the other coil. In the case of cylindrical coils, it may be derived from an expression for the mutual inductance of two circular turns of fine wire by summing up the voltage in every turn of one coil, produced by the current in every turn of the other. If the space for insulation is assumed to have negligible effect, the summation may be done by integrating.

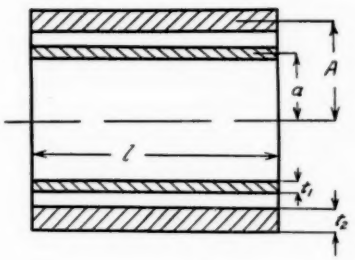

FIG. 1. Two concentric, coaxial solenoids of equal length.

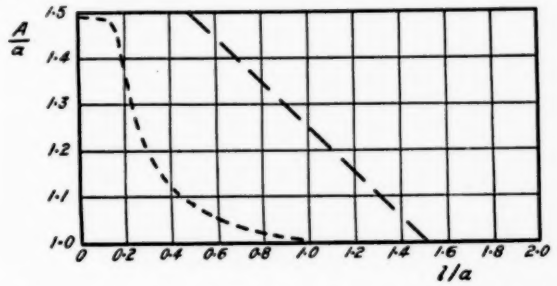

FIG. 2. Ranges of application of formulas (4) and (21).

If M_p is the M. I. of two coils of equal length and of radii $a+y_1$ and $A+y_2$, whose thickness is negligible and whose numbers of turns are N_1 and N_2, then the M. I. of two coils as in Fig. 1, of thickness t_1 and t_2, is

$$M=(1/t_1t_2)\int_{y_1=-\frac{1}{2}t_1}^{\frac{1}{2}t_1}\int_{y_2=-\frac{1}{2}t_2}^{\frac{1}{2}t_2} M_p dy_2 dy_1. \tag{1}$$

Now $M_p=f(a+y_1, A+y_2)$ and this, by Taylor's theorem, when expressed symbolically, is equal to

$$f(a, A)+(y_1D_a+y_2D_A)f(a, A)+(1/2!)(y_1D_a+y_2D_A)^2f(a, A)$$
$$+\cdots+(1/n!)(y_1D_a+y_2D_A)^nf(a, A)+\cdots, \tag{2}$$

[1] Maxwell, *Electricity and Magnetism*, Vol. II, paragraph 678.

[2] Rosa and Cohen, Bull. Bur. Stand. **3**, No. 2 (1907).

[3] Rosa and Grover, Bull. Bur. Stand. **8**, No. 1, Eq. (36) (1911) or Bur. Stand. Sci. Pap., No. 169.

[4] Maxwell, *Electricity and Magnetism*, Vol. II, paragraph 700.

where $f(a, A) = M_s$, the M. I. of the central solenoids of infinitesimal thickness. Performing the integrations indicated in (1), there is obtained[5]

$$M = M_s + \frac{t_1^2}{3!\,2^2}\frac{\partial^2 M_s}{\partial a^2} + \frac{t_2^2}{3!\,2^2}\frac{\partial^2 M_s}{\partial A^2} + \frac{t_1^4}{5!\,2^4}\frac{\partial^4 M_s}{\partial a^4} + \frac{t_1^2 t_2^2}{3!\,3!\,2^4}\frac{\partial^4 M_s}{\partial a^2 \partial A^2} + \frac{t_2^4}{5!\,2^4}\frac{\partial^4 M_s}{\partial A^4}$$
$$+ \frac{t_1^6}{7!\,2^6}\frac{\partial^6 M_s}{\partial a^6} + \frac{t_1^4 t_2^2}{5!\,3!\,2^6}\frac{\partial^6 M_s}{\partial a^4 \partial A^2} + \frac{t_1^2 t_2^4}{3!\,5!\,2^6}\frac{\partial^6 M_s}{\partial a^2 \partial A^4} + \frac{t_2^6}{7!\,2^6}\frac{\partial^6 M_s}{\partial A^6} + \cdots. \quad (3)$$

The formula for M_s in abhenries, from Scientific Paper 169 of the Bureau of Standards,[3] Eq. (36), is

$$M_s = \frac{4\pi^2 N_1 N_2 a^2 A}{l^2}\left[Q_1 + \frac{a^2}{8A^2}Q_3 + \frac{a^4}{64A^4}Q_5 + \frac{5}{1024}\frac{a^6}{A^6}Q_7 + \cdots\right] \quad (4)$$

where dimensions are in cm and are as in Fig. 1. N_1 and N_2 are the numbers of turns in the two coils,

$$r^2 = l^2 + A^2, \quad (5) \qquad \mu = A/r, \quad (6)$$
$$Q_1 = r/A - 1, \quad (7) \qquad Q_3 = 1 - \mu^3, \quad (8)$$
$$Q_5 = 1 + 4\mu^5 - 5\mu^7, \quad (9) \qquad Q_7 = 1 - 8\mu^7 + 28\mu^9 - 21\mu^{11}. \quad (10)$$

Derivatives of M_s with respect to a and A can be directly written down and substituted in (3) and the following terms giving the correction for thickness are obtained:

$$M = M_s + \Delta M \quad (11)$$

$$\Delta M = \frac{4\pi^2 N_1 N_2}{l^2}\left[\frac{t_1^2 A}{24}\left(2Q_1 + \frac{3}{2}\frac{a^2}{A^2}Q_3 + \frac{15}{32}\frac{a^4}{A^4}Q_5 + \frac{35}{128}\frac{a^6}{A^6}Q_7 + \cdots\right)\right.$$
$$+ \frac{t_2^2 A}{24}\left(\frac{a^2}{A^2}R_1 + \frac{a^4}{4A^4}R_3 + \frac{a^6}{16A^6}R_5 + \frac{5}{1024}\frac{a^8}{A^8}R_7 + \cdots\right)$$
$$+ \frac{t_1^4}{1920A}\left(3Q_3 + \frac{45}{8}\frac{a^2}{A^2}Q_5 + \frac{525}{64}\frac{a^4}{A^4}Q_7 + \cdots\right)$$
$$+ \frac{t_1^2 t_2^2}{576A}\left(2R_1 + 3\frac{a^2}{A^2}R_3 + \frac{15}{8}\frac{a^4}{A^4}R_5 + \frac{35}{128}\frac{a^6}{A^6}R_7 + \cdots\right)$$
$$\left. + \frac{t_2^4}{1920A}\left(3\frac{a^2}{A^2}S_3 + \frac{3}{8}\frac{a^4}{A^4}S_5 + \frac{45}{64}\frac{a^6}{A^6}S_7 + \frac{105}{128}\frac{a^8}{A^8}S_9 + \cdots\right) + \text{terms in } t_1^6 \text{ etc.}\right] \quad (12)$$

where Q_1 to Q_7 are given by Eqs. (7) to (10),

$$R_1 = \mu - \mu^3, \quad (13)$$
$$R_3 = 1 - \mu^3 + (15/2)\mu^5 - (15/2)\mu^7, \quad (14)$$
$$R_5 = 3 + 2\mu^5 - 40\mu^7 + (455/4)\mu^9 - (315/4)\mu^{11}, \quad (15)$$
$$R_7 = 30 - 16\mu^7 + 616\mu^9 - 3402\mu^{11} + 5775\mu^{13} - 3003\mu^{15}, \quad (16)$$
$$S_3 = -\mu^3 + 6\mu^5 - 5\mu^7, \quad (17)$$

[5] H. B. Dwight, Trans. A. I. E. E., Eq. (12), p. 1689 (1919).

$$S_5=8+12\mu^5-195\mu^7+490\mu^9-315\mu^{11}, \tag{18}$$

$$S_7=8-8\mu^7+252\mu^9-1253\mu^{11}+2002\mu^{13}-1001\mu^{15}, \tag{19}$$

$$S_9=10+8\mu^9-414\mu^{11}+3399\mu^{13}-(77649/8)\mu^{15}+(45045/4)\mu^{17}-(36465/8)\mu^{19}. \tag{20}$$

As a numerical example of (12), the pair of coils described on page 77 of Scientific Paper No. 169[3] may be used, giving each coil a thickness of 1 cm. We have

$$a=5, \quad A=10, \quad t_1=t_2=1, \quad l=200, \quad M_s=(4\pi^2N_1N_2/l^2)\times 4764.3,$$

$$r=200.25, \quad Q_1=19.025, \quad Q_3=0.9999, \quad Q_5=1.000, \quad R_1=0.0498, \quad R_3=0.9999, \quad R_5=3.00.$$

The series involving t_1^2 in the square bracket of (12) is

$$(10/24)(38.050+0.375+0.029+0.004+\cdots)=38.46/2.4=16.02.$$

The corresponding series in t_2^2 is

$$(10/24)(0.012+0.016+0.003+\cdots)=0.031/2.4=0.01,$$

$$\Delta M=(4\pi^2N_1N_2/l^2)[16.02+0.01+\cdots],$$

$$\Delta M/M_s=16.0/4764.3=0.0034 \text{ or } 0.34 \text{ percent.}$$

Formula (4) of this paper is most rapidly convergent for very long solenoids. It is one of its advantages, however, that it can be used in many cases with short solenoids, as is shown by Example 36, page 79 of Scientific Paper 169.[3] There is a limit beyond which the solenoids are too short for this formula. This is shown by Fig. 2 where, if the ratios A/a and l/a lie to the left of the curved dotted line, the mutual inductance is not given with even ordinary slide-rule accuracy.

A formula has been developed to cover this part of the range, which is more rapidly convergent than formula (4) up to approximately the location of the sloping, dotted, straight line of Fig. 2. It is as follows:[6]

$$M=\pi gN_1N_2\left[\left(\log\frac{16g^2}{b^2+p^2}\right)\left(1+\frac{p}{g}+\frac{b^2}{8g^2}+\frac{p^2}{4g^2}-\frac{b^2p}{8g^3}-\frac{p^3}{4g^3}-\frac{b^4}{64g^4}+\frac{7}{64}\frac{b^2p^2}{g^4}+\frac{17}{64}\frac{p^4}{g^4}+\cdots\right)\right.$$
$$+\frac{p^2}{b^2}\left(\log\frac{b^2+p^2}{p^2}\right)\left(1+\frac{p}{g}-\frac{p^2}{8g^2}+\frac{p^3}{8g^3}-\frac{9}{64}\frac{p^4}{g^4}+\cdots\right)-4\frac{p}{b}\left(1+\frac{p}{g}\right)\tan^{-1}\frac{b}{p}-1$$
$$\left.+\frac{p}{g}+\frac{b^2}{16g^2}+\frac{13}{8}\frac{p^2}{g^2}+\frac{3}{16}\frac{b^2p}{g^3}-\frac{11}{24}\frac{p^3}{g^3}+\frac{b^4}{48g^4}-\frac{5}{16}\frac{b^2p^2}{g^4}+\frac{p^4}{24g^4}+\cdots\right], \tag{21}$$

where the solenoids are of infinitesimal thickness, of equal length, b cm, and of diameters g and $g+2p$ cm and where log denotes natural logarithm.

The formulas described in this paper consist of groups of infinite series. If, in the case of any of the series, the last term used is not almost negligibly small and is not smaller than the preceding term, then the series should not be used. The numerical precision which is obtained should be watched by the user of the formula, for each separate problem.

By means of a few numerical examples, an approximate description of the precision to be expected will be given in the following paragraphs but this should not be relied on exclusively. The chief reliance should be on the observation of the relative values of the terms actually obtained, as already described.

First, the cases will be considered where the coils have practically equal radii and negligible thickness. These have for a limit the case of self-

[6] Formula (1), H. B. Dwight and P. W. Sayles, J. Math. and Phys. p. 162 (1930).

inductance. These cases can be described simply by the equations:

$$a = A \qquad \text{and} \qquad t_1 = t_2 = 0.$$

The percentages given are approximate. It is to be noted that there is a difference in notation between (4) and (21). When $l/a = 2$, Eq. (4) to 4 terms has about 0.4 percent error. The value of the 8th term is 0.03 percent of the total. For the same case, Eq. (21) has about 0.2 percent error. When $l/a = 1.4$, Eq. (4) to 4 terms has about 0.6 percent error and the value of the 8th term is 0.05 percent of the total. For this case, Eq. (21) has about 0.1 percent error. The terms involving b^4/g^4 are 0.3 percent of the total.

By using an average value of the first logarithm in (21), the sum of the last terms used in the series in b/g is approximately $(1/24)\ (b^4/g^4)$, which gives directly an indication of the order of accuracy obtained by (21) when p is less than b.

When $A/a = 6/5$, that is, $p/g = 1/10$, the accuracy of (21) is not changed unless b/g is less than $1/10$. The accuracy of (4) is considerably improved, however, because the power series in a/A become more rapidly convergent than when $a = A$. Thus when $A/a = 1.5$ and $l/a = 1$, the error in using 4 terms of (4) is $1/10$ as much as when $A = a$ and $l/a = 1$.

Formula (21) should not be used for larger values of A/a than about 1.5 but this restriction does not apply to (4), which becomes more rapidly convergent as A/a becomes larger. Formula (21) should not be used for larger values of l/a than about 1.6.

When a power series is differentiated, factors are put in the numerators of the terms and the series become less rapidly convergent or they may become divergent. Thus, the series of (12) are less rapidly convergent than (4) and cannot be used with such short solenoids. This is almost automatically shown in using the series. If t/a is less than about $1/3$, the usefulness of (12) usually depends more on the values of a/A and A/r being small than on the smallness of t/a.

When $l/a = 1$ and $A/a = 1.5$, the 4 terms of (12) in t_1^2 are just convergent to a practical extent. For the long solenoids whose calculation is shown in this paper in detail, where $l/a = 40$ and $A/a = 2$, the precision of the series in t^2 is $1/100{,}000$ of the total mutual inductance.

The terms in ΔM involving the 6th powers of t have been calculated and may be found in the S. M. thesis of S. H. Chen in the library of the Massachusetts Institute of Technology. They are most suitable for very long solenoids and for those of comparatively unequal diameters.

In calculating the mutual inductance of coils, the dimensions of the cross sections should be taken so as to extend to the limits of the metal wires. One reason for this is the lack of a correction formula for the shape and insulation of the wires, in calculating mutual inductance.

In calculating self-inductance, such a correction formula is available, namely, Eq. (93) of Scientific Paper 169.[3] For this correction formula, it is necessary to take each dimension of the cross section as equal to the number of wires in the dimension, multiplied by the pitch distance between centers of wires.

If example 57, page 126 of Scientific Paper 169[3] be recalculated by finding $L_u = 47011.9\pi$ by using Eq. (84), p. 79, *Standard Handbook for Electrical Engineers*, edition of 1933, with the thickness $c = 0.1$ cm and $b = 1$ cm and $\Delta_2 L = 373.9\pi$ by Eq. (93) of Scientific Paper 169,[3] the sum is $L = 47{,}385.8\pi$ which agrees with the precisely calculated value on page 127 of Scientific Paper 169.[3]

If Eq. (93)[3] is not used, however, the value of $L_u = 47{,}011.9\pi$ is not by itself a good approximation. It is evident from physical reasons that a thick current sheet which is to be closely equivalent to a row of wires should have a thickness not greater than the diameter of the metal wires. This can be checked by calculating L_u putting $c = 0.08$ cm and $b = 0.98$ cm, the result being $47{,}384.1\pi$ which is a good approximation to the precise value $47{,}385.8\pi$,

This is a matter of some importance in connection with this paper, since in solenoids of one or two layers of wire there is a considerable difference in the values of t_1 and t_2 when measured over the metal wires or over the insulation.

The formulas in this paper are based on there being no magnetic material in or near the coils and on the current density being uniform.

Low Voltage Impulse Circuits

L. B. SNODDY, *General Electric Company, Schenectady, New York*

(Received May 27, 1933)

Three different types of low voltage circuits suitable for supplying impulse voltages in oscillographic work are discussed. These circuits use Thyratrons as the connecting and timing switches in place of the spark gaps ordinarily employed in transient investigations. Charged condensers are used as the source of voltage. Two circuits are of the single tube type and the third is a multiple tube system in which a number of condensers are charged in multiple and discharged in series by means of Thyratrons. Oscillograms of the voltage form obtainable in each case are given and the time lag of starting determined.

IN the oscillographic study of the transients which occur during the initial ionization and final deionization of gaseous discharge devices it is often necessary to connect a source of potential to the test circuit and to synchronize the time of this connection and the time of starting of the sweep motion of the oscillograph. For slow sweep motions this can be done by some kind of mechanical switch but for investigations in which the variation between the times of starting must not be more than one or two microseconds any mechanical device is out of the question.

Since the source of potential is usually a charged condenser, this synchronization is made comparatively simple for high voltage circuits by the use of three electrode sphere gaps as the connecting switches. This works quite satisfactorily down to perhaps 10 kv; below this it becomes increasingly difficult to regulate accurately and measure the voltage and also to prevent the introduction of excessive extraneous voltages during the breakdown of the sphere gaps.

For low voltage work the sphere gap connecting switch may very advantageously be replaced by Thyratrons. In this way voltages from a few volts (66 volts is the lowest that the author has actually used) up to the limit of the tube may be obtained.

It is the purpose of this paper to discuss some of the impulse circuits in which Thyratrons may be used and to determine the time of starting and the type of wave obtained.

The simplest possible type of circuit is that shown in Fig. 1. It consists of the condenser C charged from some constant voltage supply (B batteries are quite satisfactory) through the resistance R_1, the Thyratron T with its filament transformer F and the discharge resistance R. The test circuit is connected across R. The time constant RC is made large so that the voltage applied to the test circuit can be considered as constant for relatively short intervals of time. The grid of the Thyratron T is charged negatively with respect to the cathode by the battery b through the resistance R_2. To start the discharge through the tube a positive potential is applied to R_3 from an auxiliary circuit. The values of R_2 and R_3 will depend upon the speed of starting desired and upon the amount of negative bias necessary to prevent accidental discharge. In all of this work the grid was kept from 70 to 135 volts negative with respect to the

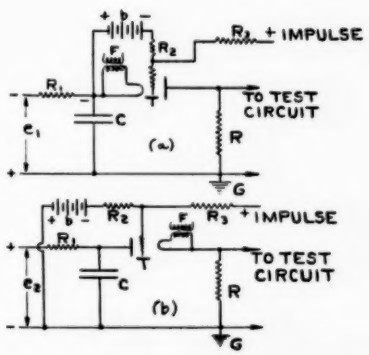

FIG. 1. Single tube circuit arranged to supply either negative (a) or positive (b) potential to the test circuit.

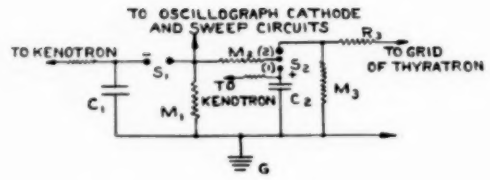

FIG. 2. Oscillograph and auxiliary circuit used for supplying power to the oscillograph and the starting impulse to the grid of the Thyratron.

cathode. In Fig. 1a the circuit is arranged to supply negative voltage and in Fig. 1b positive.

Oscillograms of the voltage appearing across R were taken with the General Electric oscillograph of the DuFour type (HC-2). This employs a high voltage cold cathode discharge to give the electron beam and depends entirely upon gas focussing.

It was consequently convenient to produce the positive starting impulse, as shown in Fig. 2. The condenser C_2 is kept charged to within a few percent of the breakdown value of $S_2(1)$; i.e., to a value as close as possible to the setting of $S_2(1)$ without producing accidental discharges. To take an oscillogram, the voltage of C_1 is gradually increased until S_1 sparks over. This applies voltage to the oscillograph cathode and sweep circuits and at the same time trips S_2 (both 1 and 2) (time lag very short—not over 5×10^{-8} sec.). The positive potential appearing across M_3 is used to charge the grid of the Thyratron and start the discharge. The rate of charging can be varied by changing R_3.

The constants of the oscillograph and starting circuit are given below:

$C_1=0.226$ mf, $R_3=1.47\times10^6$ ohms,
$C_2=0.0085$ mf, $S_1=60$ kv,
$M_1=6\times10^4$ ohms, $S_2(1)=30$ kv,
$M_2=1.4\times10^6$ ohms, $S_2(2)=15$ kv
$M_3=2\times10^6$ ohms,

Oscillograms of the voltage across R are given in Fig. 3a and b, for the circuits of Figs. 1a and 1b, respectively. The circuit constants are as follows:

$C=0.915$ mf, $e_1=-254$ volts,
$R_1=R_2=2.5\times10^5$ ohms, $e_2=+170$ volts,
$R=1000$ ohms, $b=90$ volts.

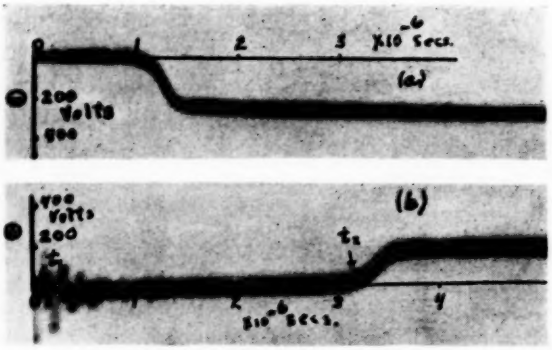

FIG. 3. Oscillograms of the voltage form obtainable from the circuits of Fig. 1.

The Thyratron used for the single tube circuits is known as FG-33.

In Fig. 3b the time of application of the starting impulse is shown at t_1. Complete breakdown occurs at t_2. The interval t_2-t_1 represents the total time lag between the appearance of potential across M_3 (Fig. 2) and discharge through the Thyratron. This interval was measured in several cases and found to be approximately 3×10^{-6} sec. It depends upon the tube design, the rate of charging of the grid and the mercury vapor pressure. For a given tube design and rate of charging it becomes shorter and more constant in value as the vapor pressure is increased. Since in this type of circuit the tube is only carrying current a small fraction of the time it does not reach the normal operating temperature. It is advisable to compensate for this by wrapping part of the bulb with cloth tape.

The potential attained by the grid before breakdown occurs was not measured but the maximum possible potential can easily be computed. After the application of potential to R_3, the grid circuit is essentially as shown in Fig. 4. With the following constants,

$C=40\times10^{-12}$ f, $E=+30$ kv,
$R_3=1.47\times10^6$ ohms, $e=-344$ volts,
$R_2=2.5\times10^5$ ohms,

the potential of the grid reaches that of the cathode in 1.7×10^{-7} sec. and at the end of 3×10^{-6} sec. is approximately 980 volts. The actual potential reached is probably less than this because of the electrons drawn from cathode to grid prior to complete breakdown. It is inter-

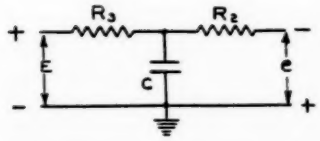

FIG. 4. Equivalent grid circuit used in computation of maximum grid voltage.

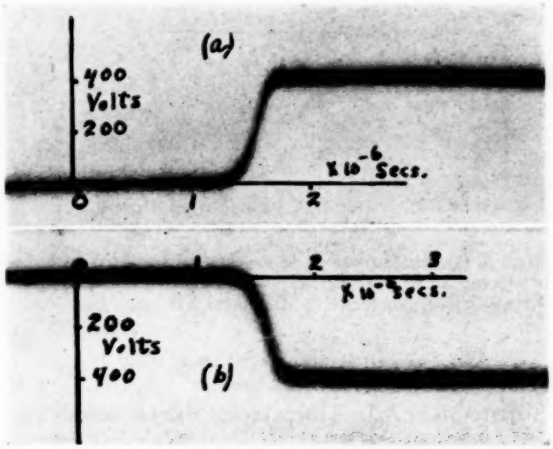

FIG. 6. Oscillograms of the voltage form obtainable from the circuit of Fig. 5.

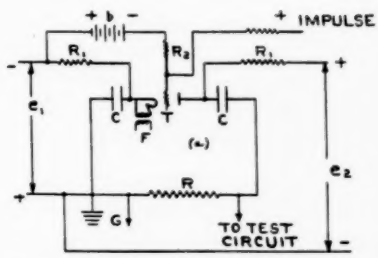

FIG. 5. Single tube circuit with two condensers as voltage sources.

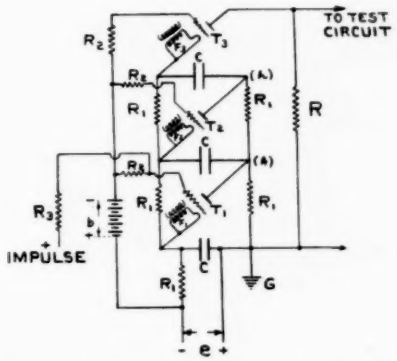

FIG. 7. Multiple tube circuit arranged for charging of the condensers in multiple and discharging in series.

esting to note that in all the cases investigated in this work the actual breakdown took place very abruptly.

It is sometimes convenient to use the circuit shown in Fig. 5 in which the two capacitances C, C are charged to different polarities. This has the advantage that opposite polarities may be applied to the test circuit by simply changing the ground terminal from one capacitance to the other. In order to avoid oscillations and obtain a rapid rate of potential increase across R it is, of course, understood that in all of these circuits the connecting wires should be as short as possible, R itself be wound non-inductively and the condensers C be free from inductance.

Oscillograms of the voltage drop across R with a circuit of this type are given in Fig. 6. The circuit constants are the same as before with $e_1 = -254$ volts and $e_2 = +170$ volts. In Fig. 6a positive potential is applied to the test circuit and in Fig. 6b negative potential.

Since in many laboratories power voltages above 2 or 3 hundred volts are not readily obtainable, the circuit shown in Fig. 7 has been developed to furnish impulse voltages in approximately integral multiples of the available supply. This circuit is analogous to the ordinary high voltage impulse circuit of the Marx type in which the capacitances are charged in multiple and then discharged in series by means of spark gaps.

The three condensers, C, (Fig. 7) are charged in multiple from the supply, e, through the resistances R_1. The magnitude of R_1 is relatively unimportant. Its lower limit should be such that the time constant R_1C is considerably greater than RC/n where n is the number of condenser units. Its upper value depends upon the leakage of the condenser. This leakage current must not decrease the voltage applied to the capacitances if it is desired that the voltage appearing across R should be accurately ne—(sum of tube drops).

The action of the circuit is readily understood from the diagram. The positive impulse applied to the grid of the first tube, T_1, starts the discharge and raises the point k to a potential $e - V_1$ where V_1 is the voltage drop across the

tube T_1. This, in turn, starts T_2 by making its cathode more negative than the grid. The breakdown of T_2 raises the point h to a potential $2e-(V_1+V_2)$. This process may be continued as far as desired. The arrangement for this work used only the three sections shown in the diagram. It would perhaps be better to have all the Thyratrons of the same type but it is not at all necessary. In this circuit T_1 was an FG-33, T_2 and T_3 were both FG-57's. To obtain a positive voltage it is necessary simply to change the grounded side of R to the anode side of the third Thyratron and place a charging resistance R_1 in the positive side of the supply line.

It is of interest to consider the maximum current and energy available from a system of this kind. If C represents the capacity of each unit, e the voltage and n the number of separate units, the total energy is given by

$$W = C(ne)^2/2n = \tfrac{1}{2}Cne^2$$

and is consequently directly proportional to the number of sections. This neglects the energy dissipated in the tube.

The maximum current available on direct short circuit, assuming all wire and contact resistance as well as tube limitations negligible, is

$$I_{\max.} = n(e-V_T)(C/nL)^{\frac{1}{2}} = (e-V_T)(Cn/L)^{\frac{1}{2}},$$

where L is the inductance of the necessary connecting loop. This inductance cannot be computed accurately as a function of n but it is evident that it increases as n increases since the connecting loop must become larger. The maximum current consequently increases at a rate slower than the $n^{\frac{1}{2}}$.

The rate of increase of voltage across R for the system of Fig. 7 is shown in Fig. 8. For Fig. 8a only two units were used and for Fig. 8b all three units were charged. Two consecutive discharges are shown in each case. The total time lag in this case was also approximately 3×10^{-6} sec. If necessary, this can easily be reduced to 0.8×10^{-6} sec. by increasing the energy input to the grid. However, if this is done, it is necessary to shield the Thyratron circuit rather carefully to avoid the introduction of extraneous voltage into the test circuit from the starting system.

In the use of these circuits it is necessary to consider the current limitations imposed by the Thyratrons. All Thyratrons have a definite upper limit to the amount of emission obtainable from the cathode. It is obvious that the current taken by the test circuit must not exceed this value or the wave front will be greatly distorted.

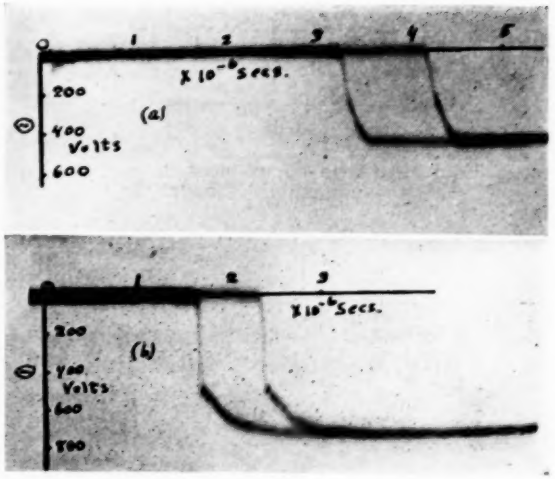

FIG. 8. Oscillograms of the voltage form obtainable from the circuit of Fig. 7. In (a) two units are charged and in (b) three. Two consecutive discharges in each case.

An oscillogram of the drop across an 8.7 ohm resistance (R), with the circuit of Fig. 5 with an FG-33, is shown in Fig. 9. The voltage rise is smooth and steep up to a value corresponding to 9.5 amperes (a) flowing through R. The increase is then slow and irregular up to 34 amperes (b). This forced emission is possibly due to the formation of hot spots on the cathode by positive ion bombardment. It is evident that this

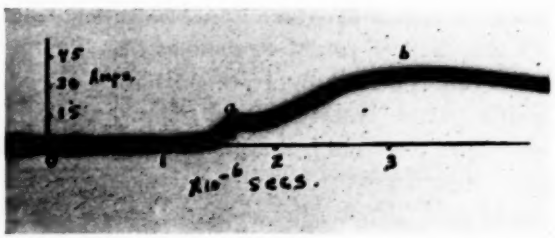

FIG. 9. Oscillogram showing the change in wave form produced when the current limitation of the tube is exceeded. This particular Thyratron (FG-33) will give excellent results provided the current shown at "a" (9.5 amp.) is not exceeded.

particular tube can be used provided the current taken by the test circuit does not exceed 9.5 amperes. This is usually amply sufficient as circuits of this type are ordinarily used simply as a voltage source with no great current demand beyond the charging current to the capacities of the test circuit.

If greater current capacity is desired, it is necessary to use a Thyratron of higher rating. An oscillogram of the same type of circuit, with an FG-41 in place of the FG-33, is given in Fig. 10. In this case a perfectly smooth curve is obtained with a maximum of 129 amperes. The maximum in this case was determined by the voltage of the condensers and was not a tube limitation. The maximum emission was not measured, as 129 amperes is sufficient for the test circuits in which a low voltage supply of this kind is used.

The voltage increase across R in Fig. 10 is limited principally by the inherent inductance of the connecting wires, etc., since this inductance is the primary factor in determining the rate at which current can increase in the circuit. As the time constant of this circuit is small (1.5×10^{-6} sec.), the current decreases very rapidly after the maximum is reached. This rate of decrease depends entirely upon the circuit constants and is not a tube characteristic.

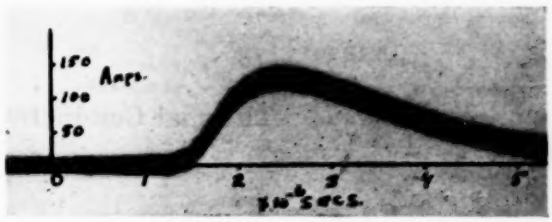

FIG. 10. Oscillogram of the current obtainable from an FG-41. The current increase is smooth up to the maximum of 125 amperes which was determined by voltage limitations and is not the limit of this particular cathode when used in the circuit of Fig. 5. The rate of decrease depends upon the time constant of the circuit.

Thermal Conductivity of Acheson Graphite

A. P. CRARY, *Lehigh University*

(Received June 5, 1933)

Thermal conductivity of Acheson graphite is reported for the temperature range −150°C to +700°C. Cylindrical blocks of the material were placed above and below a flat electric heater and lateral losses balanced out by auxiliary coils wound on the surface of the sample. The results show a continual decrease in thermal conductivity with temperature over the entire range. The law, $k/aC = A/T + B$, proposed by Bidwell for certain other materials is found to hold accurately for graphite.

CONSTRUCTION OF THE APPARATUS

TWO cylindrical blocks of the graphite 10.2 cm (4 in.) in diameter and 17.8 cm (7 in.) long were placed in a vertical position end to end with a flat electric heater between them. This heater consisted of nickel resistance wire, No. 22, wound across and through a circular mica sheet of the same diameter as the cylinders. Current and potential leads of heavy nickel wire were fused to the heater wire. The heat input per second was measured electrically. The diagram of the apparatus is shown in Fig. 1 where the

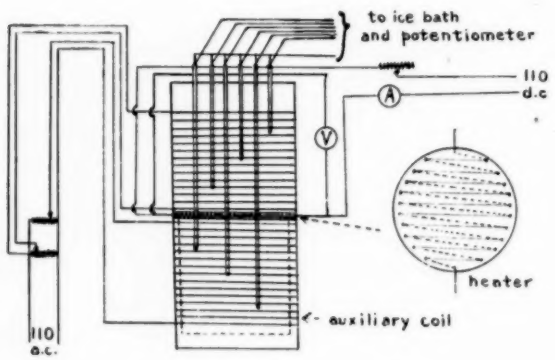

FIG. 1. Diagram of apparatus.

method of winding the heater element is also shown.

Three Alumel-chromel thermocouples of No. 28 wire were placed every 3 cm in the graphite both above and below the heater element. The chromel wire was insulated from the alumel by threading the former through small quartz beads and both wires were put in a quartz tube which was sealed at the bottom. The thermo-junction tubes were placed in holes, drilled down from the top of the sample to the correct level. Thermal e.m.f.'s were measured with a Wolff potentiometer.

The two auxiliary coils consisted of nickel resistance wire, No. 23, wound over a layer of asbestos paper around the sample and then coated with cement. The coils extended in each case from the heater to about 2 cm past the level of the outer thermocouple. For high temperature this apparatus was lowered into a nichrome furnace consisting of an iron pipe 40 cm long and 12 cm in diameter, wound with nichrome ribbon on a layer of asbestos paper. For low temperatures the apparatus was lowered into an evacuated Dewar cylinder and cooled with liquid CO_2 or liquid air.

METHOD OF PROCEDURE

The sample was allowed to come to the desired temperature and the thermocouples read. The heater current was then turned on and after waiting about half an hour in order that sufficient time might elapse for a steady state to be reached, readings were again taken. In order to correct for slight original gradients in the sample and for differences in the individual thermocouples, each couple reading was subtracted from its first steady state reading for a given temperature, i.e., the reading with no heat flowing. From these differences the differences between couples at different depths were found. Heat was then introduced gradually from the auxiliary coils and readings taken continually until a linear gradient both above and below the heater was obtained.

This condition was reached when the temperature differences between adjacent thermocouples on the same side of the heater were the same. When this condition was reached, all lateral heat losses were assumed compensated for. The total heat input was found and the conductivity obtained. Inasmuch as the thermal contact resistance both above and below the heater could never be made exactly the same, the formula was applied separately to the two parts. Thus

$$H_1 = kA\Delta t_1/l, \qquad H_2 = kA\Delta t_2/l.$$

Adding we get

$$H = (kA/L)(\Delta t_1 + \Delta t_2).$$

Results

The plot of thermal conductivity against temperature is shown in Fig. 2. The conductivity is

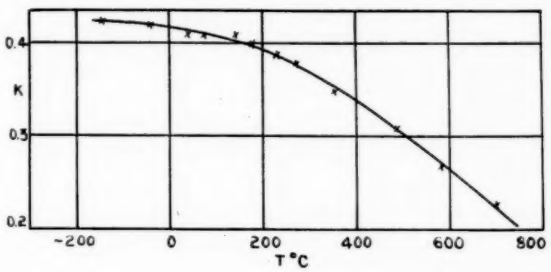

FIG. 2. Thermal conductivity of Acheson graphite.

seen to decrease very slightly between -150°C and 200°C and then fall off more rapidly at higher temperatures.

C. C. Bidwell[1] has found for certain metals a relation of the form

$$k/aC = A/T + B$$

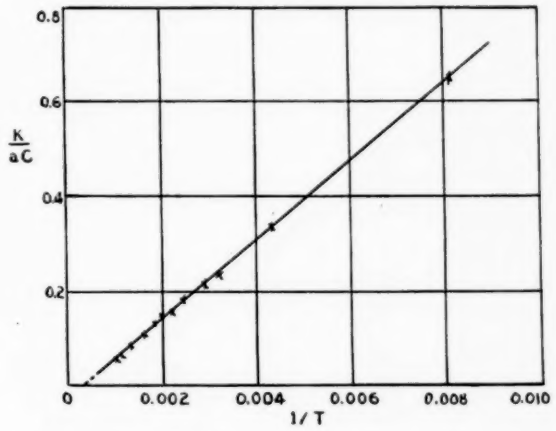

FIG. 3. Variation of k/aC with $1/T$.

where k is thermal conductivity; A and B, constants. This equation is plotted for graphite in Fig. 3 and is seen to hold with good precision over the entire range. The values of atomic heat, aC, were obtained from data published by the Acheson Graphite Company.[2] Due to the uncertainty of the values of aC at liquid air temperature the straight line which best fitted the other points was extended to a value of $1/T$ corresponding to this temperature. The value of k/aC for this temperature was then read from the curve and by using the observed values of k, the value of aC was computed. This value was then plotted on the atomic heat curve and is the lowest point on the curve. It is seen that this point is a good fit on the atomic heat curve as averaged through the points obtained from the published tables.

In conclusion the author wishes to acknowledge his debt to Professor C. C. Bidwell, under whose guidance the work was carried on, and also to Professor C. E. Berger for his many valuable suggestions.

[1] Bidwell, Phys. Rev. **32**, 311–314 (1928).

[2] *Acheson Electrodes. The Nature and Properties.* A pamphlet issued by the Acheson Graphite Company.

The Theory of the Psychrometer. II. The Effect of Velocity

J. HOWARD ARNOLD, *Department of Chemical Engineering, University of Minnesota*

(Received March 8, 1933)

The psychrometric constant ψ, defined as the ratio of **A** (corrected for radiation) to the **A** predicted by the convection theory, is shown to be a function of velocity. At infinite velocity, the new equation reduces to that of August ($\psi=1$); at zero velocity, to the result obtained by Maxwell, $\psi=K/D$. An improved method of obtaining the true wet-bulb temperature is given, together with values of ψ, accurate to about 1 percent, for toluene, chlorbenzene and xylene. Straight lines are obtained when ψ for the latter two liquids against ψ for toluene at the same velocity. The theoretical psychrometric line for water is found; it is shown from theory that the line uncorrected for radiation possesses a stationary minimum value at velocities between 1000 and 10,000 ft./min., the radiation error just balancing the deviation from the August theory. In this range **A** is constant at 630×10^{-6}, while at lower velocities it varies rapidly because of the change in the radiation error. For accurately reproducible results, the air velocity must be maintained at 1000 ft./min. or more.

IN the first paper of this series, a new psychrometric theory was developed leading to the equation[1]

$$\psi=\frac{\mathbf{A}/(M_aC/M_v\lambda)}{1+h_r/h_g}=\left\{\frac{(1-r)/r+(CZ/k)(K/D)}{(1-r)/r+(CZ/k)}\right\}. \tag{1.33}$$

It is the purpose of this paper to investigate the nature and degree of the dependence of ψ on gas velocity and to substantiate further the validity of the equation.

It has long been suspected on empirical grounds[2] that the August result is a limiting value, correct at infinite velocity, although no theory existed to show this. The physical basis for this behavior is found in the relative magnitudes of the resistances of film and convection zone to heat and vapor transfer. The convectional resistance varies inversely as the product fu, by Eqs. (1.07) and (1.37), when r is small, while the film thickness, which determines the film resistance, varies as r/fu. The determining factor is r, which varies as a small fractional power of u; hence, as the velocity approaches infinity, the film resistance disappears more rapidly than the convective resistance and August's result becomes valid. As u varies from zero to infinity, the limits of variation of r are unity and zero, while $(1-r)/r$ changes from zero to infinity. At low velocities, $(1-r)/r$ becomes negligible, and Eq. (1.33) reduces to the Maxwell result, while at high velocities $(1-r)/r$ is of controlling importance.

At infinite velocity, therefore, all systems possess the same value of ψ, regardless of the value of K/D. Conversely, another special case exists when $K/D=1$, ψ then being independent of velocity, since the numerator and denominator of Eq. (1.33) become identical. For this case also, the August equation is valid, not because the film resistances disappear, but because their ratio becomes identical with that of the convective resistances when the diffusivities of heat and vapor are the same. The over-all resistances may then be treated as though they were wholly convective (or diffusive).

ANALYSIS OF THE DATA

The experimental data to be analyzed consist of determinations of the value of **A** for each of the three liquids used, in a transverse current of air at each of several velocities. In the first paper, data were obtained by using a parallel current of air, as is found in the aspiration psychrometer of Assmann,[3] widely used in European practice. For the present research, however, it was considered desirable to use a

[1] Arnold, Physics **4**, 255 (1933).

[2] Regnault, Ann. Chim. Phys. **37**, 257 (1853).

[3] Assmann, Zeits. f. Instrumentenk. **12**, 1 (1892).

transverse current in order that the results obtained might be applied to the whirling (sling) psychrometer, and to the industrially important case of a wet-bulb thermometer inserted in the air ducts of a dryer or air conditioner.

As before, in the treatment of the data it is assumed that Eq. (1.33) is applicable to the wet bulb as a whole, despite its derivation for point conditions. The agreement obtained indicates that this procedure is justified, evidently because the theoretical value of ψ changes but little from point to point; although the individual resistances to heat transfer and evaporation vary markedly around the wet-bulb circumference, their ratio remains fairly constant.

It is desirable to plot the data in such a way that a straight line is obtained. The reduction of the general equation to the Maxwell and August results cannot be shown by plotting ψ against u, or $1/u$, since, at the limits, the slopes of the curves become infinite. A suitable graphical method may be secured by the elimination of r from Eq. (1.33), just as the pressure is eliminated in the Dühring method of vapor pressure estimation:

$$1+(1-r)/r(CZ/k)=(K/D-1)/(\psi-1). \quad (2.01)$$

Since r and CZ/k are practically unaffected by the nature of the liquid on the wet bulb, each side of this equation is constant at a given velocity. Thus, if D_1 and ψ_1 refer to toluene, and D_2 and ψ_2 to xylene,

$$(K/D_1-1)/(\psi_1-1)=(K/D_2-1)/(\psi_2-1) \quad (2.02)$$

or, rearranging,

$$\psi_2=\psi_1\left\{\frac{K/D_2-1}{K/D_1-1}\right\}-\left\{\frac{K/D_2-K/D_1}{K/D_1-1}\right\}. \quad (2.03)$$

ψ_2 is, therefore, a linear function of ψ_1.

If values of ψ for a number of liquids be plotted against ψ for a reference liquid, at various velocities, a family of straight lines results, converging to $\psi=1$ at $u=\infty$, with slopes and intercepts determined by the corresponding values of K/D. At $u=0$ the Maxwell result is obtained, $\psi=K/D$. Consequently, if K/D is known for any liquid, the psychrometric line can readily be constructed; conversely, the value of K/D may be determined experimentally from psychrometric data.

The Wind Tunnel

The function of the wind tunnel was to provide a stream of air of constant velocity, uniform over a cross section large enough to include the wet-bulb thermometer; a tunnel diameter, large compared to the thermometer bulb, was therefore indicated. However, it was desirable to keep the diameter small in order to obtain as high a velocity as possible. The tunnel was made ten feet long and four inches square inside. It was built of composition board (Masonite Presdwood), with the thermometer supports of wood. The Pitot tubes and thermometers were mounted near the outlet end (Fig. 1); most of the tunnel

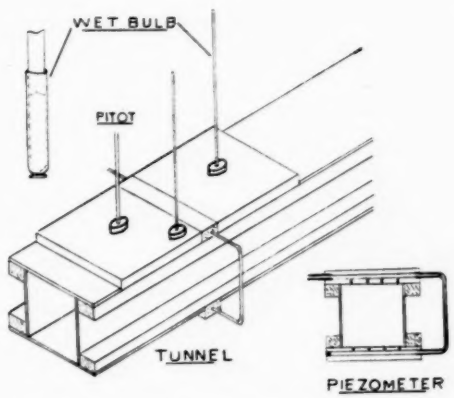

Fig. 1. Isometric drawing of wind tunnel showing placement of thermometers; sectional view of piezometer ring; diagram of wet-bulb wick.

was therefore utilized as a calming section. Air was supplied by a Roots figure-eight rotary blower, size $3\frac{1}{2}$, through a two-inch pipe projecting into the open end of the tunnel; the space between the pipe and the tunnel wall was not closed, the injector-effect thus obtained increasing the maximum velocity obtainable from 1350 to 3300 ft./min.

The wind velocity was measured by a Pitot tube, made from brass tubing of 5 mm outside and 3 mm inside diameter, bent into an L-shape, with the lower branch of the L placed at the axis of the tunnel. Static pressures were obtained with the aid of a piezometer 'ring' consisting of two strips of wood, one at the top and

one at the bottom of the tunnel, each containing four 1 mm pressure openings connecting with a large duct drilled through the long axis of the strip. The readings obtained with this arrangement agreed with those given by a standard double-concentric-tube instrument. Pressure differences were read from an inclined manometer, similar to the ordinary draft gauge, with an inclination of 1 : 10. The gauge reading varied from 0.45 cm at 500 ft./min. to 16.2 cm at 3000 ft./min. Over a central area of about 4 cm diameter, Pitot tube explorations indicated a negligible small variation in velocity; the Pitot tube was accordingly fixed in place at the axis of the tunnel. It was found possible, through by-passing part of the blower output, to secure and maintain any desired velocity from 500 to 3000 ft./min.

The Thermometers

The thermometers used in this investigation were graduated in 0.1°C intervals; they were carefully selected from the available supply and agreed almost exactly over the entire range used. The dry-bulb thermometer was used only as a reference, being compared with the wet-bulb thermometer (with the wick removed) at the start of each run, so that both t_a and t_w were really measured with the same thermometer. The wet-bulb thermometer was compared with a standard calibrated by the Bureau of Standards and agreed with it as nearly as the latter could be read, 0.03°C. The thermometers were mounted in rubber stoppers to facilitate insertion into the tunnel.

The wick was made from unbleached muslin cloth having 18 threads/cm each way. It was wrapped around the bulb in three layers, sewn tightly in place and gathered and tied at the free end so as to cover the bulb completely with a nearly cylindrical form, Fig. 1. Its over-all length was 43 mm, and its outside diameter (in place) 8 mm. The thermometer bulb was 32 mm long and 6.5 mm in diameter; the wick extended 8 mm beyond the upper end of the bulb. The same wick was used in all runs, being carefully cleaned when changing liquids by soaking in benzene and subsequent drying.

The dry-bulb thermometer was placed six inches downstream from the wet bulb to avoid disturbing the air in front of the wet bulb; to keep it out of the cooled air in the wet-bulb wake, the dry bulb was placed $\frac{9}{16}$ inch from the tunnel wall. As a further precaution, dry-bulb readings were taken both before and after the wet-bulb readings. Velocity measurements were made with the wet-bulb thermometer removed from the tunnel.

The liquids used on the wet bulb were purified commercial toluene, chlorbenzene and meta-xylene, dried over phosphorus pentoxide and twice fractionated through an eleven-bulb glass rectifying column. The fractions reserved for psychrometric use were very pure; the boiling ranges were: toluene, 0.2°; chlorbenzene, 0.3°; xylene, 0.2°.

Wet-Bulb Thermometry

A very important part of the research was the devising of a simple, reliable method of obtaining the wet-bulb equilibrium temperature. Water, with its high latent heat, low vapor pressure and consequent low rate of evaporation, is the ideal psychrometric liquid. The use of volatile organic liquids presents considerable difficulty because of the ease with which the wick dries out, making impossible the maintenance of the true wet-bulb temperature for any length of time, especially at high gas velocities.

The continuous feeding of liquid to the wet bulb involves the inherent possibility that a false equilibrium may result, conditioned by the rate of feeding as well as by the variables under study. Any system depending on capillarity is particularly objectionable, since its very effectiveness depends upon a partial drying-out of the wick, without which there could be no gradient of liquid concentration and hence no capillary rise. The rate of evaporation is thereby decreased, since the wetted area may be less, and the liquid must be drawn by capillarity from below the surface of the wick; the effect was discussed by Sherwood[4] in connection with industrial drying. This has been found[5] to lead to a dependence of **A** on the material of the wick. A conspicuous example of the great inaccuracy arising from continuous feeding is to be found in the recent

[4] Sherwood, Ind. Eng. Chem. **21**, 976 (1929).

[5] Svensson, Meteorol. Zeits. **43**, 140 (1926); Ekholm, Arkiv Matem. Astron. Fysik **4**, No. 15 (1908).

results of Sherwood and Comings.[6] Their disagreement with the present theory, ascribable largely to the lack of wet-bulb adiabaticity, is also increased by the use of hygroscopic liquids in undried air and the omission of the radiation correction.

In order to secure reproducible evaporative conditions, it is desirable to present to the air stream an unbroken film of liquid on the wet bulb. It was therefore considered necessary to isolate the wet bulb as much as possible and to eliminate all inflow of liquid to the wick. After much experimentation, a satisfactory method was developed, involving neither continuous feed nor long evaporation time, and making possible the determination of t_w to 0.01°. It is obviously necessary to supply volatile liquids to the wet bulb at a temperature near t_w. The liquid, in a 1×4 in. test tube, was therefore pre-cooled in an ice bath to about 3° below t_w. When this temperature had been attained, the test tube was removed from the bath and its temperature permitted to rise slowly. The wet-bulb thermometer was dipped into the liquid at its lowest temperature, removed, and plunged into the tunnel at zero time, as recorded by a stopwatch. The wet-bulb temperature was read at 10 and at 20 seconds after the insertion of the thermometer into the air stream; the reading at zero time was also taken, but was used only for reference. The thermometer was then removed from the tunnel, replaced in the test tube to replenish the liquid, now at a slightly higher temperature, because of the inflow of heat from the room, and again inserted in the tunnel, temperature readings being taken as before at 0, 10, and 20 seconds. On plotting t_{20} against t_{10}, a straight line results, from which the true wet-bulb temperature is obtained by locating the point $t_{20}=t_{10}=t_w$; this is easily done graphically by finding the intersection of the line with another drawn at 45°. Usually from ten to twenty sets of readings were taken, over a temperature interval of about 6°C. Fig. 2 illustrates the graphical method, showing the 45° line obtained for zero interval between readings, the points experimentally secured for a ten-second interval and the horizontal line representing an infinite interval, at the end of which the wet-bulb temperature is hypothetically t_w.

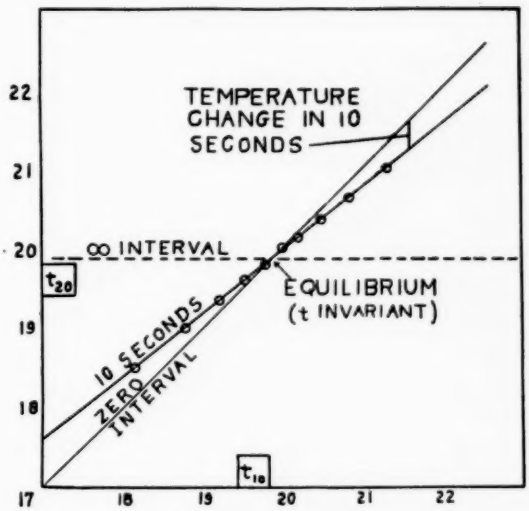

FIG. 2. Working graph for the determination of true equilibrium wet-bulb temperature from temperature-time data.

The method proved to be extremely accurate since it amounts to an averaging of a number of runs. Because of the short time, 20 seconds, there is no possibility of drying of the wick. The drying-out time for toluene at the highest velocity used was found to be 60 seconds, so the margin of safety is considerable. The method has the further important advantage of requiring only a small amount of liquid. The accuracy is apparently limited only by the operator's visual acuity in following a moving thread of mercury and it is favored by the decrease in thread velocity as the equilibrium point is approached. The individual points showed no systematic deviations from the straight line; incidental deviations never exceeded 0.10°, and were infrequently greater than 0.03°.

The method is based, of course, upon the fact that, at the true wet-bulb equilibrium temperature, the thermometer reading does not change with time. The same end might be attained with a single trial, starting with the reservoir liquid at nearly the equilibrium temperature but there is then no protection, such as is afforded by a method involving a number of readings, against the occasional erratic results. The analytical theory of the method is quite simple; it will be considered in a later paper.

[6] Sherwood and Comings, Trans. Am. Inst. Chem. Eng., Dec. (1932).

The Radiation Correction

Because of the small ratio of the wet-bulb area to the area of the enclosure, in this case the wind tunnel, the Stefan-Boltzmann relation, Eq. (1.30), may be simplified still further to

$$h_r = \epsilon_w C(4T^3). \qquad (2.04)$$

The emissivity of the enclosure disappears for this case. ϵ_w is taken as 0.90.

For the estimation of h_g, empirical correlations have recently been advanced by Ulsamer and King,[7] plotting hd/k against $du\rho/Z$. In this paper, Ulsamer's curve has been used. Because of the increased turbulence at the free end of the thermometer, somewhat higher values of h_g are to be expected.

Experimental Results

The data obtained are collected in Table I, together with the calculated values of **A** and ψ. Vapor pressures and diffusivities were found as in the first paper and the latent heats calculated from the Dieterici equation as before. These latent heats agree fairly well with those found from the slopes of the vapor-pressure curves by the Clapeyron equation.

In Fig. 3, values of ψ for chlorbenzene and for xylene are plotted against those for toluene at the same velocity, with straight lines resulting; a third line has been drawn in for toluene, for comparison. These lines may be regarded as theoretically determined, with one end at $\psi = 1$ and the other end at the appropriate K/D, with the experimental points falling along the central portions of the lines. Taking as correct the calculated value of D for toluene, values of K/D may be found for the other liquids; this involves fixing the position of the abscissa corresponding to $u = 0$, at which $\psi = K/D$. For chlorbenzene, K/D found in this way is identical with that calculated, 2.68; for xylene, the graphical value of K/D is 2.86, with 2.82 calculated (Table II).

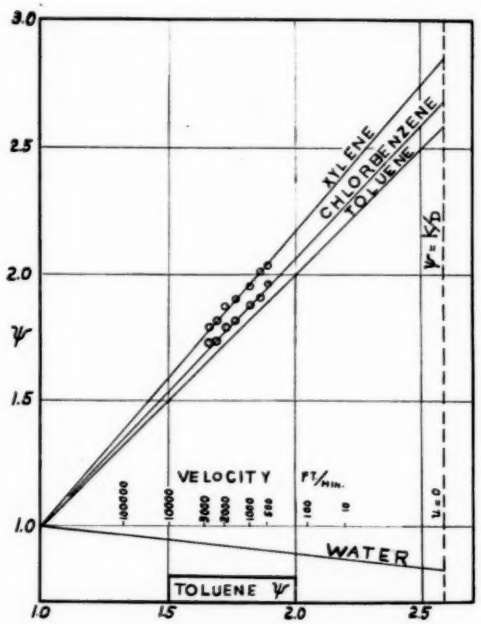

Fig. 3. Rectilinear treatment of data by elimination of velocity functions with theoretical limits K/D and 1.

Table I. *Experimental data and calculated values of* **A** *and* ψ.

u ft./min.	t_a °C	t_w	$t_a - t_w$	p_w mm Hg	P mm Hg	10^6**A**	$\frac{10^6\mathbf{A}}{1+h_r/h_g}$	ψ
Toluene								
3000	29.50	13.25	16.25	15.02	745.5	1239	1197	1.665
2500	29.00	13.14	15.86	14.93	745.5	1261	1214	1.689
2000	28.79	13.24	15.55	15.01	745.5	1295	1242	1.726
1500	28.63	13.40	15.23	15.15	745.5	1334	1272	1.770
1000	25.88	12.26	13.62	14.20	747.4	1394	1313	1.826
700	28.48	13.92	14.56	15.63	745.5	1440	1340	1.862
500	28.43	14.12	14.31	15.84	745.5	1483	1363	1.895
Chlorbenzene								
3000	29.36	19.65	9.71	8.62	741.4	1197	1157	1.720
2500	29.00	19.50	9.50	8.55	741.4	1212	1166	1.733
2000	28.54	19.45	9.09	8.52	745.1	1256	1204	1.790
1500	26.83	18.40	8.43	8.03	744.5	1280	1220	1.814
1000	28.18	19.60	8.58	8.60	745.1	1344	1266	1.881
700	30.40	21.20	9.20	9.42	744.5	1376	1280	1.903
500	30.30	21.40	8.90	9.53	744.5	1439	1320	1.961
Xylene								
3000	27.30	20.25	7.05	6.52	747.4	1237	1196	1.786
2500	27.04	20.16	6.88	6.49	747.4	1261	1214	1.813
2000	26.69	20.08	6.61	6.46	747.4	1307	1253	1.870
1500	26.26	19.88	6.38	6.38	747.4	1337	1274	1.902
1000	26.06	19.90	6.16	6.39	747.4	1386	1305	1.950
700	26.31	20.27	6.04	6.53	747.4	1446	1346	2.010
500	26.12	20.25	5.87	6.52	747.4	1485	1365	2.040

Table II.

Substance	M_v	λ	$\frac{M_v\lambda}{M_aC}$	$\frac{10^6 M_aC}{M_v\lambda}$	D_0	$(K/D)_0$
Toluene	92	105.6	1390	720	0.0705	2.59
Chlorbenzene	112.5	92.4	1487	672	.0680	2.68
Xylene	106	98.5	1494	670	.0646	2.82
Water	18	592	1526	655	.220	0.832

Figs. 3 and 5 contain scales of abscissae showing the velocities corresponding to the various values of ψ.

The deviation of the individual points from the straight lines of Fig. 3 in no case exceeds one

[7] Ulsamer, Forschung **3**, 94 (1932); King, Mech. Eng. **54**, 410 (1932).

percent, although such deviations include errors in the values of the abscissae as well as the ordinates. The experimental accuracy is about 0.5 percent, though with a more refined apparatus this error undoubtedly could be still further reduced. The absolute values of ψ, of course, contain all the errors in the latent heat, vapor pressure and radiation correction, which may be much larger than the observational errors. The graphically-determined values of K/D are affected by small errors from these several sources, some of which may counteract each other.

In Fig. 4, ψ is plotted against K/D at the various velocities used, as in the first paper. For illustration, additional curves representing very

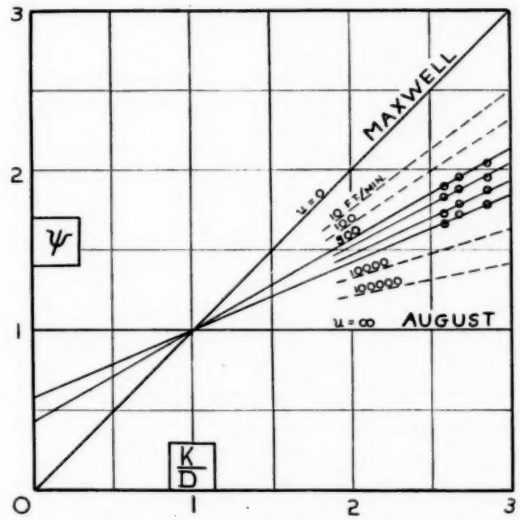

FIG. 4. Lines of constant velocity, showing reduction of theory to Maxwell and August results at velocity limits.

low and very high velocities have been added by using extrapolated values of r. The slope of such lines decreases with increasing velocity, varying from unity at $u=0$ to zero at $u=\infty$, these limits representing the Maxwell diffusional and the August convectional theories. For the range of velocities covered by the experiments, values of r are readily calculable from Eq. (2.01) and may be compared with those found from Eq. (1.35); as the former represent averages over the wet-bulb surface, good agreement is not to be expected.

THEORIES OF GROSSMANN AND WEBER

Grossmann[8] has proposed an empirical equation of approximately correct form:

$$\mathbf{A}=(M_aC/M_v\lambda)[(a+bu)/(1+bu)]. \quad (2.05)$$

With $a=K/D$, this reduces to the correct limits but the velocity function is incorrect. The equation was designed to allow for the inadequacy of August's hypotheses.

Weber[9] recently advanced the relation

$$\mathbf{A}=(M_aC/M_v\lambda)(K/D)^n \quad (2.06)$$

also derived by Svensson[10] for a laminar gas stream. Weber based this equation on Boussinesq's equation[11] for heat transfer and a similar one for evaporation; but since the basic assumptions are physically incorrect,[12] Weber's theory also is invalid. For values of n between zero and unity, Eq. (2.06) predicts *curved* lines in Fig. 4; though Weber's formula is inherently capable of giving better agreement with experiment than Maxwell's or August's, the correspondence must be regarded as largely fortuitous.

THEORY OF HUMIDITY MEASUREMENT

The psychrometric line for water has been constructed in Fig. 3 by drawing a straight line between the points (1, 1) and (2.59, 0.832); K/D for water and air is 0.183/0.220, or 0.832, while at $u=0$, ψ for toluene is 2.59. The same line has been shown in Fig. 5, together with a curved line representing the value of ψ with the radiation correction omitted, that is, of $\mathbf{A}/\mathbf{A}_\infty$, where $\mathbf{A}_\infty$ is the convection theory result. The psychrometric line thus lies below the line $\psi=1$ predicted by August, as has been shown experimentally by Grossmann.[8] At velocities below 1000 ft./min., the curved line rises very steeply, largely because of the radiation error. Above 100 ft./min., the radiation error becomes comparable in magnitude with the theoretical deviation from the August equation, but opposite

[8] Grossmann, Meteorol. Zeits. **24**, 164 (1889); Ann. d. Hydrog. u. Marit. Meteor. **44**, 592 (1916).

[9] Weber, Kung. Danske Videns. Selskab Medd. **3**, No. 19 (1921).

[10] Svensson, Arkiv Matem. Astron. Fysik **A22**, No. 23 (1932).

[11] Boussinesq, Comptes Rendus **133**, 257 (1901).

[12] Russell, Proc. Phys. Soc. **22**, 432 (1909).

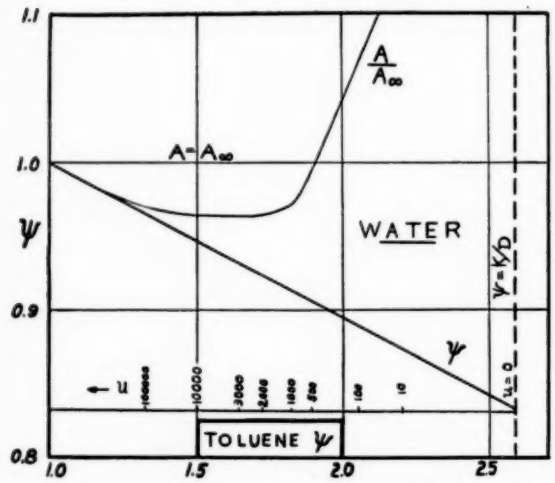

FIG. 5. Psychrometric lines for water; curved line represents theory without the radiation correction.

in direction; at a sufficiently high velocity, a flat minimum results, extending over the range 2000 to 10,000 ft./min. The position of the minimum is dependent upon the air temperature and the nature of the apparatus.

This behavior has been confirmed by experiment. Bongards,[13] using Edelmann's data, found such a minimum. No change of **A** with velocity was observed by Sieper[14] above 600 ft./min.; by Watt,[15] from 880 to 8000 ft./min.; and by Lepinay,[16] from 800 to 2000 ft./min. It is noteworthy that the use of a high velocity in sling psychrometry serves to secure a constant (minimum) value of **A**, not, as is commonly supposed, to render negligibly small the error due to radiation. At the usual sling psychrometer velocity of about 1000 ft./min., **A** is about 0.97 $\mathbf{A}_\infty$, whence the approximate experimental confirmation of the convection theory; however, the radiation correction is still 6.2 percent.

Further consideration of humidity measurements, particularly at high temperatures, is reserved for a later paper. Since **A** is the ratio of two differences, it is greatly affected by errors in either temperatures or partial pressures. In order to secure decisive test data, very precise measurements of p_a and t_w are necessary, particularly at low values of the wet-bulb depression. Much of the work reported in the literature does not possess the required accuracy, largely because of errors in the determination of p_a.

With a few refinements in the experimental arrangement and with the introduction of several secondary effects into the theory, the psychrometer will take its place among physical instruments of high precision.

ACKNOWLEDGMENT

For their assistance in securing the grant of an honorary fellowship, the writer is indebted to Professors G. H. Montillon and S. C. Lind of the School of Chemistry; to Dr. Burrell F. Ruth for several valuable suggestions during the course of the experimental work; and to Mr. A. B. Algren of the Experimental Engineering Laboratories for the loan of apparatus.

[13] Bongards, Zeits. f. Instrumentenk. **52**, 498, 542 (1932).
[14] Sieper, *Dissertation*, Darmstadt (1926).
[15] Watt, Proc. Phys. Soc. **34**, lxiv (1921).
[16] Lepinay, J. de Physique **10**, 17 (1881).

Some Physico-Mathematical Aspects of Nerve Conduction

N. RASHEVSKY, *Westinghouse Research Laboratories, East Pittsburgh*

(Received March 18, 1933)

It has been shown previously by the author that, from the physical point of view, the process of propagation of the nerve impulse is essentially different from the propagation of other kinds of disturbances usually studied in physics. Instead of being described by a differential equation, this type of propagation leads to a simple integral equation. In the domain of the inorganic similar types of propagation are met in the spread of activation on the surface of passive metals. In the present paper the problem of such types of propagation is treated mathematically for two different cases. In the first case it is assumed, that the nerve is electrically uniform all along its length. In this case the final formula for the velocity of propagation reduces to a rather simple expression which applied to the ischiadicus of the frog, leads to a value of 15 meters per second for the velocity of propagation. In the second case the nerve sheath is assumed to be completely insulating, except at the Ranvier nodes, where its continuity is broken, so that the electrical properties of the nerve vary periodically along its length. For the second case a more complicated formula is obtained, which reduces to the first one, when the distance between the nodes tends to zero. Effects of possible distributed capacity are briefly discussed.

PROBLEMS of nerve excitation have always been on the borderland between physiology and physics. Ever since the classical work of W. Nernst[1] the problem of movement and equilibria of ions in the field of an electric current has preoccupied the minds of the nerve physiologists. Much less attention however was given to the physico-mathematical side of another phenomenon in the nerve physiology, namely that of propagation of the nervous impulse. Yet it is perhaps just from the physico-mathematical point of view that this problem is the most fascinating. For, according to the present-day views the propagation of the nerve impulse, though the latter is electric in its nature, is physically quite different from the propagation of either any other electric disturbance, or any kind of wave propagation. Facts of nerve physiology and R. S. Lillie's ingenious experiments[2] on artificial "models" of nerves, all point to the following picture for the propagation of the nerve impulse.

An excited region of the nerve becomes, for reasons which need not to be discussed here, electronegative with respect to the unexcited regions. This results in the production of a local electric current, which will flow in such a way that it is directed from outside into the nerve at the excited place, and in the opposite direction in the unexcited region (Fig. 1). On the other hand, it is known that an electric current, flowing through the nerve, excites at the cathode where it is directed outwards. Hence if the region E (Fig. 1)

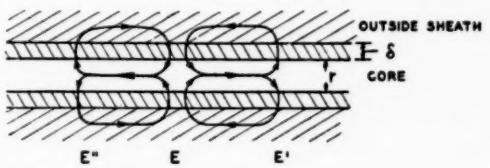

FIG. 1.

becomes excited, the electric current created because of its electronegativity will be such as to cause an excitation at E' and E''. The excitation will thus spread along the nerve. The picture is a rather simple one.

If, however, we try to establish equations which govern such a process of propagation, we shall meet with a peculiar difficulty. The latter lies in the circumstance, that the excitation by the electric current is determined at a given moment not by the instantaneous value of the current, but by the variation of the current previous to its establishment. For the excitation in

[1] Nernst, Gottingen Nachr; Math.-Phys. Klasse, p. 104, 1899.

[2] Lillie, *Protoplasmic Action and Nervous Action*, Chicago University Press, 1923. J. Gen. Physiol. **7**, 473 (1925).

the region occurs when the concentration of the ions, contained in the nerve, exceeds in that region a critical value. The variation of this concentration caused by the current is described by a differential equation and is therefore determined at a given moment both by the initial conditions and the variation of the current at all times previous to that moment. When a region of the nerve is excited, the bio-electric current is not limited to the adjacent region only, but spreads along the whole nerve. Its distribution along the nerve is determined by the physical constants of the latter. Thus the concentration of the ions begins to vary *in the whole nerve as soon as one place is excited*. As the excitation spreads, the distribution of the current along the nerve varies, and that variation is a function of the velocity of spreading of excitation. At a given point of a nerve therefore the concentration of the ions is determined not by the conditions prevailing in the adjacent regions, but actually by the condition of the whole nerve and at all previous times. The problem reduces to an integral equation, whereas in all other problems of disturbance propagation dealt with in physics, the propagation is described by a differential equation, being determined by conditions in the immediate neighborhood of the point considered.

As has been shown elsewhere,[3] the consequence of this situation is that in spite of the fact that the nerve may be physically uniform all along its length, the velocity of propagation need not be constant. Whether it will be constant or not depends on the type of differential equation assumed to govern the variation of the concentration of the excitatory substance.

Unfortunately up to the present physiologists do not yet agree as to the proper kind of such an equation. We shall put at the basis of our considerations an equation recently proposed by H. A. Blair.[4] It has the advantage, besides being simple and representing a number of data very adequately, of permitting an exact solution of the resulting integral equation for the velocity of propagation to be obtained. As we shall see, the numerical value of the velocity of propagation also is in fair agreement with experimental data.

[3] N. Rashevsky, J. Gen. Physiol. **14**, 517 (1931).
[4] Blair, J. Gen. Physiol. **15**, 709 (1932).

In inorganic phenomena the same type of propagation of a disturbance is found in the spread of activation on the surface of passive metals. For instance an iron wire immersed in properly diluted nitric acid becomes covered with a thin layer of higher oxides, which make the metal passive. If the surface of the wire is scratched so as to remove this layer, it becomes activated again, and this activation spreads along the wire.

It is agreed that local electric currents are responsible for this process in a manner similar to that explained above for a nerve.

I.

Considering the nerve as consisting of an inside conducting core, an outside conducting layer (perineurium) and an insulating sheath between, the distribution of the current along the nerve, when a limited region of the latter is excited and therefore electronegative, is easily calculated.

The accepted interpretation of the action currents is that at the place of excitation the drop of potential across the membrane of the nerve fiber is zero, and that it has a constant value along the unexcited part of the axon, the inside being negative. However, mathematically the problem is equivalent to one in which a constant e.m.f. is assumed at the excited region, outside being negative and the potential becoming zero for infinite distance from that excited region. It is merely a question of choice of the zero-point for the scale of potentials.

Let the nerve fiber consist of a core of radius r and specific resistivity ρ. Let the insulating sheath have a thickness δ and specific resistivity $\bar{\rho}$ (Fig. 1). We shall call it "intermediate sheath." Let us denote the potential at any point inside the nerve by V, the potential at an outside point by V'. The current flowing through the cylindrical surface of length dx at a point x is equal to

$$2\pi r dx(V-V')/\delta\bar{\rho}. \tag{1}$$

But this current is equal to the difference di of the currents flowing through the cross sections of the core at x and $x+dx$, as well as to the difference di' of the currents flowing through the cross section of the outside sheath at the same points. Hence

$$di/dx=(2\pi r/\bar{\delta\rho})(V-V')=di'/dx. \quad (2)$$

On the other hand, Ohm's law requires

$$i=(\pi r^2/\rho)dV/dx. \quad (3)$$

If we denote by γ the ratio of the resistance of an unit length of the core to that of an unit length of the outside sheath, we have similarly

$$i'=(\pi r^2\gamma/\rho)dV'/dx. \quad (4)$$

From (2) we have $i=i'+$const. and since for $x=\infty$, both i and i' must vanish, the constant is equal to zero, so that

$$i=i'. \quad (5)$$

Differentiating (2) and combining it with (3), (4) and (5), we find

$$\frac{d^2i}{dx^2}=\frac{2\pi r}{\bar{\delta\rho}}\left(\frac{dV}{dx}-\frac{dV'}{dx}\right)=\frac{2\rho}{\bar{\delta\rho}r}\left(1-\frac{1}{\gamma}\right)i. \quad (6)$$

The general integral of this equation is:

$$i=Ae^{\alpha x}+Be^{-\alpha x}$$

with

$$\alpha=\{[(\gamma-1)/\gamma](2\rho/\bar{\delta\rho}r)\}^{\frac{1}{2}}. \quad (7)$$

Since for $x=\infty$, i must be zero, A must be equal to zero and B to the current I at $x=0$. So that we finally have:

$$i=Ie^{-\alpha x}. \quad (8)$$

Blair's fundamental equation is:

$$dp/dt=Ki-kp, \quad (9)$$

where K and k are constants, i, the exciting current, and p is the quantity which must reach or exceed a critical value h, in order that excitation should occur.

Let the excitation at the point $x=0$, caused by an external exciting current, occur at the time $t=0$. That is, the current distribution described by (8) is established at that time. The region in the immediate vicinity of $x=0$ is then subject to the action of a constant current I, suddenly established at $t=0$.

By integrating Eq. (9) we find[4] that the excitation will occur in the immediate vicinity of $x=0$ only after a time

$$t_1=\frac{1}{k}\log\frac{KI}{KI-kh}. \quad (10)$$

In order that t_1 should be finite, we must have $I>kh/K$. This quantity

$$R=kh/K \quad (11)$$

is known technically as the "rheobase" of the nerve and represents the lower limit, which a suddenly established constant current must exceed in order that excitation should take place.

Hence only after this time has past will this excitation begin to spread in both directions from E. Since the whole phenomenon is symmetrical with respect to the original position of E, we shall consider only the propagation in one direction.

Consider any other point along the nerve, x_0. At the moment $t=0$ a current

$$i(x_0)=Ie^{-\alpha x_0}$$

is established at that point. But as soon as the excitation begins to spread from E, the current at x_0 begins to increase, because the distance s from this point to the excited region decreases.

Let the velocity of propagation of the nervous impulse, in other words the velocity of this spread of excitation, be in general some function of time, which we shall denote by $v(t)$. It is the shape of this function $v(t)$ that we wish to determine.

Since the propagation begins only at the moment $t=t_1$, the distance s of the point x_0 from the excited region at any time $t>t_1$ is given by:

$$s=x_0-\int_{t_1}^{t}v(t)dt=x_0-u(t). \quad (12)$$

Hence between $t=0$ and $t=t_1$ the current at x_0 is constant and has the value

$$Ie^{-\alpha x_0} \quad (13)$$

whereas after $t=t_1$ the current at x_0 varies with time according to the expression:

$$Ie^{-\alpha x_0+\alpha u(t)}. \quad (14)$$

Hence introducing (14) into (9) we find for the variation of p at the point x_0 the equation:

$$dp/dt=KIe^{-\alpha x_0+\alpha u(t)}-kp. \quad (15)$$

The integral of this equation is

$$p=Ce^{-kt}+KIe^{-kt-\alpha x_0}\int e^{\alpha u(t)+kt}dt. \quad (16)$$

C is a constant, which is determined by the initial conditions, that is by the value $p_{x_0}{}^{t_1}$, which p must have at the point x_0 and at the moment t_1. This quantity $p_{x_0}{}^{t_1}$ is easily calculated. For at $t=0$, p equals zero all along the nerve. Between $t=0$ and $t=t_1$, a constant current $Ie^{-\alpha x_0}$ flows at the point x_0.

Substituting this value for i in Eq. (9) and integrating the latter we find for the variation of p at the point x_0 between $t=0$ to $t=t_1$.

$$p=(KIe^{-\alpha x_0}/k)(1-e^{-kt}). \tag{17}$$

To find $p_{x_0}{}^{t_1}$ we must substitute for t in Eq. (17) the value t_1 from Eq. (10) .This gives

$$p_x{}^{t_1}=\frac{KIe^{-\alpha x_0}}{k}(1-e^{-kt_1})$$

$$=\frac{KIe^{-\alpha x_0}}{k}\left(1-\frac{KI-kh}{KI}\right)=he^{-\alpha x_0}. \tag{18}$$

Hence C is determined by the condition

$$Ce^{-kt_1}+KIe^{-kt_1-\alpha x_0}\left[\int e^{\alpha u(t)+kt}dt\right]_{t_1}=he^{-\alpha x_0}. \tag{19}$$

The expression in the square brackets means the value of the integral in the square brackets for $t=t_1$ and is a constant, independent both of x_0 and t. We shall denote it by A.

Substituting in Eq. (19) for t_1 its value from Eq. (10) and solving with respect to C, we find

$$C=(hKI/(KI-kh)-AKI)e^{-\alpha x_0}, \tag{20}$$

which introduced into Eq. (16) gives

$$p=\left(\frac{hKI}{KI-kh}-AKI\right)e^{-\alpha x_0-kt}$$

$$+KIe^{-\alpha x_0-kt}\int e^{\alpha u(t)+kt}dt. \tag{21}$$

The excitation at x_0 occurs when p reaches the value h. Hence the time when this happens is given by

$$\left(\frac{hKI}{KI-kh}-AKI\right)e^{-\alpha x_0-kt}$$

$$+KIe^{-\alpha x_0-kt}\int e^{\alpha u(t)+kt}dt=h. \tag{22}$$

Eq. (22) solved with respect to t gives the time for which the excitation will reach the point x_0. But this in its turn means that if resolved with respect to x_0, Eq. (22) will give the distance travelled during the time $t-t_1$ by the excitation from the point $x=0$, at which it started. But that distance is equal to $u(t)$. Hence substituting[3] $u(t)$ for x_0 in Eq. (22), we find the equation for the determination of $u(t)$.

Performing this substitution and making some rearrangements we find

$$hKI/(KI-kh)-AKI+KI\int e^{\alpha u(t)+kt}dt$$

$$=he^{\alpha u(t)+kt}, \tag{23}$$

which is the integral equation sought.

Differentiating with respect to t,

$$KIe^{\alpha u(t)+kt}=h(\alpha du/dt+k)e^{\alpha u(t)+kt}, \tag{24}$$

and this gives for du/dt, which according to (12) is equal to v, the expression:

$$v=du/dt=(KI-kh)/\alpha h. \tag{25}$$

The velocity of propagation is in this case strictly constant all along the nerve.

On account of (11) we can write Eq. (25) thus

$$v=(I-R)k/\alpha R. \tag{26}$$

Introducing (7) into (26) we find:

$$v=(I-R)k(\gamma\bar{\rho}\delta r)^{\frac{1}{2}}/R[2(\gamma-1)\rho]^{\frac{1}{2}}. \tag{27}$$

Other conditions kept constant, v will vary as the square root of the radius of the fiber. This however holds only if we consider I as an independent constant of a nerve fiber. Actually this is hardly the case. The primary thing is the electromotive force produced by the nerve; and I is determined by it and by the resistance of the nerve fiber. From Eqs. (1)–(6) it is easily seen, that V and i satisfy similar differential equations. We have $V=V_0e^{-\alpha x}$, V_0 being the value of V at $x=0$. Furthermore we see, that $V'=V/\gamma$ and $V_0'=V_0/\gamma$. Hence from (3)

$$i=\frac{\pi r^2\alpha}{\rho}V_0e^{-\alpha x}=\frac{\pi r^2\alpha\gamma}{\rho}V_0'e^{-\alpha x}.$$

Since V_0' is negative, v is positive (the current in

the core flows *from* the excited place). For convenience we shall use the absolute value of V_0' and omit the minus sign.

I is found by putting $x=0$, that is

$$I=\pi r^2\alpha\gamma V_0'/\rho. \tag{28}$$

But V_0' is nothing else but the peak value of the action potential as recorded from the surface of the nerve fiber. Introducing (18) into (26), we find:

$$v=\{[(\pi r^2\alpha\gamma/\rho)V_0'-R]k\}/\alpha R. \tag{29}$$

It may be argued, that the rheobase R should also be expressed in volts, and not in terms of the current. However, from the meager knowledge which we possess about the physical nature of excitation, we would rather believe that it is the exciting current and not the voltage, that plays the primary rôle. For practical purposes, as long as the two are proportional to each other, either may be used. Especially so, because the usually measured rheobase is a relative quantity, measured for a nerve trunk consisting of hundreds of nerve fibers. In our formula R means the minimal current which must flow through a *single fiber*, in order to excite it.

In order to calculate the actual value of v from (29) we need data which are scarcely available An exact calculation cannot therefore be made at present, but at least an estimate may be attempted. From a paper by Rosenberg and Ruhl[5] we find that for the ischiadicus of the frog the liminal intensity of the current is about 2×10^{-6} amp. The cross section of the nerve is about 2×10^{-3} cm^2 (Rosenberg and Schnauder),[6] for the radius of the fiber let us take about 4×10^{-4} cm (Gerard).[7] This gives its cross section approximately 5×10^{-7} cm^2. Hence the liminal current per fiber is about

$$(2\times10^{-6}\times5\times10^{-7})/(2\times10^{-3})=5\times10^{-10}\text{ amp.}$$

But it must be remembered, that the actual liminal current pro fiber is much smaller, for a great part of the current flows through the "outside" sheaths. According to Keil and Müllaur,[8] and Keil and Schultz,[9] γ may be as large as 3, in which case only 1/4 of the total current will flow through the cores of the fibers, and 3/4 will flow through the outside sheaths. All this gives for R as a plausible value 10^{-10} amp. V_0' is about 30 millivolts. As to α, we are again at a loss for lack of exact data. Assuming, that $\bar{\rho}$ and ρ are of the same order of magnitude and taking $\delta=10^{-4}$ cm we find $\alpha\sim5\times10^3$. The values for k vary very much (Blair,[4] p. 712). Taking as one of the largest values $k=497$, and assuming $\rho=200$ ohm·cm,[6] we find $v\sim15$ meters per second. This is in fair agreement with the actual value for the frog's ischiadicus (15–25 m/sec.).[10] A better approximation can be expected only with data more reliable than those available.

With the data used, we find that R is negligible as compared with $\pi r^2\alpha\gamma V_0'/\rho$ so that (29) reduces, with rough approximation to

$$v=\pi r^2\gamma V_0'k/\rho R. \tag{30}$$

We see, that v must vary as the square of r provided R and k are independent on the size. The data of Gasser and Erlanger[11] show definitely, that heavier fibers conduct more rapidly, and that apparently there is a linear relation between v and r, though not without exceptions. Granting the exactitude of this conclusion, their results should be interpreted in terms of the above analysis as indicating a dependence of either R or k, or both on r. Little can be said definitely until on the one hand our knowledge of the mechanism of excitation is more complete, and on the other hand more exact experiments are available on the dependence of v on r.

II.

The circumstance, that the myelin sheath, which covers a nerve fiber, is not continuous, but is broken at intervals of a fraction of a millimeter at the so-called nodes of Ranvier, has led several physiologists (Gerard,[7] Lillie[2]) to assume that the process of propagation of the nerve impulse is not a continuous one, but that the excitation "jumps" from one Ranvier node to another, the Ranvier nodes being the only places where the

[5] Rosenberg and Ruhl, Cremer's Beitrage zur Physiol. **2**, 61 (1924).

[6] Rosenberg and Schnauder, Tabulae Biologicae, Vol. **2**, p. 350. W. Junk, Berlin, 1925.

[7] Gerard, Quart. Rev. Biol. **6**, 59 (1931).

[8] Keil and Müllaur, Cremers Beitrage **2**, 89 (1924).

[9] Keil and Schultz, Cremers Beitrage **2**, 209 (1924).

[10] Reference 6, p. 332.

[11] Gasser and Erlanger, Am. J. Physiol. **82**, 644 (1927); **80**, 522 (1927); **92**, 43 (1930).

bio-electric current can pass from the core. A similar condition has been reproduced by R. S. Lillie for the spread of activation in a passive iron wire. When the latter is covered with a glass tube, broken at regular intervals, the activation also does not spread over the whole wire, but "jumps" from one break to another. Let us calculate the velocity in this case.

Let the internodal distance be equal to a and let ρ have the same meaning as before. Let the current flowing through the n-th internodal interval along the core be i_n. Let the potential of the core at the n-th node be V_n and the potential outside the core V_n'. When the current flowing through the n-th node is given by

$$\bar{\imath}_n = (V_n - V_n')/\omega \tag{31}$$

if ω denotes the resistance of the node. Further we have

$$i_{n+1} - i_n = \bar{\imath}_n = i'_{n+1} - i_n' \tag{32}$$

and

$$\left.\begin{aligned} i_n &= (\pi r^2/\rho a)(V_n - V_{n-1}), \\ i_n' &= (\pi r^2 \gamma/\rho a)(V_n' - V_{n-1}'). \end{aligned}\right\} \tag{33}$$

From (32) it follows, that $i_n = i_n' + \text{const.}$, and for the same reasons as before this constant must be equal to zero, so that $i_n' = i_n$. But then (33) gives $V_n - V_{n-1} = \gamma(V_n' - V_{n-1}')$ which gives $V_n' = V_n/\gamma$. (31) now becomes

$$\bar{\imath}_n = \frac{1}{\omega}\frac{\gamma-1}{\gamma} V_n. \tag{34}$$

(32) and (34) give

$$i_n = \frac{\pi r^2 \omega}{\rho a}\frac{\gamma}{\gamma-1}(\bar{\imath}_n - \bar{\imath}_{n-1}). \tag{35}$$

(35) combined with (32) gives

$$i_n = \frac{\pi r^2 \omega}{\rho a}\frac{\gamma}{\gamma-1}(i_{n+1} - 2i_n + i_{n-1})$$

or raising all indexes by one and rearranging:

$$i_n - 2\left(1 + \frac{\rho a}{2\pi r^2 \omega}\frac{\gamma-1}{\gamma}\right) i_{n+1} + i_{n+2} = 0. \tag{36}$$

This is an equation in finite differences of second order. Its general solution is[12] $i_n = A\beta_1^n + B\beta_2^n$, A and B being constants, and β_1 and β_2 being the roots of the equation

$$y^2 - 2\left(1 + \frac{\rho a}{2\pi r^2 \omega}\frac{\gamma-1}{\gamma}\right) y + 1 = 0. \tag{37}$$

Hence

$$\left.\begin{aligned} \beta_1 &= 1 + \frac{\rho a}{2\pi r^2 \omega}\frac{\gamma-1}{\gamma} + \left[\left(1 + \frac{\rho a}{2\pi r^2 \omega}\frac{\gamma-1}{\gamma}\right)^2 - 1\right]^{\frac{1}{2}} \\ \text{and} \quad \beta_2 &= 1 + \frac{\rho a}{2\pi r^2 \omega}\frac{\gamma-1}{\gamma} - \left[\left(1 + \frac{\rho a}{2\pi r^2 \omega}\frac{\gamma-1}{\gamma}\right)^2 - 1\right]^{\frac{1}{2}}. \end{aligned}\right\} \tag{38}$$

It is easily seen, that $\beta_1 > 1$; $\beta_2 < 1$; hence since i should not become infinitive with increasing n, $A = 0$. Writing now β for β_2, we have

$$i_n = I\beta^n. \tag{39}$$

I is determined by the initial conditions, namely, $I\beta$ is equal to the current through the core in the first internodal interval. A similar expression is obtained for V

$$V_n = V_0\beta^n. \tag{40}$$

(39) gives the current through any node at any time. n is the serial number of the node, counting from the one which the excitation has already reached.

Let us now denote by t_1, t_2, $\cdots t_n$ the moments at which the excitation reaches the 1st, 2nd $\cdots n$th node. We propose to calculate t_1, $t_2 - t_1$, $t_3 - t_2$, $\cdots t_n - t_{n-1}$,

t_1 can be readily calculated. For this is the time it takes to excite the first node, through which a constant current $I\beta$ is flowing. From Eq. (10) we find:

$$t_1 = \frac{1}{k}\log\frac{KI\beta}{KI\beta - kh}. \tag{41}$$

[12] Nörlund, *Differenzrechnung;* p. 296. J. Springer, Berlin, 1924.

Let us denote by $p^g{}_i$ the value p at the ith node at the moment t_g $(g<i)$. We have $p_1{}^1=h$. Remembering that at the moment t_{i-1} the excitation has reached the $(i-1)$st node and that therefore at that time the current through the ith node is $I\beta$, we find from (9):

$$\int_{p_i{}^{i-1}}^{h}\frac{dkp}{KI\beta-kp}=k(t_{i-1}-t_i) \tag{42}$$

or

$$\frac{1}{k}\log\frac{KI\beta-kp_i{}^{i-1}}{KI\beta-kh}=t_i-t_{i-1}. \tag{43}$$

And similarly

$$\frac{1}{k}\log\frac{KI\beta^2-kp_i{}^{i-2}}{KI\beta-kp_i{}^{i-1}}=t_{i-1}-t_{i-2}. \tag{44}$$

Eq. (44) gives

$$kp_i{}^{i-1}=KI\beta^2(1-e^{-k(t_{i-1}-t_{i-2})})+kp_i{}^{i-2}e^{-k(t_{i-1}-t_{i-2})}. \tag{45}$$

Since $p_2{}^0=0$ and $t_0=0$, (45) gives

$$kp_2{}^1=KI\beta^2(1-e^{-kt_1})=k\beta h. \tag{46}$$

Eq. (43) gives

$$t_2-t_1=\frac{1}{k}\log\frac{KI\beta-kp_2{}^1}{KI\beta-kh} \tag{47}$$

and introducing $p_2{}^1$ from (46) we find:

$$t_2-t_1=\frac{1}{k}\log\frac{KI\beta-\beta kh}{KI\beta-kh}. \tag{48}$$

Again from (44) we have

$$t_3-t_2=\frac{1}{k}\log\frac{KI\beta-kp_3{}^2}{KI\beta-kh} \tag{49}$$

and from (48)

$$kp_3{}^2=KI\beta^2(1-e^{-k(t_2-t_1)})+kp_3{}^1e^{-k(t_2-t_1)}. \tag{50}$$

But $p_3{}^1$ is calculated from

$$\int_0^{p_3^1}\frac{kdp}{KI\beta^3-kp}=kt_1 \text{ or } \log\frac{KI\beta^3}{KI\beta^3-kp_3{}^1}=kt_1, \tag{51}$$

which gives

$$kp_3{}^1=KI\beta^3(1-e^{-kt_1}). \tag{52}$$

Introducing (52) into (50) and the latter into (49) and substituting for t_1 and t_2-t_1 their values from (41) and (48), we find after some elementary calculations

$$t_3-t_2=\frac{1}{k}\log\frac{KI\beta-\beta kh}{KI\beta-kh}=t_2-t_1. \tag{53}$$

By the so-called method of conclusion from n to $n+1$, it can be shown, that the same expression holds for any $t_{n+1}-t_n$. So that

$$t_{n+1}-t_n=(1/k)\log[(KI\beta-\beta kh)/(KI\beta-kh)]. \tag{54}$$

Hence except for the first interval t_1, all the others are equal and given by (54). The velocity of propagation is constant and given by

$$v=\frac{a}{t_n-t_{n-1}}=ak\Big/\log\frac{KI\beta-\beta kh}{KI\beta-kh} \tag{55}$$

or using again $KR=kh$

$$v=ak\Big/\log[\beta(1-R)/(I\beta-R)]. \tag{56}$$

For the first interval t_1 we find similarly

$$t_1=(1/k)\log[I\beta/(I\beta-R)]. \tag{57}$$

Now again we must introduce V_0' instead of I. Eq. (33) together with (40) gives:

$$i_1=I\beta=\frac{\pi r^2}{\rho a}(V_1-V_0)=\frac{\pi r^2\gamma}{\rho a}(1-\beta)V_0'. \tag{58}$$

(We again shall use the absolute value of V_0'.) So that (56) becomes

$$v=ak\Big/\left\{\log\left[\frac{\pi r^2\gamma}{\rho a}(1-\beta)V_0'-\beta R\right]-\log\left[\frac{\pi r^2\gamma}{\rho a}(1-\beta)V_0'-R\right]\right\}. \tag{59}$$

We shall now prove that when the internodal distance a tends to zero, expression (59) tends to expression (29). To do this, let us first see how ω is connected with the average specific resistance $\bar{\rho}$ of the nerve sheath.

The resistance of a uniform intermediate sheath to a radially flowing current is equal per unit length to $\delta\bar{\rho}/2\pi r$. If, however, the sheath is insulated except at the nodes, the resistance to a radial current per unit length is equal to ωa, because per unit length there are $1/a$ nodes, connected in parallel. Hence the average specific resistance $\bar{\rho}$, that is the specific resistance obtained with the assumption that the sheath is uniformly conducting, is given by:

$$\delta\bar{\rho}/2\pi r=\omega a \quad \text{or} \quad \omega=\delta\bar{\rho}/2\pi r a. \tag{60}$$

Introducing this into (38) we find

$$\beta=1+\frac{\rho a^2}{\delta\bar{\rho}r}\frac{\gamma-1}{\gamma}-\left[\left(1+\frac{\rho a^2}{\delta\bar{\rho}r}\frac{\gamma-1}{\gamma}\right)^2-1\right]^{\frac{1}{2}}. \tag{61}$$

When a approaches zero, β approaches unity. Expanding (61) and neglecting terms with a^2 and higher orders we find

$$\left.\begin{aligned}\beta&=1-a\left[\frac{2\rho}{\bar{\rho}r\delta}\frac{\gamma-1}{\gamma}\right]^{\frac{1}{2}}=1-\epsilon,\\ \epsilon&=\alpha a,\end{aligned}\right\} \tag{62}$$

ϵ being a small quantity.

Now we may write the Eq. (59) as follows:

$$v=ak\Big/\left\{\log\left[\frac{\pi r^2\gamma\alpha}{\rho}V_0'-(1-\epsilon)R\right]-\log\left(\frac{\pi r^2\gamma\alpha}{\rho}V_0'-R\right)\right\}$$

or

$$v=ak\Big/\left\{\log\left[\frac{\pi r^2\gamma\alpha V_0'}{\rho}-R+\epsilon R\right]-\log\left[\frac{\pi r^2\gamma\alpha V_0'}{\rho}-R\right]\right\}=ak\Big/\left\{\log\left[1+\frac{R}{\pi r^2\gamma\alpha V_0'/\rho-R}\epsilon\right]\right\}. \tag{63}$$

Expanding the log in the denominator and omitting higher powers of ϵ than the first, we have

$$v=ak[\pi r^2\gamma\alpha V_0'/\rho-R]\Big/\epsilon R,$$

which on account of (62) is identical with (29).

The variation of v with a, the internodal distance, as given by (59) is rather complicated, for a enters in β. It can be easily seen, that for very small a, v is larger than v for $a=0$. In order to see that, we need only to take the next term in the expansion of the log in (63). This gives, by using (62):

$$v=\frac{ak}{\dfrac{R\alpha}{\dfrac{\pi r^2\gamma\alpha V_0'}{\rho}-R}a-\dfrac{1}{2}\left(\dfrac{R\alpha}{\dfrac{\pi r^2\gamma\alpha V_0'}{\rho}-R}\right)^2a^2}.$$

For $a=0$ this reduces to (29), but with increasing a, V increases. This increase does not go on, however, indefinitely. From the expression (38) for β it can be seen, that for a approaching zero, β tends to unity, but for very large a it tends to zero, varying like $1/a$. Therefore as a increases the second log in denominator of (59) tends to zero, and the whole denominator tending to infinity, v tends to zero. The physical meaning of this is clear: as the internodal distance becomes larger, the resistance of the fiber between two subsequent nodes becomes larger and the current produced by a given e.m.f. in one node and flowing through the next, becomes smaller, until finally it fails to excite. v has therefore a maximum for a certain a. Using the same data as above we find that v becomes zero for $a=0.17$ cm. For $a=0.1$ cm, v has approximately the same value as for $a=0$. The insufficiency of our knowledge of the physical constants of the nerve do not permit to decide between (59) and (29). More exact determinations of those constants of the nerve are very desirable for a better understanding, by means of analysis similar to this one, of the true nature of nervous conduction.

A closer inspection of the Eq. (59) shows that v increases with r, though the law of increase is rather complicated.

In the above analysis we have assumed, that when the excitation spreads along the nerve, the

distribution of the current in the unexcited regions, given by (8), simply "travels along," thus leading to expression (14). But Eq. (8) represents a stationary state which is reached only after a finite time after the application of a constant e.m.f. at $x=0$. The transition from (8) to (14) means a tacit assumption, that the time of establishing the condition (8) is negligible, which physically means neglecting the possible distributed inductance and capacity of the nerve. There is nothing that indicates any appreciable inductance of a nerve fiber. But the work of Bishop[13] shows that the capacity of the nerve is not negligible. Taking into account the distributed capacity would however complicate very much the problem mathematically. We shall reserve such a rigorous treatment to a subsequent paper. Here we shall only roughly estimate, how large a correction this may introduce into our formulae. Bishop's results indicate, that the distribution of capacity and resistance in a nerve is quite a complicated one. The nerve may be considered as approximately equivalent to three coupled capacity-resistance circuits. The table on p. 626 of Bishop's paper gives the values for these various circuits. If we reduce all his data for 1 cm length of the nerve, we shall find that the time factors, which give the order of magnitude of the time it would take to reach a stationary state (relaxation time) in the circuits, and which is given by the product capacity$\times$resistance (ohm$\times$farad = one second), vary from 2×10^{-4} sec. and down. But during that time the excitation will have travelled only about 0.1–0.2 cm. In other words, the "relaxation time" per unit length is small, though not negligible, as compared with the time it takes the excitation to travel that unit length. Taking into account the relaxation time will therefore change our final formulae by 10 percent–20 percent at most, but will not alter the order of magnitude.

[13] Bishop, Am. J. Physiol. **89**, 618 (1929).